2017-12-21

Small Molecule Modulation of GLUT1-Mediated Glucose Transport

Ogooluwa A. Ojelabi
University of Massachusetts Medical School

SMALL MOLECULE MODULATION OF GLUT1-MEDIATED GLUCOSE TRANSPORT

A Dissertation Presented

By

OGOOLUWA ADEGOKE OJELABI

Submitted to the Faculty of the
University of Massachusetts Graduate School of Biomedical Sciences, Worcester
in partial fulfillment of the requirements for the degree of

DOCTOR OF PHILOSOPHY

December 21, 2017

Department of Biochemistry and Molecular Pharmacology

SMALL MOLECULE MODULATION OF GLUT1-MEDIATED GLUCOSE TRANSPORT

A Dissertation Presented

By

OGOOLUWA ADEGOKE OJELABI

Dissertation Defense Committee Members

Mary Munson, Ph.D.
Biochemistry and Molecular Pharmacology

Silvia Corvera, M.D.
Program in Molecular Medicine

William Kobertz, Ph.D.
Biochemistry and Molecular Pharmacology

Chair of Dissertation Committee
Reid Gilmore, Ph.D.
Biochemistry and Molecular Pharmacology

External Dissertation Committee Member
Paul Pilch, Ph.D.
Professor, Boston University School of Medicine

Thesis Advisor
Anthony Carruthers, Ph.D.
Biochemistry and Molecular Pharmacology

Student Program
Biochemistry and Molecular Pharmacology

December 21, 2017

DEDICATION

To Ife and Ola

I hope the efforts of your mom and I to attain excellence in our endeavors will always inspire you to work hard to acquire the skills that will bring you success

Ecclesiastes 10:10

ACKNOWLEDGEMENTS

I am eternally grateful to my advisor and mentor, Dr. Anthony Carruthers, for his loving support, guidance, encouragement, and help all through this graduate program. Tony always made time for me in spite of his busy schedule and he made sure I had everything I needed to succeed. He always encourages me to do my best work, and is truly excited about my progress. Thank you, Tony, for believing in me and for genuinely caring about the well-being of my family and I.

When I first spoke to Tony about joining his lab, he told me that he and the members of his lab will do everything in their power to see that I succeed, and that is exactly what Tony and the Carruthers' lab have done! I am grateful to the all members of Carruthers lab, both past and present, for creating a great working environment, and for their help. Particularly, I would like to thank Dr. Julie De Zutter for her help with experiments and for her true interest in my success. I also want to thank Dr. Anthony Cura, who mentored me when I first rotated in the lab, and taught me the fundamentals I so much needed. Special thanks to Dr. Jay Sage, Andrew Simon and Kenny Lloyd for their help and amazing support.

I appreciate the support of my TRAC members – Dr. Reid Gilmore, Dr. Silvia Corvera and Dr. Mary Munson. I am grateful for their valuable suggestions and insights toward my thesis research, and for their sincere interests in my success and progress. I would also like to thank Dr. Bill Kobertz for agreeing to serve on my dissertation committee, and for his many signatures and support as the director of the department's graduate program. I sincerely want to thank Dr. Paul Pilch for accepting our invitation to serve as the external member of my dissertation committee, and for his time and input.

I would like to thank Navitor Pharmaceuticals for providing the navitor compounds used in this study and for funding the navitor compounds project. I especially will like to thank Drs. Sengupta, Saiah and Vlasuk for their support and encouragement.

I have enjoyed a remarkable support from all the members of the BMP department. I am thankful for their encouragement, support and for making this place a friendly and collaborative environment for science.

I would like to acknowledge my friends here at UMass Medical School who truly understand and share in the travails of biomedical research, and with whom I have shared the joys of our progress in science and outside of science. Special thanks to Chido Kativhu, Zach Maben, Ken Aryee, Amena Arif, and Eugene Bah for been my solid support system.

I am grateful to my friends, the members of my church, and my family for their unconditional love, prayers and support over the years. Words cannot express enough how much I appreciate you all. Thank you, I am grateful.

To the love of my life, Ayomi, thank you for loving me. Your unconditional love provides the much-needed drive to get through each day. Thank you for your encouragement, your prayers, your patience, your understanding, and for taking care of me and the kids too. I cannot imagine going through this journey without you. Thank you for making it worthwhile.

Finally, to Ife and Ola, thank you for your understanding, and for honing my ability to focus and to maximize the use of my time away from home. As this program ends, I hope to create more time for you both and to be truly there for you.

ABSTRACT

The glucose transport protein, GLUT1, is highly expressed in rapidly proliferating cells, including cancer cells, while decreased GLUT1 levels are found in diseases such as GLUT1 deficiency syndrome and Alzheimer's. There is increased interest in developing GLUT1 inhibitors as novel anticancer therapeutics, and the discovery of compounds that directly stimulate GLUT1 function. This work investigates how small molecules stimulate and/or inhibit GLUT1-mediated glucose transport, either directly or through the AMPK pathway.

Using sugar transport assays and docking analyses to explore Ligand–GLUT1 interactions and specificity of binding, we show that: 1) Ligands inhibit GLUT1 by competing with glucose for binding to the exofacial or endofacial sugar binding sites; 2) Subsaturating inhibitor concentrations stimulate sugar uptake; 3) Ligands inhibit GLUT1–, GLUT3– and GLUT4–mediated sugar uptake in HEK293 cells; and 4) Inclusion of a benzonitrile head group on endofacial GLUT1 inhibitors confers greater inhibitory potency.

Furthermore, we investigated AMPK-regulated GLUT1 trafficking in cultured blood-brain barrier endothelial cells, and show that inhibition of GLUT1 internalization is not responsible for increased cell surface levels of GLUT1 observed with AMPK activation in these cells.

This study provides a framework for screening candidate GLUT1 inhibitors for specificity, and for optimizing drug design and delivery. Our data on transport stimulation at low inhibitor concentrations support the idea that GLUT1 functions as a cooperative oligomer of allosteric alternating access subunits.

TABLE OF CONTENTS

LIST OF TABLES

LIST OF FIGURES

LIST OF PUBLISHED MATERIALS PRODUCED BY THE AUTHOR

Chapter II of this dissertation was published as:

Ojelabi, O. A., Lloyd, K. P., Simon, A. H., De Zutter, J. K., and Carruthers, A. (2016) WZB117 (2-Fluoro-6-(m-hydroxybenzoyloxy) Phenyl m-Hydroxybenzoate) inhibits GLUT1-mediated sugar transport by binding reversibly at the exofacial sugar binding site. *Journal of Biological Chemistry* 291, 26762-26772

LIST OF ABBREVIATIONS

2DG	2-deoxy-D-glucose
3MG	3-O-methyl-D-glucose
AAT	Alternating access transporter
AICAR	aminoimidazole carboxamide ribonucleotide
AMPK	5’- adenosine-monophosphate-dependent kinase
APC	Amino acid-polyamine-organocation superfamily
BAY-876	N4-[1-[(4-cyanophenyl)methyl]-5-methyl-3-(trifluoromethyl)-1H-pyrazol-4-yl]-7-fluoro-2,4-quinolinedicarboxamide
BBB	Blood-brain barrier
bEnd.3	Murine brain microvascular endothelial cell line
CB	Cytochalasin B
CFTR	Cystic Fibrosis membrane conductance Regulator protein
CNS	Central nervous system
DHA	Dehydroascorbic acid
DTT	Dithiothreitol
ECG	(–)-Epicatechin-3-gallate
EGCG	(−)-Epigallocatechin-3-gallate
FST	Fixed-site transporter
G6PT	Glucose-6-phosphate translocase
Glc	Glucose
Glc-6-P	Glucose-6-phosphate
GlcP	Glucose/mannose transporter
GLUT	Glucose transport protein
GLUT1DS	GLUT1 deficiency syndrome
HEK293	Human embryonic kidney cells 293
HMIT	H+/myo-inositol symporter
KCN	Potassium cyanide
LacY	Lactose permease
MFS	Major facilitator superfamily
Na^+–K^+ ATPase	Sodium-potassium adenosine triphosphatase

NAD^+	Nicotinamide adenine dinucleotide
NADPH	Nicotinamide adenine dinucleotide phosphate
NV-5440	o-{4-[(5-{[4-(o-cyanophenyl)-1-piperazinyl]methyl}-2,4-xylyl)carbonyl]-1-piperazinyl}benzenesulfonamide
qPCR	Quantitative reverse-transcriptase polymerase chain reaction
Rab-GAP	Rab GTPase-Activating Protein
SDS-PAGE	Sodium dodecyl sulfate-polyacrylamide gel electrophoresis
SGLT	Sodium–dependent glucose transporters
SLC	Solute-linked carrier protein
STF-31	4-[[[[4-(1,1-Dimethylethyl)phenyl]sulfonyl]amino]methyl]-N-3-pyridinyl-benzamide
SWEET	Sugars will eventually be exported transporters
TCEP	Tris(2-carboxyethyl)phosphine
TfR	Transferrin receptor
TOG	Transporter-opsin-G protein-coupled receptor superfamily
Tris	2-amino-2-(hydroxymethyl)-1,3-propanediol
WZB117	2-fluoro-6-(mhydroxybenzoyloxy)phenyl m-hydroxybenzoate
XylE	D-xylose-proton symporter

CHAPTER I

Introduction

Solute transport across cell membranes

The plasma membrane encloses all living cells and acts as a physical barrier that limits the movement of substances in and out of cells. This barrier function allows a cell to define and distinguish the contents of its interior, from the extracellular environment (1). The plasma membrane, like all other biological membranes, is a complex, dynamic non-covalent macromolecular structure comprising a lipid bilayer containing embedded and membrane-spanning proteins. The lipid bilayer comprises amphipathic phospholipids arranged in such a way that the nonpolar fatty acid tails self-associate to form a hydrophobic interior of about 2 – 3 nm in thickness, shielded from the polar interstitial and cytoplasmic environments by their hydrophilic phosphate head groups (1).

Simple diffusion

Given enough time, virtually all substances will diffuse across an artificial lipid bilayer down an electrochemical gradient (1). The ability of a molecule to diffuse across the plasma membrane and enter into the cell depends on its size and relative hydrophobicity (1,2). Small nonpolar molecules (e.g. carbon dioxide, oxygen, benzene, and steroid hormones) cross lipid membranes readily by simple diffusion. Small uncharged polar molecules (e.g. ethanol, water and glycerol) also diffuse across lipid membranes but slowly. In contrast, larger uncharged polar substrates (e.g. glucose, amino acids and nucleotides) and charged ions (e.g. H^+, Na^+, K^+, and Cl^-) are unable to cross lipid membranes by simple diffusion (1,2).

Protein-mediated transport

Cells utilize specialized membrane proteins which span the membrane to facilitate the rapid transbilayer movement of hydrophilic molecules and ions, which otherwise could not cross the cell membranes by simple diffusion at physiologically meaningful rates. This protein-mediated transport system creates a path for polar solutes to cross cells membranes without interacting directly with the hydrophobic interior of the lipid bilayer (1,3). Membrane transport proteins can be classified into 2 major classes: 1) channels and 2) transporters.

Channels form narrow and highly selective hydrophilic pores across cell membranes which allow rapid passage of specific solutes in the order of tens of millions per second (4). The most characterized channels include: 1) ion channels, that transport specific inorganic ions (e.g. Na^+, K^+, Ca^{2+} and Cl^-), and 2) aquaporins, water channels, which allow rapid transport of water but exclude ions (2). Unlike the aquaporins, ion channels are gated, and they open and close rapidly in response to signals such as voltage, mechanical stress or binding of a ligand (1). Transporters, on the other hand, move specific substrates or a class of substrates across cell membranes by undergoing substrate-induced conformational changes that shuttle substrates between either side of the membrane.

Unlike most transporters, channels interact with transported solutes with low affinity but are able to transport solutes at much faster rates, typically more than 1,000-fold greater than transporters (5). This may simply reflect selective pressure to transport cations at prevailing substrate levels (high mM) and at rates compatible with function (e.g. allow the conduction of action potentials). Another striking difference between transporters and

channels is that channels can only mediate passive transport of solutes, while transporters facilitate both passive and active transport (1,3,6).

Passive versus active transport

Passive transport describes the net movement of solutes down a concentration gradient (or electrochemical gradient for charged solutes), while active transport describes the net transport of solutes against a concentration or electrochemical gradient and requires energy input (1,6). The free energy source for active transport is either derived directly from transporter-catalyzed ATP hydrolysis (primary active transport; e.g., Na^+–K^+ ATPase) or indirectly (secondary active transport) by coupling the uphill transport of substrate to the downhill transport of a second solute (usually a cation) down an electrochemical gradient established by the action of a primary active transporter (7). Secondary active transporters can either mediate the cotransport of 2 different solutes in the same direction (symporters; e.g., Na^+–dependent glucose cotransporters [SGLTs]) or in different directions (antiporters; e.g., Na^+–Ca^{2+} and Na^+–H^+ exchangers). Symporters and antiporters dependent on the electrochemical gradients created and maintained by primary active transporters (e.g., Na^+ gradients generated by Na^+–K^+ ATPase). Transporters that catalyze passive transport of a single solute down its concentration gradient are referred to as uniporters (e.g., glucose transporter proteins [GLUTs]) (1,6).

Clinical relevance of membrane transport proteins

The biological significance of membrane transport proteins is revealed in various inherited human diseases caused by mutations that impair transport of specific solutes by their transporters. Mutations in the glucose transporter 1 (GLUT1), stymies the import of

glucose into the brain, resulting in GLUT1–deficiency syndrome, characterized by retarded mental development with manifestations such as abnormally small head, ataxia and seizures (8-10). Mutations in the genes (SLC7A9 and SLC3A1) encoding transporter proteins responsible for cysteine transport from urine to the blood causes accumulation of cysteine in urine (cystinuria), which results in the formation of cysteine stones in kidneys and ultimately kidney damage if not properly treated (11). Point mutations in the membrane transport protein cystic fibrosis membrane conductance regulator protein (CFTR), which mediates chloride ion transport across plasma membranes of epithelial cells, cause reduced transporter activity or prevent CFTR expression at the cell surface and give rise to cystic fibrosis (12).

Glucose transport across cell membranes

Three families of glucose transport proteins have been identified in humans: 1) the facilitative glucose transporters, GLUTs (SLC2); 2) the secondary active sodium–dependent glucose transporters, SGLTs (SLC5); and 3) the recently identified sugars will eventually be exported transporters, SWEETs (SLC50) (13-16). GLUTs catalyze the passive, facilitative transport of glucose down its concentration gradient, and mediate sugar transport in almost all mammalian cells (5). SGLTs couple the energy released from the flow of Na^+ down its concentration gradient to the uphill transport of glucose across cell membranes, and are primarily responsible for the absorption and reabsorption of glucose at the mucosal membranes of the small intestine and kidney respectively (16,17). SWEETs, found in animals, plants and bacteria, have been shown to catalyze the facilitative diffusion of sugars across the plasma membrane and endoplasmic reticulum membrane in plants, but their physiological role in mammals is still uncharacterized

(15,18). Figure 1.1 shows a model for cellular transport of glucose in humans, depicting the roles (or possible roles, as in the case of SWEETs) of each of these glucose transport proteins.

The glucose transporter (GLUT) proteins

The GLUT proteins belong to the major facilitator superfamily (MFS) of proteins which are ubiquitously expressed in living organisms, and transport a wide range of substrates including sugars, ions, drugs and toxins (19,20). There are 14 members of the GLUT protein family (GLUT1 – 12, 14 and HMIT) – each containing ~500 amino acids, and sharing an overall sequence identity of 25% – 68% (13,21). Hydropathy plot analysis reveals that GLUT proteins, like other members of the MFS superfamily, contain 12 transmembrane (TM) domains, with intracellular N– and C–termini and a single exofacial glycosylation site at either loop 1 (between TM1 and TM2) or loop 9 (between TM9 and TM10) (5,22). Like the rest of the MFS transporter proteins, GLUTs are divided into 2 symmetrical halves connected by a large intracellular loop between TM6 and TM7 (22,23). The GLUT proteins contain a highly conserved RXGRR/K motif between TM2 and TM3, which is thought to maintain their proper topology within the membrane (24). Additionally, the GLUTs contain sugar-transporter signature motifs which appear to be important for substrate/inhibitor sensitivity and selectivity. These include: PMY (in TM4), PESPRY/FLL (in loop 6), QQLSGIN (in loop 7), GXXXXP (in TM10), and VPETKG (in the C-terminus) (25). Based upon sequence similarity analysis, GLUTs are subdivided into 3 classes. Class 1 comprises GLUT1–4 and GLUT14; Class 2 comprises GLUT5, 7, 9 and 11; and Class 3 comprises GLUT6, 8, 10, 12 and HMIT1 (21). Table 1.1

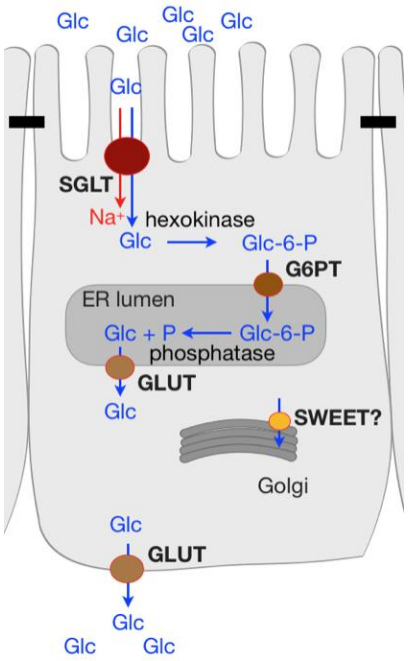

Figure 1.1: A model for cellular glucose transport mediated by different glucose transport proteins in human intestinal epithelial cells

Glucose (glc) from the small intestinal lumen is taken up into the cytoplasm of enterocytes by the Na^+–dependent glucose transporter, SGLT1. Cytoplasmic glc is either transported out of the cell by passive diffusion mediated by the facilitative glucose transporter, GLUT2 or phosphorylated by hexokinase to form glucose-6-phosphate (Glc-6-P). Glc-6-P, especially in the liver, and during gluconeogenesis can be shuttled into the endoplasmic reticulum (ER) lumen by the antiporter, glucose-6-phosphate translocase (26), where Glc-6-P is dephosphorylated and glucose shuttled back into the cytoplasm by GLUTs, probably by GLUT8 (27). Although the role of SWEETs in mammalian cells is still unclear, SWEET proteins are localized to the Golgi in mammalian cells, suggesting a possible role for this glc transporter in the Golgi (18).

shows the classification of human GLUTs, their characteristics and their tissue distribution. With the exception of HMIT (a H^+/myo-inositol symporter), all GLUTs transport glucose, fructose, or both sugars (13). The crystal structures of human GLUT1 (28,29) and GLUT3 (30) were recently reported. These, together with the crystal structures of *Bos taurus* and *Rattus norvegicus* GLUT5 (31), and their bacterial homologs XylE (32-34) and GlcP (35), provide structural insights to the transport mechanisms of the GLUT proteins.

The Na^+–dependent glucose cotransporter (SGLT) proteins

SGLTs belong to the amino acid-polyamine-organocation (APC) superfamily of transporter proteins containing 5+5 or 7+7 inverted repeat folds (36). Unlike the GLUTs, SGLTs are secondary active glucose transporters that cotransport the uphill flow of glucose and downhill flow of Na^+ in the same direction, by harnessing the free energy of the Na^+ electrochemical gradient to transport of glucose against its concentration gradient (17). The favorable Na^+ electrochemical gradient exploited by SGLTs is created and maintained by Na^+–K^+ ATPase (1). Six SGLT proteins (SGLT1–6) have been identified in humans which share amino acid sequence identity of 21% – 70% with SGLT1 (14,17). SGLTs contain 580 – 718 amino acid residues and are predicted to have 14 transmembrane helices (37). The best-characterized members of the SGLT proteins are SGLT1 and SGLT2 (16). SGLT1, a high affinity glucose and galactose transporter (K_m = 0.5 – 1 mM) (38,39), is primarily expressed in the small intestine where it mediates the absorption of glucose and galactose from the intestinal lumen (17). Relative to SGLT1, SGLT2 is a low affinity glucose transporter (K_m for glucose = 5 mM (39)) and is predominantly expressed in the kidney cortex where it facilitates the concentrative reabsorption of glucose from the glomerular filtrate (17). Unlike SGLT1, SGLT2 does not

Table 1.1: Classification, tissue distribution and characteristics of GLUT proteins

Isoform	Class	Amino acid residues & (molecular weight)	Substrate	K_m (mM)	Tissue distribution	Ref.
GLUT1	1	492 (54 kDa)	Glucose Galactose Glucosamine DHA Mannose	3–7 17 2.5 1.1 20	Ubiquitous expression	(40-42)
GLUT2	1	524 (55 kDa)	Glucose Fructose Galactose Glucosamine Mannose	17 76 92 0.8 125	Liver, kidney, small intestine, pancreas	(40,43-45)
GLUT3	1	496 (45 kDa)	Glucose Galactose	1.4 8.5	Brain, testis, leukocytes	(44,46,47)
GLUT4	1	509 (55 kDa)	Glucose Glucosamine DHA	5 3.9 0.98	Muscle, fat, heart	(48,49)
GLUT5	2	501 (55 kDa)	Fructose	6	Kidney, intestine, testis	(50-52)
GLUT6	3	507 (46 kDa)	Glucose		Brain, spleen, leukocytes	(53,54)
GLUT7	2	524 (53 kDa)	Fructose Glucose	0.2 0.3	Small intestine, testis, colon, prostate	(54,55)
GLUT8	3	477 (51.5 kDa)	Glucose	2	Brain, testis, liver, lung, fat, spleen,	(56)
GLUT9	2	511 (66 kDa) 540 (46 kDa)	Urate Fructose Glucose	0.9 0.42 0.61	Kidney, liver, pancreas, placenta	(57,58)
GLUT10	3	541 (57 kDa)	Glucose Galactose	0.3	Brain, liver, heart, lung, pancreas, muscle, kidney, placenta	(59,60)
GLUT11	2	496 (54 kDa)	Fructose Glucose	0.16 0.16	Kidney, heart, fat, muscle, placenta, pancreas	(61-64)
GLUT12	3	617 (67 kDa)	Glucose		Heart, fat, muscle, small intestine, placenta, prostate	(65)
HMIT	3	618 (69 kDa)	Myoinositol	0.1	Brain	(66)
GLUT14	1	497 (N/A) 520 (N/A)	N/A		Testis	(67)

transport galactose efficiently (K_m for galactose > 100 mM) (39). Mechanistically, SGLT1 couples the transport of 2 Na^+ ions with the transport of 1 glucose molecule, while SGLT2 couples the transport of 1 Na^+ ion to each transported glucose molecule (17). Only one SGLT crystal structure is available and this structure is of the bacterial homolog vSGLT (68,69)

SWEET proteins

The SWEET protein family is a recently discovered, diverse family of glucose transport proteins, belonging to the transporter-opsin-G protein-coupled receptor (TOG) superfamily (70). Eukaryotic SWEETs have 7 transmembrane domains arranged in a 3+1+3 repeat (70), whereas most bacterial SWEETs (commonly referred to as SemiSWEETs) contain only 3 TMs (15). While an average of 20 SWEET paralogs are found in plants, only 1 SWEET gene has been identified in animals (except for *Caenorhabditis elegans* with 7 SWEET paralogs) (15). In plants, SWEETs are localized to different cellular compartments, including: the plasma membrane (71-74), Golgi (73,74), and tonoplast (75,76) where they mediate the transport of sucrose and hexose (15). Although animal SWEETs have been shown to transport glucose (18), the physiological role of SWEET in mammals is yet to be characterized (15). No mammalian crystal structures of SWEETs have been resolved yet, but different crystal structure conformations of their bacterial homologs have recently been reported (77-79). These structures reveal that a single protomer of SemiSWEET is incapable of forming a functional transporter by itself, so two protomers dimerize in these crystal structures, suggesting that the dimer is the basic functional unit of SemiSWEETs (77-79).

Kinetic and structural characteristics of GLUT1

The kinetics of GLUT1–mediated sugar transport are analogous to those of enzyme catalyzed reactions. Accordingly, enzyme kinetics principles, such as Michaelis–Menten kinetics, are used to define the catalytic properties of GLUT1-mediated sugar transport (6). Being a passive transporter, GLUT1 mediates both unidirectional sugar uptake and exit. Net transport is a vector – the sum and net direction of unidirectional uptake and exit. Thus, if net transport is positive, unidirectional uptake is greater than exit. If net transport is negative, unidirectional uptake is less than exit. At equilibrium, when intracellular [glucose] = extracellular [glucose], net transport is zero because unidirectional uptake and exit are identical.

Affinity for substrate

GLUT proteins have affinities for sugars (measured as apparent K_m for transport ($K_{m(app)}$)), that are commensurate with the extracellular sugar concentration of their respective environments. $K_{m(app)}$ for GLUT1 (3–7 mM) and GLUT4 (5 mM) is comparable to serum glucose concentration of 4–6 mM under normal physiologic conditions (25,80). Neuronal GLUT3 has a K_m of 1.4 mM, consistent with the brain interstitial fluid glucose concentration of 1–2 mM (81). The glucose concentration in human liver is > 10 mM (82), which rationalizes why the K_m for hepatic GLUT2 is ~ 17 mM (25).

Although GLUT1 also transports galactose, glucosamine and L-dehydroascorbic acid (DHA) (40,83-85), the main physiological substrate of GLUT1 is glucose (21). Biochemical studies have demonstrated that GLUT1 sugar binding sites interact with hydroxyl groups on glucose through hydrogen bonding (86-88). Hydrogen bonds with C1 and C3 hydroxyls

of glucose are required for binding to the exofacial sugar site. Hydrogen bonding with C4 hydroxyl group enhances affinity for the exofacial sugar site, while C6 hydroxyl group is not important for substrate interaction at the exofacial sugar binding site (86-88). Conversely, hydrogen bonding with C3 and C6 hydroxyl groups of glucose are needed for interaction with the endofacial sugar site, while C1 hydroxyl is not required (86-88).

Asymmetry of GLUT1-mediated glucose transport

Sugar transport is described as asymmetric when K_m and V_{max}, for sugar influx into sugar-free cells (zero-trans uptake) and sugar efflux into sugar-free medium (zero-trans exit) are different. Transport asymmetry is observed with GLUT1-mediated glucose transport in human red blood cells where K_m and V_{max} for glucose exit are 5 – 10 times greater than K_m and V_{max} for uptake (89,90). Asymmetry is pronounced at low temperatures. At 4ºC, the V_{max} for exit is 10-fold greater than V_{max} for uptake, but as temperature increases V_{max} and K_m for uptake increase, and asymmetry falls (91). Cytoplasmic ATP has been shown to contribute to transport asymmetry observed with GLUT1 (92). Depletion of intracellular ATP results in loss of transport asymmetry with K_m and V_{max} for sugar uptake approaching the values for sugar exit (92). The physiological relevance of GLUT1 asymmetry may be that it allows cells to equilibrate more rapidly with extracellular sugar (93).

Trans-acceleration

Trans-acceleration or accelerated exchange transport describes a phenomenon whereby the presence of sugar at the opposite (trans) side of the membrane increases the rate of unidirectional sugar transport from the other (cis) side of the membrane (6,93). Trans-acceleration has been shown in human erythrocytes where intracellular glucose stimulates

the rate of unidirectional glucose uptake, and extracellular glucose increases the rate of unidirectional glucose exit (94,95). Unlike GLUT1, GLUT4 does not show trans-acceleration (96). By swapping transmembrane (TM) domains between GLUT1 and GLUT4 using homology scanning mutagenesis, Vollers and Carruthers show that TM6 in GLUT1 is important for trans-acceleration (97). Trans-acceleration, just as with asymmetry can accelerate the rate at which a cell equilibrates with extracellular glucose (97).

Structure of GLUT1

GLUT1 comprises 492 amino acid residues (molecular weight = 54 kDa), and forms 12 transmembrane α-helices (TMs) with both the N– and C–termini located within the cytoplasm (13,21,98). Like other class I GLUTs, GLUT1 has a single N-glycosylation site (Asn45) in loop 1, which is heterologously glycosylated causing the protein to appear as a smeared band running from 45 – 65 kDa when resolved by SDS-PAGE and Western blot (99). Deglycosylation does not interfere with GLUT1 targeting to the plasma membrane but reduces glucose uptake and affinity for glucose (100).

The crystal structure of human GLUT1, capturing the inward–open conformation, was first reported in 2014 (28). This structure confirms the following predictions of GLUT structure based on the structures of prokaryotic MFS homologs, XylE, GlpT and LacY (32,101,102): 1) GLUT1 contains 12 TMs; 2) These TMs are divided into 2 symmetrical halves connected by a large intracellular loop (now referred to as intracellular helices, ICH); 3) TMs in GLUT1 are organized in a similar way as XylE; and 4) GLUT1 also share the MFS fold with its bacterial homologs. TM arrangement and GLUT1 structure is shown in figure 1.2. Since 2014, the number of GLUT crystal structures has been steadily growing, with 3

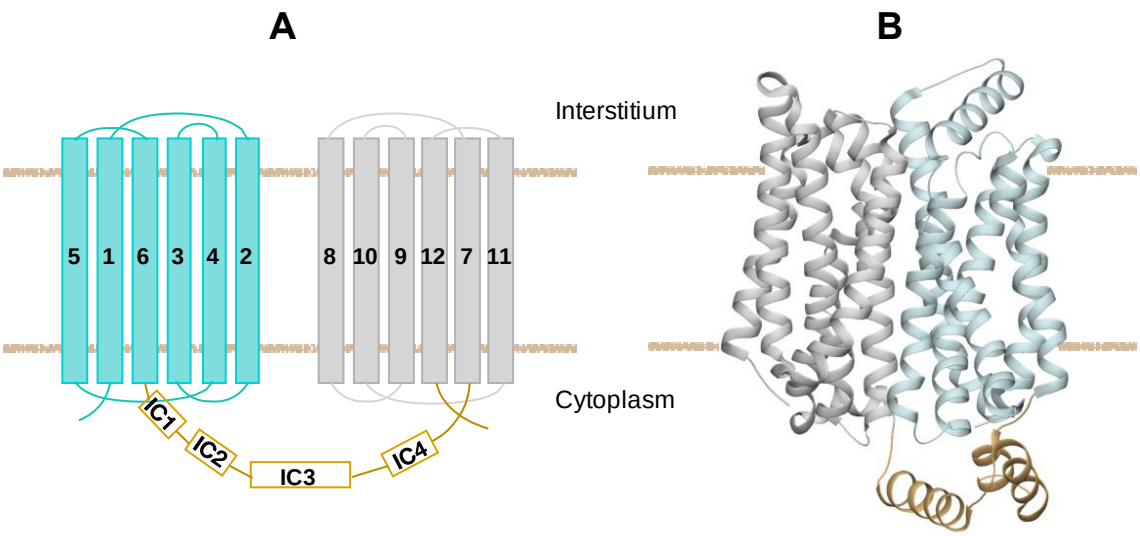

Figure 1.2: Structure of human GLUT1

A, Arrangement of the 12 transmembrane helices (TM) of GLUT1, as refined by the recent crystal structure shown in B. The 12 TMs are divided into 2 symmetrical halves, N–domain (cyan) and C–domain (grey), and connected by the intracellular helices (ICH; gold) domain. **B,** Crystal structure of human GLUT1 (PDB code: 4PYP)

more inward–open human GLUT1 structures, 3 human GLUT3 crystal structures captured in the outward–open and outward–occluded conformations, and bovine and rat GLUT5 captured in the inward–open and outward–open conformations respectively (29-31).

Mechanisms of GLUT1–mediated sugar transport

Two prevailing models have been proposed for how GLUT1 mediates sugar transport: 1) Alternating access transporter (AAT) model, and 2) Fixed-site transporter (FST) model.

The alternating access transporter model argues that the transporter alternately presents either the exofacial or endofacial sugar binding site at any instant (95,103-105). Accordingly, the carrier must undergo cycles of reversible conformational change between the exofacial and endofacial states whether sugar is bound or absent. Thus, sugar bound to the transporter at one side of the membrane is translocated to the other side via this alternating access mechanism. Conformational reorientations of the carrier between the two sides of the membrane in the presence of bound sugar is termed “translocation,” and in the absence of sugar is called “relaxation” ((3,5); figure 1.3A).

The fixed-site transporter model depicts a carrier that simultaneously exposes the exofacial and endofacial sugar binding sites (89,106,107). Hence, the transporter must allow sugars bound at both sugar binding sites to bypass each other as they translocate in opposite directions ((5); figure 1.3B).

Early biochemical evidence to support the AAT model came from equilibrium ligand binding experiments to purified GLUT1 isolated from human erythrocytes in the presence of reducing agents. These studies showed that the stoichiometry of binding between GLUT1 and cytochalasin B (CB; an endofacial GLUT1 ligand) is 1:1, and the carrier

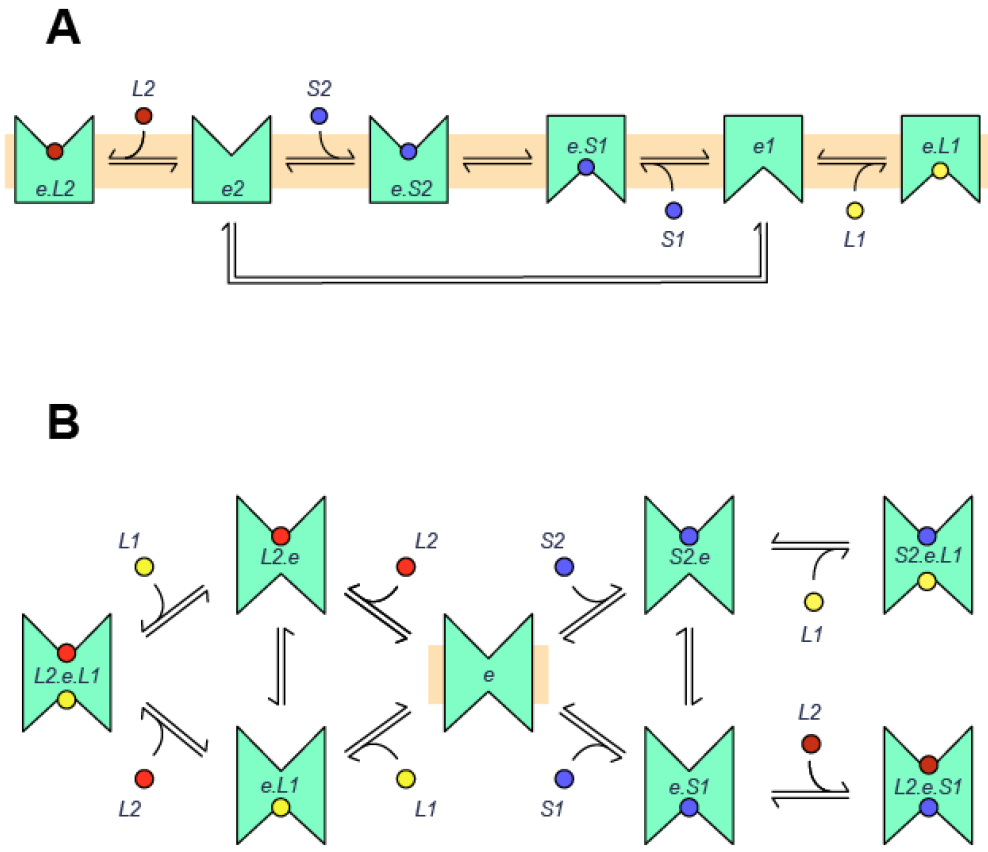

Figure 1.3: The Alternating Access Transporter (AAT) and the Fixed Site Transporter (FST)

A, The AAT. The carrier alternates between conformations exposing an exofacial sugar binding site (e2) and an endofacial sugar binding site (e1). Extracellular inhibitor (L2) and extracellular sugar (S2) compete for binding to e2. Intracellular inhibitor (L1) and intracellular sugar (S1) compete for binding to e1. Conformational changes between e2 and e1 are called "translocation" when sugar is bound and "relaxation" when no sugar is bound. **B**, The FST. The carrier, e, presents exofacial and endofacial sugar binding sites simultaneously. Extracellular sugar (S2) and inhibitor (L2) compete for binding at the exofacial site. Intracellular sugar (S1) and inhibitor (L1) compete for binding at the endofacial site. The carrier can form ternary complexes with intra- and extracellular sugars (S2.e.S1, intra- and extracellular inhibitors (L2.e.L1), or with sugars and inhibitors (L2.e.S1, S2.e.L1).

presents no exofacial ligand binding site in the presence of saturating CB concentrations (108-110). This observation is refuted by CB binding studies to purified human erythrocyte GLUT1 isolated in the absence of reductants, which show that 2 molecules of GLUT1 are needed to bind 1 molecule of CB, consistent with the FST model (111-115). Additionally, equilibrium binding of CB to intact human erythrocytes in the presence of exofacial inhibitors (maltose, phloretin, and ethylidene glucose) reveal a behavior consistent with the FST model (116).

Sugar transport measurements in the presence of both endofacial and exofacial GLUT1 inhibitors provided another biochemical strategy to test the GLUT1 sugar transport models. By performing glucose efflux experiments in human red blood cells, in the presence of CB and phloretin (an exofacial GLUT1 inhibitor), Krupka and Deves (104) demonstrated that the exofacial and endofacial sugar binding sites in GLUT1 are mutually exclusive, and concluded (provided that binding of endofacial and exofacial ligands is not characterized by negative cooperativity) that GLUT1 functions as a simple carrier (104). If the AAT model is correct, then CB and phloretin should compete with each other for binding to GLUT1, such that the presence of another inhibitor acting at the opposite side of the membrane increases the apparent inhibitory constant ($K_{i(app)}$) for glucose transport by the first inhibitor (117,118), but this was not observed by Krupka and Deves (104). On the basis that phloretin behavior deviates from that of a simple exofacial inhibitor (117), Carruthers and Helgerson performed glucose uptake by human RBCs in the presence of maltose (an exofacial GLUT1 inhibitor) and CB and showed these ligands simultaneously bind to GLUT1, but that the binding of these ligands displays negative cooperativity (118). This was exactly the finding required to negate the conclusions of Krupka & Deves (104) and affirms the FST model (118).

The aforementioned biochemical data lend support to the FST model, by revealing that the exofacial and endofacial sugar binding sites coexist in GLUT1 at any instant. However, recent crystal structures of human GLUT1 and GLUT3, the mammalian homologs of GLUT5, as well as the bacterial homologs, XylE, LacY and GlcP all suggest that GLUT1 functions as a simple, alternating access transporter (28-32,101). Put together, these crystal structures demonstrate that GLUT1 cycles between at least 4 different conformations including the outward-open, outward-occluded, inward-occluded and inward-open conformations (30,119). These structural data, together with the biochemical data obtained with purified GLUT1, strongly suggest that each monomer of GLUT1 is a functional unit, capable of binding substrates and functions as an alternating access transporter. However, the biochemical evidence obtained from membrane-bound GLUT1 suggests that GLUT1 functions as a more complex carrier than what the alternating access transporter model proposes.

A unifying model that incorporates evidence for both the AAT and FST models, views GLUT1 as a homotetramer of alternating access carriers which simultaneously presents 2 exofacial and 2 endofacial sugar binding sites (120-122). This conclusion is reinforced by the observations that, cell membrane GLUT1 exists as homodimers and tetramers (113-115,123) and that GLUT1 exhibits trans- and cis-allostery (121,122,124).

Regulation of GLUT1 function

Glucose uptake is rate limiting in cells (e.g. adipocytes, cardiomyocytes, astrocytes and neurons) where rates of glucose metabolism can exceed rates of basal glucose transport. In these cells, the rate of net glucose uptake is rapidly stimulated in response to increased glucose utilization (125-127). For instance, GLUT4–mediated glucose uptake in muscle

and fat is stimulated by up to 50-fold in response to insulin or cellular metabolic depletion (96,125,126,128,129).

GLUT1–mediated glucose transport in mature human erythrocytes and endothelial cells occur at rates 50– to 500–fold greater than glucose utilization rates (130,131). In spite of this, erythrocytes and endothelial cell GLUT1 are subject to physiologic regulation by factors including ATP, hypoglycemia, hypoxia and growth factors (132-135). Control of GLUT1-mediated glucose transport can occur by modulation of GLUT1 intrinsic activity, as observed in human erythrocytes (111,136,137), and/or by modulating cell surface content of GLUT1 as seen in endothelial cells (132,133).

Regulation of GLUT1 activity by ATP

GLUT1 is an ATP–binding protein with no ATPase activity (138,139). ATP depletion enhances the sugar-import capacity of human erythrocyte GLUT1 or GLUT1 heterologously expressed in cultured cells, by increasing the K_m and V_{max} of sugar uptake (111,137,140-143). Conversely, cytoplasmic ATP inhibits GLUT1–mediated glucose transport by decreasing V_{max} and K_m for net sugar uptake, V_{max} for net sugar exit, and K_m for equilibrium exchange transport (144,145). ATP regulates GLUT1–mediated glucose transport by interacting at an intracellular nucleotide binding site located within the cytoplasmic loop 8 in GLUT1 (138,146). ATP modulation of GLUT1 is competitively inhibited by AMP, ADP and H^+ (139,140).

Regulation of GLUT1 activity by cellular metabolic state and AMPK

Mature human erythrocytes lack the machinery to regulate GLUT1 expression and cell surface translocation, but GLUT1 in endothelial cells is subject to control by the metabolic

status of the cell (5). Conditions of cellular energy (ATP) depletion, including hypoglycemia, hypoxia and mitochondrial poisoning, increase the V_{max} of GLUT1-mediated glucose uptake, without altering the cell's affinity for glucose (K_m for transport is unchanged) (132,147,148). This increased glucose uptake results from increasing cell surface content of GLUT1 and is dependent on activation of AMP-activated kinase (AMPK) (149-152). AMPK is a cellular energy-sensing kinase that becomes activated by an increase in intracellular AMP:ATP ratio (153). When activated, AMPK phosphorylates many targets in different metabolic pathways to decrease active ATP consumption and replenish depleted cellular energy (154). AMPK activation controls the cell surface localization of GLUT1 in endothelial cells during acute metabolic stress (151), and has been shown to upregulate increased GLUT1 mRNA transcription and protein expression under chronic metabolic stress conditions (155,156).

Mechanisms of AMPK-regulated GLUT4 trafficking in insulin-sensitive tissues, including fat and skeletal muscle, have been extensively studied. Reports indicate that AMPK inhibits GLUT4 endocytosis in adipocytes (157), whereas in skeletal muscle AMPK inhibits endocytosis (157) and stimulates exocytosis of GLUT4 (158,159). AMPK appear to stimulate GLUT4 exocytosis by directly phosphorylating the Rab–GAP proteins, TBC1D1 and TBC1D4 (160,161). It is not clear if AMPK regulates endothelial cell GLUT1 via mechanisms previously described in fat and skeletal muscle. A recent report showed that AMPK inhibits GLUT1 endocytosis in primary rat hepatocytes and in the liver hepatocellular carcinoma cell line, HepG2 cells, through a TXNIP-dependent mechanism (162).

Small molecule modulation of GLUT1 activity

A wide range of structurally unrelated compounds have been shown to inhibit GLUT1–mediated glucose transport. These include naturally-occurring, and extensively characterized compounds, such as cytochalasin B (CB) (117,163), phloretin (117,164) and maltose (118), as well as recently reported synthetized small molecules such as WZB117 (165), STF-31 (166) and BAY-876 (167). CB, for example, is a cell membrane permeable endofacial GLUT1 inhibitor (apparent inhibitory constant, $K_{i(app)}$ = 140 – 300 nM) (117), and until recently, was the most potent inhibitor of GLUT1 known. CB, phloretin and maltose have been used as tools to extensively study the structure, function and regulation of GLUT1. The observation that GLUT1 expression is highly upregulated in various forms of cancer, has made GLUT1 an attractive target for the development of novel anticancer therapeutics. CB and phloretin cannot be used as anticancer therapeutics because of their numerous off target effects. CB, for instance, interferes with actin filament polymerization, cell division, as well as blood clotting (168,169). In addition to characterizing the new generation of GLUT1 inhibitors, they can be used as tools to further understand the function and regulation of GLUT1.

Physiological and pathological roles of GLUT1

GLUT1 is ubiquitously expressed, usually at low levels, in virtually all mammalian cells, and is thought to facilitate basal glucose transport needed for respiration in mammalian tissues (170).

GLUT1 plays a crucial role in distributing absorbed glucose to peripheral tissues and the central nervous system. GLUT1 is expressed at the highest levels in erythrocytes of

primates and in other species with high brain to body mass ratios (171). It is possible, therefore, that the physiological role of the erythrocyte not only includes O_2 and CO_2 transport but also glucose transport to and from metabolically active tissues like the brain and placenta (93,172). For glucose to enter the brain, it must first transverse the endothelial cells of the blood-brain barrier, through a process mediated by GLUT1 (127).

GLUT1 is also involved in regulating blood glucose in humans. GLUT1 is the major glucose transporter expressed in the α- and ß-cells of human pancreas (173-175). This is in contrast to rodent pancreatic α- and ß-cells, which express GLUT2 (173). These cells are responsible for hormone secretion in response to changes in blood glucose levels – α-cells secrete glucan in response to reduction of blood glucose, while ß-cells release insulin during hyperglycemia, to increase glucose uptake by fat and muscle. As the major GLUT in α- and ß-cells, GLUT1 indirectly regulates glucose levels in the blood (176,177).

Elevated expression of GLUT1 in proliferating cells and activated immune cells may play a physiological role in reprogramming glucose metabolism by enabling these cells to switch to, and sustain aerobic glycolysis which is essential, not only for ATP production but also for the supply of carbon needed for biosynthesis in the growing cells, and NADPH production important for proinflammatory responses by immune cells (178-181).

Elevated GLUT1 expression also plays a pathological role in many cancer types. As with other rapidly proliferating cells, tumor cells metabolize glucose through aerobic glycolysis to generate ATP, NADPH and biomass needed for new cells (181). This over-reliance on glucose makes cancer cells more sensitive to reductions in extracellular glucose concentration than normal differentiated cells (182). Targeting GLUT1 is currently being explored as a novel strategy to develop novel anticancer therapeutics.

Mutations in the gene encoding GLUT1 as reported in GLUT1 deficiency syndrome (GLUT1DS), reduces GLUT1 expression in the patient (10). The most deleterious consequences of GLUT1DS arise from the impaired glucose transport across the blood-brain barrier (BBB) into the brain, resulting in stunted brain development and other manifestations such as seizures and ataxia (9,183). Reduced BBB GLUT1 expression and a corresponding reduction in brain glucose metabolism are also observed at the onset of Alzheimer's disease (80,184). The role of glucose metabolism in Alzheimer's disease is an active area of research, and increasing evidence suggests that early interventions targeted towards stimulating or restoring GLUT1 activity at the BBB may help prevent, or at least, delay the progression of Alzheimer's disease (80).

GLUT1 as a novel therapeutic target

GLUT1 inhibition and stimulation are promising therapeutic strategies in diseases characterized by dysfunctional regulation of GLUT1. GLUT1 expression is highly upregulated in cancers, while decreased GLUT1 levels at the blood-brain barrier (BBB) is found in GLUT1DS and Alzheimer's disease. Accordingly, there is an increased interest in developing GLUT1 inhibitors as novel anticancer therapeutics and in the discovery of compounds that directly stimulate GLUT1 function that will ameliorate GLUT1DS and Alzheimer's disease. Additionally, BBB GLUT1 is considered as a potential route for delivery of drugs into the brain for treating neurological disorders (80).

Characterizing candidate small molecule inhibitors of GLUT1

Several small molecules have been reported to inhibit GLUT1 and as a result, kill cancer cells and/or inhibit tumor growth in mice (165,166). Figure 1.4 shows the chemical

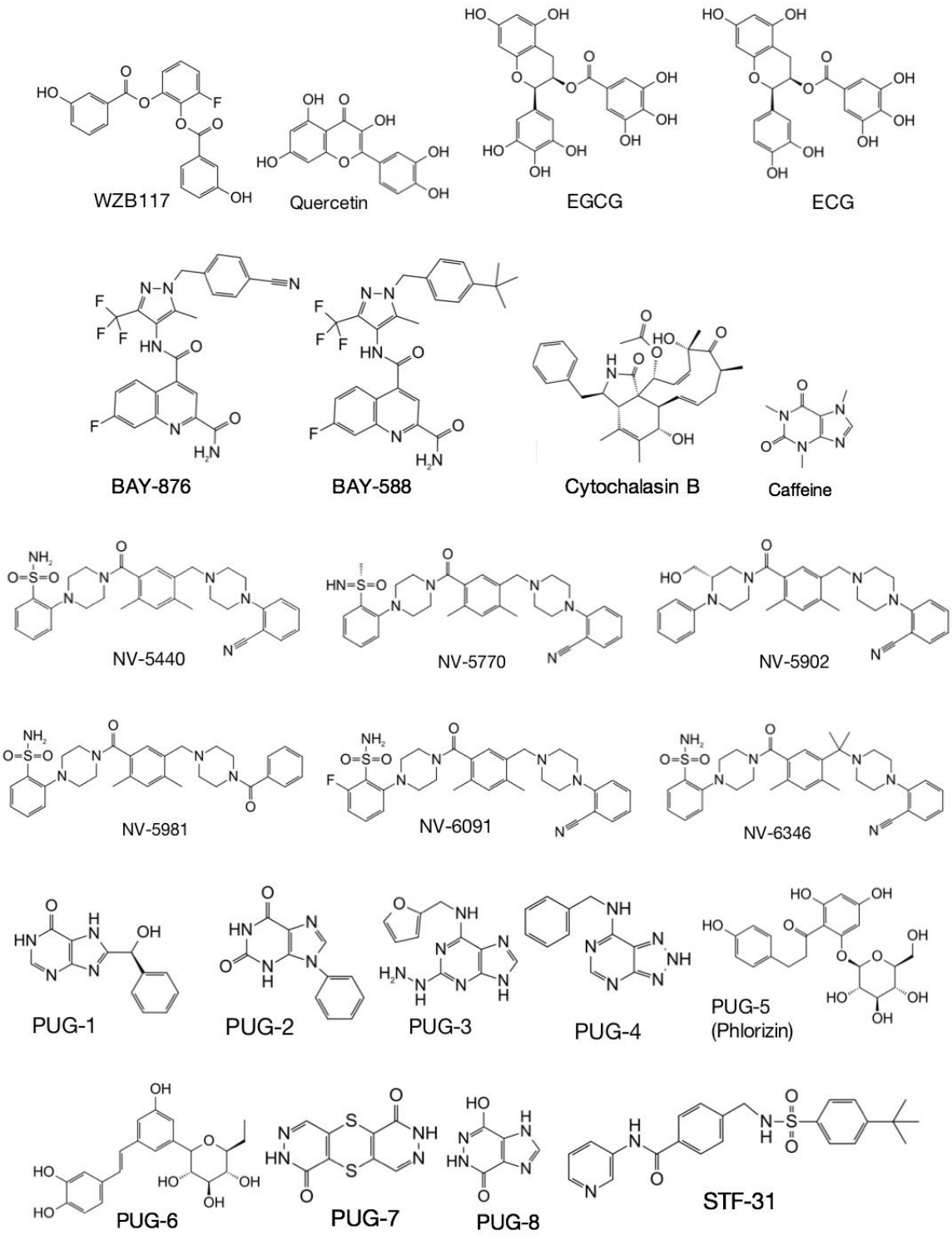

Figure 1.4: Chemical structures of candidate small molecule inhibitors of GLUT1

structures of a wide range of structurally unrelated candidate small molecule inhibitors of GLUT1. These include naturally occurring flavonoids (quercetin, EGCG and ECG) abundant in the human diet, as well as synthesized molecules discovered from high throughput screening (e.g., WZB117 (165) , BAY-876 (167) and NV-5440 developed by Navitor Pharmaceuticals, MA) and by computational methods (PUG1–8) (185).

In this study, we used a combination of sugar transport assays and molecular biology techniques in human erythrocytes and cultured mammalian cells, as well as *in silico* ligand docking, to define the mechanism of GLUT1 inhibition by these small molecules. Our approach included the following:

- Validation of small molecules as GLUT1 inhibitors by testing their effects on sugar uptake by human erythrocytes.
- Determination of sidedness of action of inhibitors on GLUT1. Taking advantage of the fact that GLUT1 exhibits Michaelis-Menten kinetics (104,118,186), we tested the effects of inhibitors on the V_{max} and K_m of sugar transport in human erythrocytes. Based on Michaelis–Menten kinetics of sugar transport, as well as radioactive ligand binding assays, we defined each compound as either an exofacial (acting on the outside) or endofacial (acting on the inside) inhibitor of GLUT1. Figure 1.4 illustrates the different modes of glucose transport assays used and the graphical representation and interpretation of data obtained.
- Tested isoform specificity of inhibition by assessing the effects of these compounds on sugar uptake in cultured mammalian cells stably expressing GLUT1, GLUT3 or GLUT4.

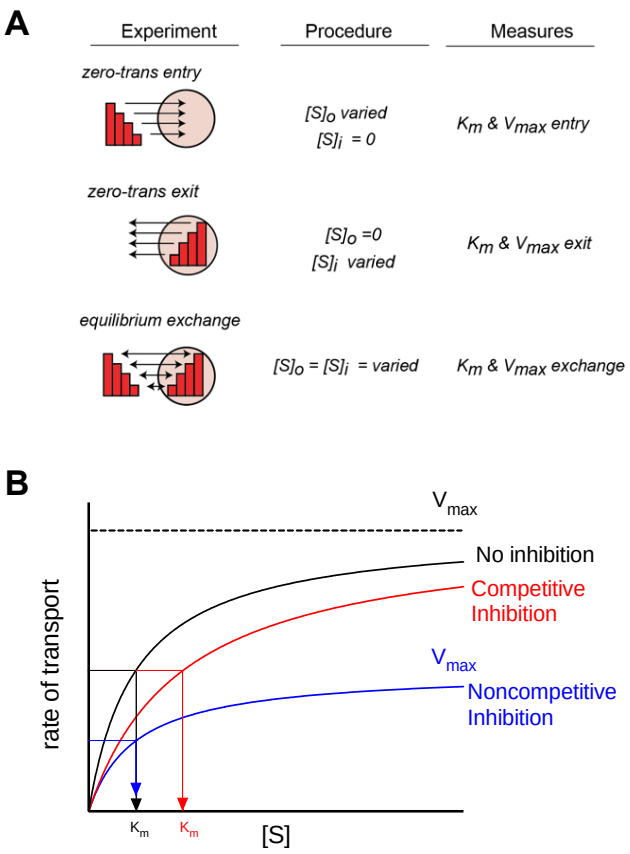

Figure 1.5: Determination of sidedness of action of GLUT1 inhibitors

A. Procedure for determining the sidedness of action of GLUT1 inhibitors in human erythrocytes. Experiments are designed to measure radioactive sugar: 1) uptake into sugar–depleted cells (zero-trans entry), 2) exit into sugar-free medium (zero-trans exit), and 3) exchange in cells loaded with equal concentrations of non-radioactive sugar as their medium (equilibrium exchange). Data from these experiments are analyzed by Michaelis–Menten kinetics and provide the K_m and V_{max} of sugar transport. **B.** Analysis of transport data by Michaelis–Menten kinetics. A plot of the rate of transport versus substrate concentration yields the Michaelis–Menten parameters, K_m and V_{max}. If an inhibitor competes with glucose for binding at the sugar binding site on the side of the membrane where sugar transport is initiated, we will observe an increase in K_m with no change in V_{max} (red curve). If inhibitor does not compete with glucose for binding at the side of the membrane where transport is initiated, it will reduce V_{max} without changing K_m (blue curve). Any deviation from competitive or noncompetitive inhibition will suggest that inhibitor interaction with GLUT1 is more complex, and that inhibitor binds GLUT1 at a site different from the sugar binding site.

- Guided by our biochemical data, we used homology modeling and ligand docking analyses to computationally predict the molecular interactions between these compounds and GLUT1.

In addition to uncovering the mechanisms of GLUT1 inhibition by these small molecules, the GLUT1 inhibitors served as molecular probes that revealed valuable insights for the mechanism of GLUT1 function.

Significance of study

This study provides a framework for screening candidate GLUT1 inhibitors for specificity, and optimizing drug design and delivery. The human erythrocyte robustly expresses GLUT1 as its only glucose transport protein. Therefore, the ability of a compound to inhibit human erythrocytes glucose transport should be a “gold standard” for confirming a potential GLUT1 inhibitor. Furthermore, understanding the sidedness of action of an inhibitor on GLUT1 will help in drug delivery. For instance, exofacial GLUT1 inhibitors do not need to cross cell membranes, which potentially simplifies the drug delivery process, and alleviates concerns about off target interaction of drugs with cellular targets. Also, testing a wide range of structurally diverse compounds, reveals functional groups essential for greater inhibitory potency, and these can be used to optimize drug design.

Finally, this study provides further experimental evidence concerning the function and regulation of GLUT1, supporting the idea that GLUT1 functions as a cooperative oligomer of allosteric alternating access subunits.

CHAPTER II

Preface

Chapter II of this dissertation was published in the Journal of Biological Chemistry, as:

Ojelabi, O. A., Lloyd, K. P., Simon, A. H., De Zutter, J. K., and Carruthers, A. (2016) WZB117 (2-Fluoro-6-(m-hydroxybenzoyloxy) Phenyl m-Hydroxybenzoate) inhibits GLUT1-mediated sugar transport by binding reversibly at the exofacial sugar binding site. Journal of Biological Chemistry 291, 26762-26772

Author contributions: OAO and AC designed experiments, analyzed results and co-wrote the manuscript. OAO conducted most of the experiments. KPL undertook the molecular docking studies. AHS assisted with quantitative analysis of data. JKD conducted experiments on the isoform specificity of transport inhibition

WZB117 inhibits GLUT1-mediated sugar transport by binding reversibly at the exofacial sugar binding site

Introduction

Most cancer cells use anaerobic metabolism (glycolysis) to generate the ATP required for cellular processes and proliferation (181). This contrasts with normal, differentiated cells, which mostly use mitochondrial oxidative phosphorylation to sustain cellular function (187). The transition from aerobic to anaerobic metabolism is termed “the Warburg effect” and is driven by growth conditions, by mutations of proto-oncogenes and tumor-suppressor genes (187,188). Vander Heiden et al. (181) have proposed that the metabolism of all proliferating cells (including cancer cells) is adapted to enhance nutrient uptake and nutrient incorporation into the biomass needed to produce a new cell. This would explain why the developing central nervous system is so susceptible to glucose deprivation resulting from glucose transport-deficiency at the blood-brain barrier (189) and why cancer cells are so sensitive to limited glucose availability (190).

This has prompted several groups to propose that suppressing anaerobic metabolism may offer an effective anticancer strategy. Three approaches have been used to limit glycolysis in cancer cells; that is glucose deprivation *in vitro* (191,192), the *in vitro* and *in vivo* use of glycolysis inhibitors (193), and cellular glucose transport inhibition *in vitro* and *in vivo* (165,193). All three approaches cause cancer cell death.

Glucose transport in most mammalian cells is catalyzed by one or more members of the GLUT (SLC2A) family of passive glucose transporters (194). GLUT1 (the blood brain barrier/erythroid glucose transporter) and, in some instances, GLUT3 (the neuronal

glucose transporter) or GLUT12 expression is significantly increased in proliferating cells (195).

Successful strategies for passive glucose transport inhibition have exploited a range of molecules that bind at or close to either the exofacial (e.g. maltose, ethylidene glucose) or the endofacial sugar binding site (e.g. cytochalasin B; (86,117,196)). A number of unrelated inhibitory molecules react with the GLUT1 purine binding site (e.g. ATP, AMP, caffeine; (197)) or at other, less well defined sites (e.g. androgens, quercetin; (198) and (199)). These and related molecules have been suggested as potential scaffolds for designing inhibitors of glucose uptake in cancer cells or cancer stem cells (193,200-202).

Using such an approach, Zhang *et. al.* (203) identified a class of polyphenolic compounds with sugar transport inhibitory potency. Among these, WBZ117 (2-fluoro-6-(m-hydroxybenzoyloxy)phenyl m-hydroxybenzoate) showed the highest affinity for sugar transport inhibition and inhibited tumor growth in a nude mouse model (165).

Although a promising strategy for cancer cell elimination, glucose transport inhibition *in vivo* may present several attendant complications. These include impaired insulin secretion, elevated blood glucose, diuresis, elevated glycation, impaired glucose transport across the blood-brain barrier, and reduced metabolic capacity in healthy cells that depend upon glycolysis for normal function. We, therefore, undertook a systematic analysis of WZB117 inhibition of glucose transport.

We found that WZB117 interacts with GLUT1 at the exofacial sugar binding site and thus acts as a reversible, competitive inhibitor of net glucose uptake and exchange glucose transport but as a noncompetitive inhibitor of sugar efflux from cells. WZB117 inhibits the

insulin-sensitive glucose transport (GLUT4) with greater potency than its inhibition of either GLUT1 or GLUT3.

Materials & Methods

Reagents

[^{3}H]-Cytochalasin B ([^{3}H]-CB) and 3-O-[^{3}H]-methylglucose ([^{3}H]-3MG) were purchased from American Radiolabeled Chemicals (St. Louis, MO). Unlabeled 3MG, CB, and phloretin were purchased from Sigma. WZB117 was purchased from EMD Millipore (Billerica, MA).

Solutions

KCl medium was composed of 150 mM KCl, 5 mM HEPES, 4 mM EGTA, 5 mM $MgCl_2$, pH 7.4. Solubilization buffer was composed of KCl medium with 0.5% Triton X-100. Phosphate-buffered saline was composed of 140 mM NaCl, 10 mM Na_2HPO_4, 3.4 mM KCl, 1.84 mM KH_2PO_4, pH 7.3. Stop solution was composed of ice-cold KCl medium plus CB (CB; 10 µM) and phloretin (100 µM). Sample buffer contained 0.125 M Tris-HCl, pH 6.8, 4% SDS, 20% glycerol, and 50 mM DTT. Transfer buffer was composed of 12 mM Tris base, 96 mM glycine, 20% methanol.

Cells

De-identified whole human blood was purchased from Biological Specialty Corporation (Colmar, PA). HEK293 cells were maintained in Dulbecco's modified Eagle's medium (DMEM) supplemented with 10% fetal bovine serum, 100 units/ml penicillin, and 100 µg/ml streptomycin in a 37 °C humidified 5% CO_2 incubator.

Heterologous Expression of GLUTs

GLUT1, GLUT3, and GLUT4 heterologous expression in HEK293 cells was as described previously (97,123). Both GLUT1 and GLUT3 contain a myc-epitope in exofacial loop 1 (97). GLUT1, GLUT3, GLUT4, and NaKATPase expression in whole cell lysates was analyzed by Western blotting as previously described (97,123).

Erythrocyte Sugar Transport Measurements

All human red cell sugar transport experiments were performed at 4 °C as previously described (197,204,205).

Zero-trans Uptake—Five volumes (100 µl) of 3MG uptake medium ± WZB117 or CB were added to 1 volume (20 µl) of sugar-depleted, 50% hematocrit (Ht) red cells, and sugar uptake allowed to proceed for 0.5–1 min at 4 °C. Uptake was stopped by adding 50 volumes (1 ml) of ice-cold stop solution containing 100 µM phloretin and 10 µM CB. Cells were washed in stop solution and lysed in 3% perchloric acid, and centrifugation-clarified lysates were assayed for radioactivity in duplicates using liquid scintillation counting.

Zero-trans Exit—Sugar-depleted packed RBCs were loaded with 10 mM 3MG by incubating with 20 mM 3MG (containing 10 µCi [^{3}H]-3MG/10 ml of cold 3MG for 1 hr at 37 °C). One volume (0.5 ml) of sugar-loaded RBCs was added to 50 volumes of KCl ± medium CB or WBZ117 on a shaker with magnetic stirrer. Aliquots (0.5 ml) of the suspension were withdrawn at the indicated time intervals, washed in ice-cold stop solution, lysed, and assayed for remaining radioactivity.

Equilibrium Exchange Transport—Sugar-depleted RBCs were preloaded with 2.5–50 mM 3MG at 25 °C for 30 min. These cells were collected by centrifugation, incubated in 10 volumes of 3MG ± WZB117 or CB for 10 min at 4 °C, centrifuged again, and resuspended to 50% Ht in the appropriate 3MG and inhibitor medium. 3MG uptake medium (100 µl) ± WZB117 or CB was added to 20 µl of sugar-loaded cells (50% Ht), and the experiment was allowed to proceed for 0.5–1 min at 4 °C. Uptake was arrested by adding 50 volumes (1 ml) of ice-cold stop solution. Cells were centrifuged, and the pellet was washed in 1 ml of stop solution, collected by centrifugation, lysed in 3% perchloric acid, clarified, and assayed for radioactivity in duplicates using liquid scintillation counting.

HEK293 Cell Sugar Transport Measurements

All HEK293 cell sugar transport experiments were performed at 37 °C using 0.1 mM 2-deoxy-D-glucose as previously described (97,123).

CB Binding

Equilibrium CB binding to red cells was performed as previously described (116). Briefly, 1 volume of sugar-depleted red cells (50% Ht) was suspended in one volume of ice-cold wash buffer 150 mM KCl, 5 mM HEPES, pH 7.4, containing 0.5 µM [^{3}H]-CB, 10 µM cytochalasin D, and varying concentrations of WZB117 (1–60 µM) for 15 min at 4 °C with constant end-over-end rotation. For total CB, 2 x 10 µl of the cell suspension were lysed in 100 µl of 3% perchloric acid and clarified by centrifugation, and the associated radioactivity was assayed by liquid scintillation counting. For free CB, the cell suspension was centrifuged at 10,000 x g for 30 s, and 10 µl of clarified supernatant were assayed in duplicate by scintillation counting. Bound CB was obtained as: total CB – free CB.

Quantitative RT-PCR

Expression levels of hGLUT3 mRNA were measured by qPCR using the QuaniTect SYBR Green PCR kit (Qiagen). Reactions were performed according to the manufacturer's protocol. Total RNA was isolated from HEK293 cells stably overexpressing hGLUT1 or hGLUT4 using the RNeasy kit and Qiashredder (Qiagen). cDNA was synthesized using the QuantiTect Reverse Transcriptase kit (Qiagen). qPCR reactions contained 100 ng of the indicated cDNA and 0.3 µM each human GLUT3-specific qPCR primers (G3, 5'-qF-AGCTCTCTGGGATCAATGCTGTGT and G3 3' qR-ATGGTGGCATAGATGGGCTCTTGA, where qF denotes qPCR forward and qR denotes qPCR reverse). Samples were run in triplicate on a Research PTC-200 Peltier Thermal Cycler with a Chromo4 real time PCR detector running Opticon Monitor 3 software (Bio-Rad). Results were analyzed by using the ΔΔCt method and normalized to an internal GAPDH marker.

Data Analysis

Linear and nonlinear regression analysis of data sets and statistical tests were accomplished using GraphPad Prism (Version 7.0a; La Jolla, CA).

Michaelis-Menten inhibition of sugar transport is assumed to be described by:

$$v = v_o - \frac{v_o[I]}{K_{i(app)} + [I]} \qquad \text{(equation 2.1)}$$

Where v_o is v measured in the absence of inhibitor I, [I] is the concentration of inhibitor and $K_{i(app)}$ is that [I] producing 50% inhibition of uptake.

Michelis-Menten transport is assumed to be described by:

$$V = \frac{V_{max}[3MG]}{K_{m(app)} + [3MG]} \quad \text{(equation 2.2)}$$

Where V_{max} is the maximum rate of 3MG transport, [3MG] is the concentration of 3MG, and $K_{m(app)}$ is that [3MG] where the rate of uptake is $V_{max}/2$.

Hanes-Woolf analysis of transport assumes Michelis-Menten kinetics, and when data are plotted as [3MG]/v versus [3MG], the results fall on a straight line described by:

$$\frac{[3MG]}{V} = \frac{[3MG]}{V_{max}} + \frac{K_{m(app)}}{V_{max}} \quad \text{(equation 2.3)}$$

Where V_{max} is the maximum rate of 3MG transport, [3MG] is the concentration of 3MG, and $K_{m(app)}$ is [3MG], where the rate of uptake is $V_{max}/2$.

Transport stimulation followed by inhibition by inhibitors was approximated first by normalizing all uptake to v_o and then using the following model.

$$\frac{v}{v_o} = 1 + \frac{[I]\Delta_1}{K_1 + [I]} - [I]\frac{1 + \Delta_1}{K_2 + [I]} \quad \text{(equation 2.4)}$$

Homology Modeling

The homology models of the e2 (open) state of GLUT1 and GLUT4 were generated using the maltose-bound human GLUT3 (PDB code 4ZWC) structure (30). GLUT1 and GLUT3 have 65% sequence identity and 88% sequence similarity (194). Ligands were removed, and chain A was used as the template for each modeled structure. Sequence alignments were generated using ClustalX. Homology models were built using Modeler-9.9 and analyzed using PROCHECK. The GLUT1-e1 structure (PDB code 4PYP; Ref. (28)) was used directly.

Stochastic Docking

The GLUT1 crystal structure was obtained from the protein data bank using PDB code 4PYP. The structures for D-glucose and CB were obtained from ZINC. The WZB117 structure was generated using the three-dimensional structure generator Corina from Molecular Networks GmbH. Docking was performed using the Schrodinger software suite. The protein structure was preprocessed with the Protein Preparation Wizard, bond orders were assigned, hydrogens were added, and the H-bond network was optimized. The system was energy-minimized using the OPLS 2005 force field. Ligand structures were prepared with the LigPrep module, and the pKa of the ligands was calculated using the Epik module. Computational docking was performed by the GLIDE module in standard precision (SP) mode and default values for grid generation. Cavities for docking were calculated using the CastP server, and the grid was centered on the residues forming the cavity. No restraints were used during the docking.

Results

Sugar transport in human erythrocytes is catalyzed by GLUT1 (98). Transport theory states that ligands binding reversibly at the exofacial sugar binding site act as competitive inhibitors of sugar uptake and as noncompetitive inhibitors of exit. Conversely, ligands binding reversibly at the endofacial sugar binding site act as noncompetitive inhibitors of sugar uptake and as competitive inhibitors of exit (104,118,186). To understand whether WZB117 inhibits GLUT1 by binding at the exofacial or endofacial sugar binding site, we examined its effects on three modes of erythrocyte sugar transport: zero-trans 3MG uptake (uptake into cells lacking sugar), zero-trans 3MG exit (efflux from cells into medium

lacking sugar), and equilibrium exchange 3MG uptake (unidirectional uptake of 3MG in cells where $[3MG]_i = [3MG]_o$).

Concentration dependence of WZB117 and CB inhibition of sugar uptake by human erythrocytes

WZB117 inhibits zero-trans 3MG (0.1 mM) uptake by erythrocytes in a dose-dependent manner with $K_{i(app)}$ = 0.23 ± 0.04 μM (figure 2.1A). CB (a known GLUT1 endofacial site ligand) inhibits 0.1 mM 3MG zero-trans uptake with $K_{i(app)}$ = 0.21 ± 0.02 μM (figure 2.1B).

Inhibition of human RBC sugar transport by WZB117 is reversible

We assessed the reversibility of inhibition in two ways. The first method involved exposing RBCs to buffer containing or lacking WZB117 (3 μM) or CB (0.5 μM) for 10 min, then removing the inhibitors using a centrifugation/wash cycle and incubating the cells in inhibitor-free buffer for a further 15 min. We then measured 0.1 mM 3MG uptake in these cells. WZB117 (3 μM) or CB (0.5 μM) inhibit sugar uptake by 50% (figure 2.2). Removing the inhibitor before sugar uptake determinations restored sugar uptake to levels of 75% or greater of uninhibited controls (figure 2.2).

WZB117 is a competitive inhibitor of 3MG uptake by human erythrocytes

The second method of assessing reversibility of inhibition evaluates the type of sugar transport inhibition produced by WZB117. Competitive inhibitors act by binding reversibly either to the active site of an enzyme or to a site whose occupancy occludes occupancy of the active site and vice versa (206). Preincubation with WZB117 (7 μM) before initiation of transport measurements increased $K_{m(app)}$ for zero-trans 3MG uptake from 1.0 ± 0.2 mM

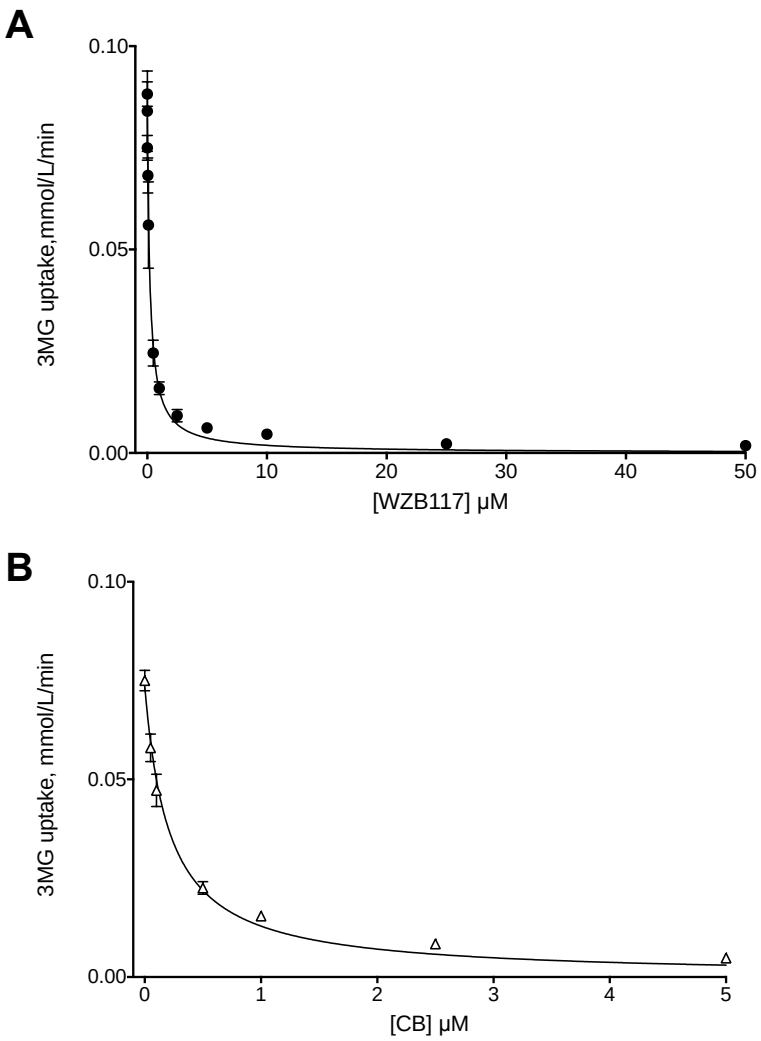

Figure 2.1: Sensitivity of zero-trans 3MG (0.1 mM) uptake by erythrocytes to inhibition by WZB117 (A) and CB (B)

Ordinate: 3MG uptake in mmol/liter of cell water/min. Abscissa: WZB117 or CB in µM. Each data point represents the mean ± S.E.M of at least three separate measurements made in duplicate. The curves drawn through the points were computed by nonlinear regression assuming uptake is inhibited completely by inhibitor in a dose-dependent manner (equation 2.1). The results are: **A,** WZB117-treated cells: $K_{i(app)}$ = 0.23 ± 0.04 µM, R^2 = 0.894, standard error of regression = 0.011; **B,** CB-treated cells: $K_{i(app)}$ = 0.21 ± 0.02 µM, R^2 = 0.933, standard error of regression = 0.007.

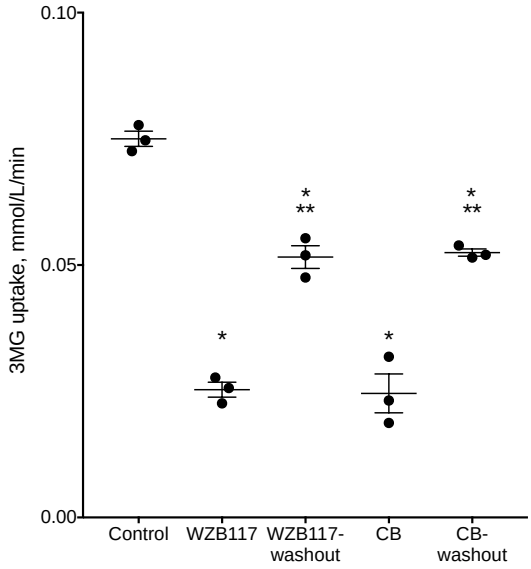

Figure 2.2: Reversibility of transport inhibition by WZB117 and by CB

Ordinate: 3MG uptake in mmol/liter of cell water/min. Abscissa: experimental treatment. Control cells saw no inhibitor during sugar uptake; WZB117 and CB cells were exposed to inhibitor (3 µM WZB117 and 0.5 µM CB respectively) for 15 min on ice before measurement of 3MG uptake in the presence of inhibitor. WZB117-washout and CB-washout cells were exposed to inhibitor (3 µM WZB117 and 0.5 µM CB, respectively) for 15 min on ice followed by inhibitor removal and exposure to inhibitor-free medium for 15 min on ice and finally measurement of 3MG uptake in the absence of inhibitor. Each symbol (●) represents the mean of duplicate measurements. The horizontal line and error bars represent the mean ± SEM of each condition. Unpaired t test analysis indicates: *, transport under all treatments is significantly lower ($p < 0.005$) than in control cells; **, transport after washout treatment is significantly greater ($p < 0.005$) than in the corresponding non-washout treatment.

to 2.8 ± 0.4 mM, but V_{max} for 3MG uptake (0.59 ± 0.03 mmol/liter of cell water/min) was unaffected (figure 2.3). This result indicated that WZB117 is a competitive inhibitor of human erythrocyte sugar uptake. If WZB117 bound irreversibly to the active site, preincubation with the inhibitor would most likely have reduced V_{max} for transport in addition to increasing $K_{m(app)}$. Conversely, CB (0.7 µM) reduces V_{max} for 3MG uptake (0.29 ± 0.05 mmol/liter of cell water/min) but has no effect on $K_{m(app)}$ (figure 2.3). This result confirms that CB is a noncompetitive inhibitor of uptake and is expected for an inhibitor which binds reversibly to the endofacial active site (118).

WZB117 is a noncompetitive inhibitor of net sugar exit

Because WZB117 competes for 3MG binding at or close to the exofacial sugar entry site, we hypothesized that WZB117 would act as a noncompetitive inhibitor of sugar exit (118). To this end, we performed sugar exit experiments where we measured the time course of zero-trans sugar exit from pre-loaded red cells into sugar-free external medium. The time course of exit was analyzed by simulating sugar exit by numerical integration using Berkeley Madonna software assuming Michaelis-Menten exit kinetics then adjusting simulated Michaelis-Menten parameters using the Levenberg-Marquardt algorithm until the fits between simulated and experimental exit data were optimal. Our analysis shows that WZB117 (0.7 µM) reduces V_{max} for 3MG exit from 2 mmol/liter of cell water/min to 0.8 mmol/liter of cell water/min, whereas $K_{m(app)}$ for exit (15 mM) was unaffected (figure 2.4A). Consistent with published data (117), CB (0.7 µM) was competitive for sugar exit, increasing $K_{m(app)}$ to 47 mM with no effect on V_{max} (figure 2.4B).

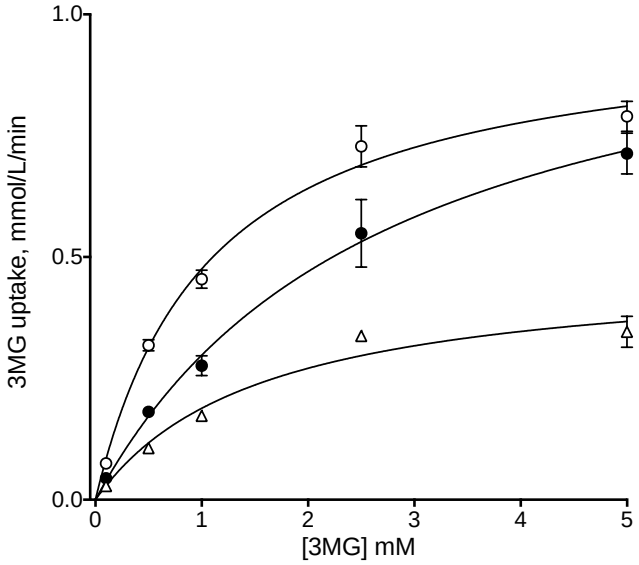

Figure 2.3: Effects of WZB117 and CB on Michaelis-Menten kinetics of zero-trans 3MG uptake

Results are shown for control cells (○), WZB117-treated cells (●), and for CB-treated cells (△). Each data point is the mean ± S.E. of three duplicate measurements. A, ordinate: 3MG uptake in mmol/liter of cell water/min. Abscissa: $[3MG]_o$ in mM. Curves drawn through the points were computed by nonlinear regression assuming Michaelis-Menten uptake kinetics (equation 2.2) and have the following results: control cells (○), V_{max} = 0.59 ± 0.03 mmol/liter of cell water/min, $K_{m(app)}$ = 1.05 ± 0.16 mM, R2 = 0.992, standard error of regression = 0.018; WZB117 treatment (●): V_{max} = 0.68 ± 0.04 mmol/liter of cell water/min, $K_{m(app)}$ = 2.77 ± 0.35 mM, R^2 = 0.997, standard error of regression = 0.018 mmol/liter of cell water/min; CB treatment (△): V_{max} = 0.29 ± 0.05 mmol/liter of cell water/min, $K_{m(app)}$ = 1.67 ± 0.63 mM, R^2 = 0.966, standard error of regression = 0.010.

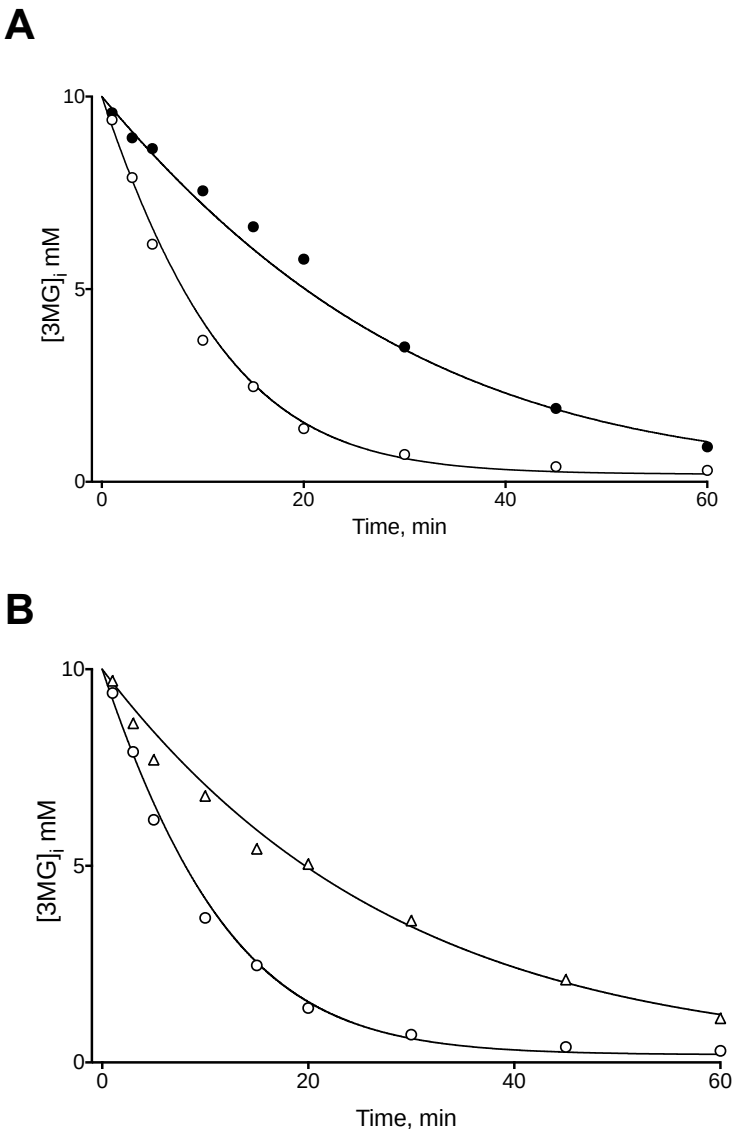

Figure 2.4: Effects of WZB117 (A) and CB (B) on Michaelis-Menten kinetics of zero-trans 3MG

Ordinates: $[3MG]_i$ in mmol/liter of cell water. Abscissa: time in minutes. Curves drawn through the points were computed by nonlinear regression and numerical integration assuming Michaelis-Menten exit kinetics and have the following results: Control cells (○): V_{max} = 2 mmol/liter of cell water/min, $K_{m(app)}$ = 15 mM; WZB117 treatment (●): V_{max} = 0.8 mmol/liter of cell water/min, $K_{m(app)}$ = 15 mM; CB treatment (△): V_{max} = 2 mmol/liter of cell water/min, $K_{m(app)}$ = 47 mM.

WZB117 is a competitive inhibitor of equilibrium exchange sugar transport

Equilibrium exchange 3MG transport in human red blood cells ($[3MG]_i = [3MG]_o$) was competitively inhibited by WZB117. WZB117 (7 μM) increased $K_{m(app)}$ for 3MG exchange transport from 40.25 ± 3.57 mM to 82.25 ± 15.30 mM but had no effect on V_{max} (13.39 ± 0.79 mmol/liter of cell water/min; figure 2.5). CB (0.7 μM), however, was a mixed-type inhibitor of equilibrium exchange 3MG transport reducing V_{max} (8.87 ± 0.33 mmol/liter of cell water/min) and increasing $K_{m(app)}$ (49.85 ± 2.56 mM; figure 2.5).

Subsaturating levels of CB and WZB117 stimulate sugar uptake in human erythrocytes

Previous studies have shown that subsaturating concentrations of CB or exofacial inhibitors of GLUT1 produce a modest stimulation of erythrocyte sugar uptake (122,124). Subsaturating levels of WZB117 (≤ 10 nM) and CB (≤ 50 nM) significantly ($p < 0.05$) stimulate zero-trans 3MG uptake in human erythrocytes by up to 40% above untreated cells (figure 2.6).

Effect of WZB117 on CB Binding

CB is membrane-permeant and rapidly crosses the cell membrane to interact with the GLUT1 endofacial sugar binding site (118,186). The simple carrier hypothesis for facilitated diffusion predicts that CB and WZB117 binding to GLUT1 are mutually exclusive (104,118,186). Accordingly, CB should competitively inhibit WZB117 inhibition of and binding to GLUT1. The $K_{i(app)}$ for CB inhibition of 3MG uptake is increased by more than 4-fold when WZB117 (200 nM) is present (figure 2.7A), suggesting that WZB117 interferes with CB inhibition of sugar uptake. Similarly, WZB117, as well as nonradioactive CB, inhibits the binding of [^{3}H]-CB to human RBCs in a dose-dependent manner (figure 2.7B).

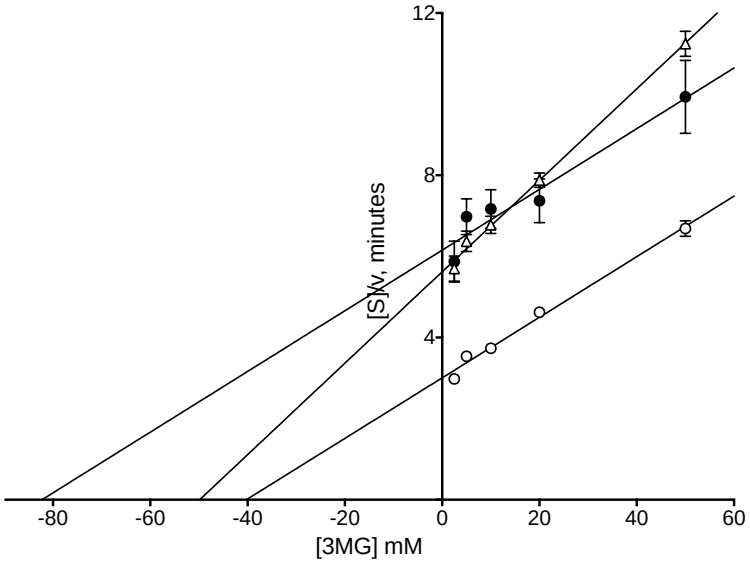

Figure 2.5: Effects of WZB117 and CB on Michaelis-Menten kinetics of equilibrium exchange 3MG uptake

Hanes-Woolf plot of equilibrium exchange transport. Ordinate: [3MG]/rate of equilibrium exchange 3MG uptake in minutes. Abscissa: intracellular and extracellular [3MG] in mM. Lines drawn through the points were computed by nonlinear regression assuming that each line is described by equation 2.3. The results are: control cells (○): V_{max} = 13.39 ± 0.79 mmol/liter of cell water/min, $K_{m(app)}$ = 40.25 ± 3.57 mM, R^2 = 0.990, standard error of regression = 0.17 min; WZB117 treatment (●): V_{max} = 13.36 ± 2.02 mmol/liter of cell water/min, $K_{m(app)}$ = 82.25 ± 15.30 mM, R^2 = 0.936, standard error of regression = 0.43 min; CB treatment (△): V_{max} = 8.87 ± 0.33 mmol/liter of cell water/min, $K_{m(app)}$ = 49.85 ± 2.55 mM, R^2 = 0.996, standard error of regression = 0.16 min

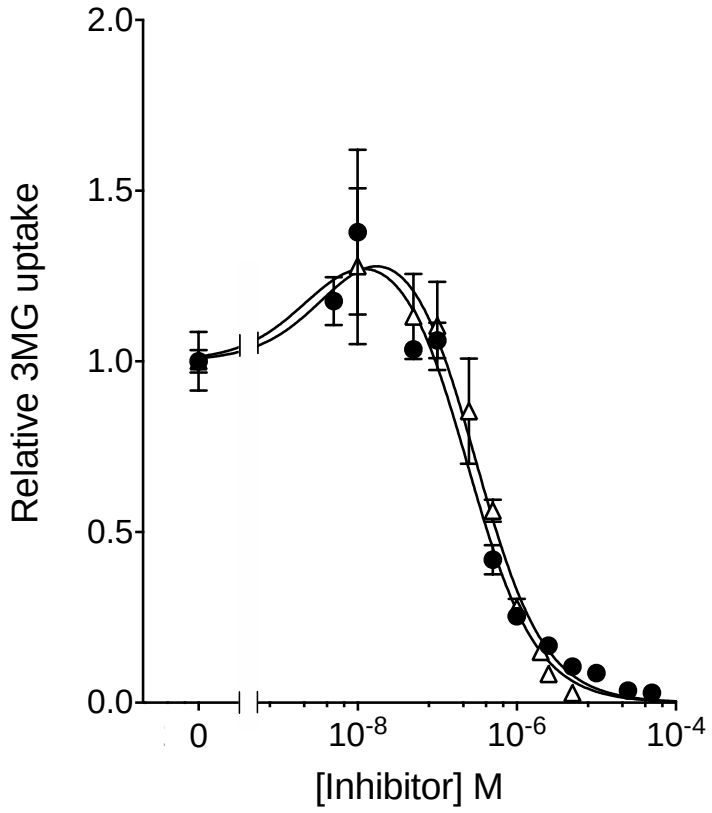

Figure 2.6: CB and WZB117 stimulate 3MG uptake at subsaturating inhibitor concentrations

Ordinate: Relative 3MG uptake. Abscissa: Inhibitor concentration in M (axis expressed in log scale). Results are shown for WZB117-treated cells (●) and for CB-treated cells (△). Each data point is the mean S.E. of three or more duplicate measurements. The curves drawn through the points were computed by nonlinear regression according to equation 2.4 and have the following constants: WZB117-treated cells (●) $\Delta_1 = 0.42 \pm 0.15$, $K_1 = 2.8 \times 10^{-9} \pm 3.6 \times 10^{-9}$, $K_2 = 2.4 \times 10^{-7} \pm 6.3 \times 10^{-7}$, $R^2 = 0.985$, standard error of regression = 0.07; CB-treated cells (△) $\Delta_1 = 0.46 \pm 0.14$, $K_1 = 4.7 \times 10^{-9} \pm 5.4 \times 10^{-9}$, $K_2 = 3.0 \times 10^{-7} \pm 6.0 \times 10^{-8}$, $R^2 = 0.988$, standard error of regression = 0.06. Differences between transport in the absence and presence of each concentration of inhibitor were analyzed by one-tailed t-test.) WZB117 (≤10 nM) and CB (≤ 50 nM significantly increased 3MG uptake ($p < 0.05$).

Together these results are consistent with the simple carrier alternating access hypothesis, suggesting that binding of WZB117 at the exofacial sugar binding site of GLUT1 prevents CB binding at the endofacial site.

Isoform specificity of transport inhibition

The GLUT (SLC2A) family of passive glucose transporters can show distinct, isoform-specific affinities for inhibitors. For example, the insulin-sensitive glucose transporter of fat and muscle (GLUT4) is inhibited by HIV protease inhibitors, but GLUT1 is not (207), whereas GLUT1, GLUT3, and GLUT4 are inhibited by CB and the intestinal fructose transporters GLUT5 and GLUT7 are not (55). We, therefore, stably transfected HEK293 cells with GLUT1, GLUT3, or GLUT4 and measured the concentration dependence of WZB117 inhibition of 2-deoxy-D-glucose (2DG, 0.1 mM) uptake at 37 °C. WZB117 inhibits GLUT1- and GLUT3-mediated 2DG uptake with $K_{i(app)} \approx 10$ μM (figure 2.8A) but is a more potent inhibitor of GLUT4-mediated uptake ($K_{i(app)} = 0.2$ μM; figure 2.8A).

GLUT12 has been reported to be the most abundant endogenous GLUT in HEK293 cells (97). Endogenous GLUT3 mRNA content is about 50% of GLUT12 mRNA, while there are only trace levels of GLUT1 and GLUT4 mRNAs in HEK293 cells (97). Heterologous expression of human GLUT1 or GLUT4 (figure 2.8E) significantly reduced endogenous GLUT3 mRNA (figure 2.8B) and protein (figure 2.8, C and D) levels in HEK293 cells as judged by qPCR and Western blotting analyses. This explains why high affinity, WZB117 inhibition of transport in GLUT4-transfected cells reduced transport more effectively than observed in untransfected cells (figure 2.8A). We hypothesize that endogenous GLUT3 expression is reduced in GLUT4- and GLUT1-transfected cells as a compensatory response to increased cellular sugar uptake.

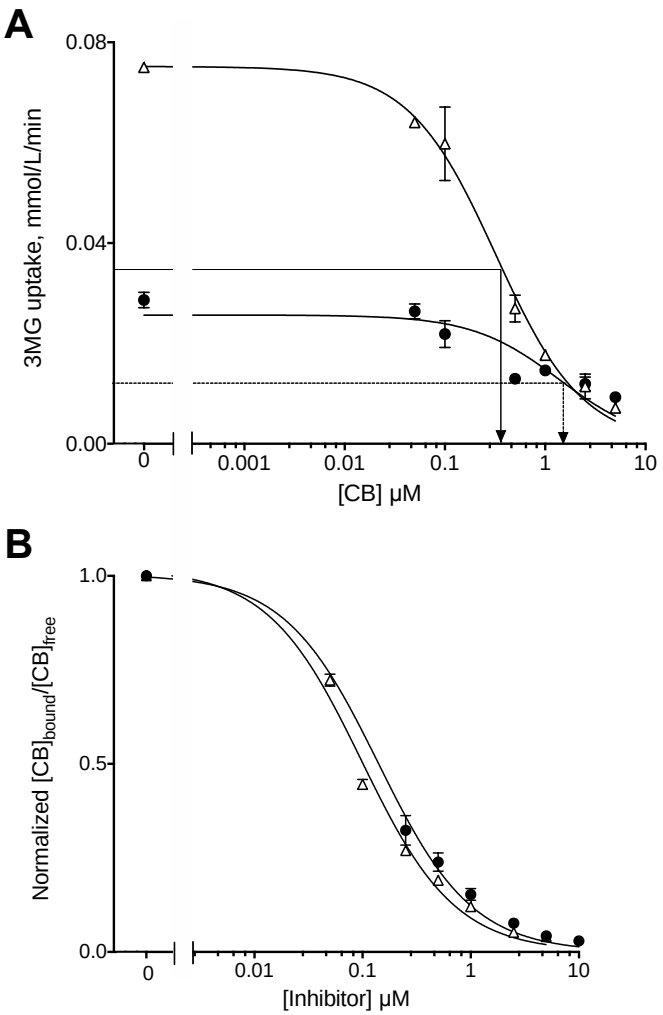

Figure 2.7: WZB117 inhibits endofacial CB binding to human red blood cells

A, WZB117 interferes with CB inhibition of 3MG uptake by human RBCs. Ordinate: 3MG uptake in mmol/L cell water/min. Abscissa: Concentration of inhibitors in µM (expressed in log scale). Results are shown for CB-treated cells (△), and CB-treated cells plus 200 nM WZB117 (●). Each data point represents the mean ± SEM of at least 3 duplicate measurements. The curves drawn through the data points were computed by nonlinear regression using equation 2.1 and have the following results: CB only treatment (△): $K_{i(app)}$ = 0.323 ± 0.042 µM, R^2 = 0.966, standard error of regression = 0.005; CB + 200 nM WZB117 (●): $K_{i(app)}$ = 1.376 ± 0.355 µM, R^2 = 0.734, standard error of regression = 0.004. **B,** Inhibition of [^{3}H]-CB binding to human RBCs. Ordinate: Normalized ratio of bound [^{3}H]-CB to free [^{3}H]-CB. Abscissa: Concentration of WZB117 (●) or nonradioactive CB (△) in µM (expressed in log scale). Each data point represents the mean ± SEM of duplicate measurements of 3 separate experiments. The curves drawn through the data points were computed by nonlinear regression using equation 2.4, with the following results: WZB117 treatment (●): $K_{i(app)}$ = 0.140 ± 0.010 µM, R^2 = 0.981, standard error of regression = 0.046; nonradioactive CB treatment (△): $K_{i(app)}$ = 0.098 ± 0.006 µM, R^2 = 0.989, standard error of regression = 0.036.

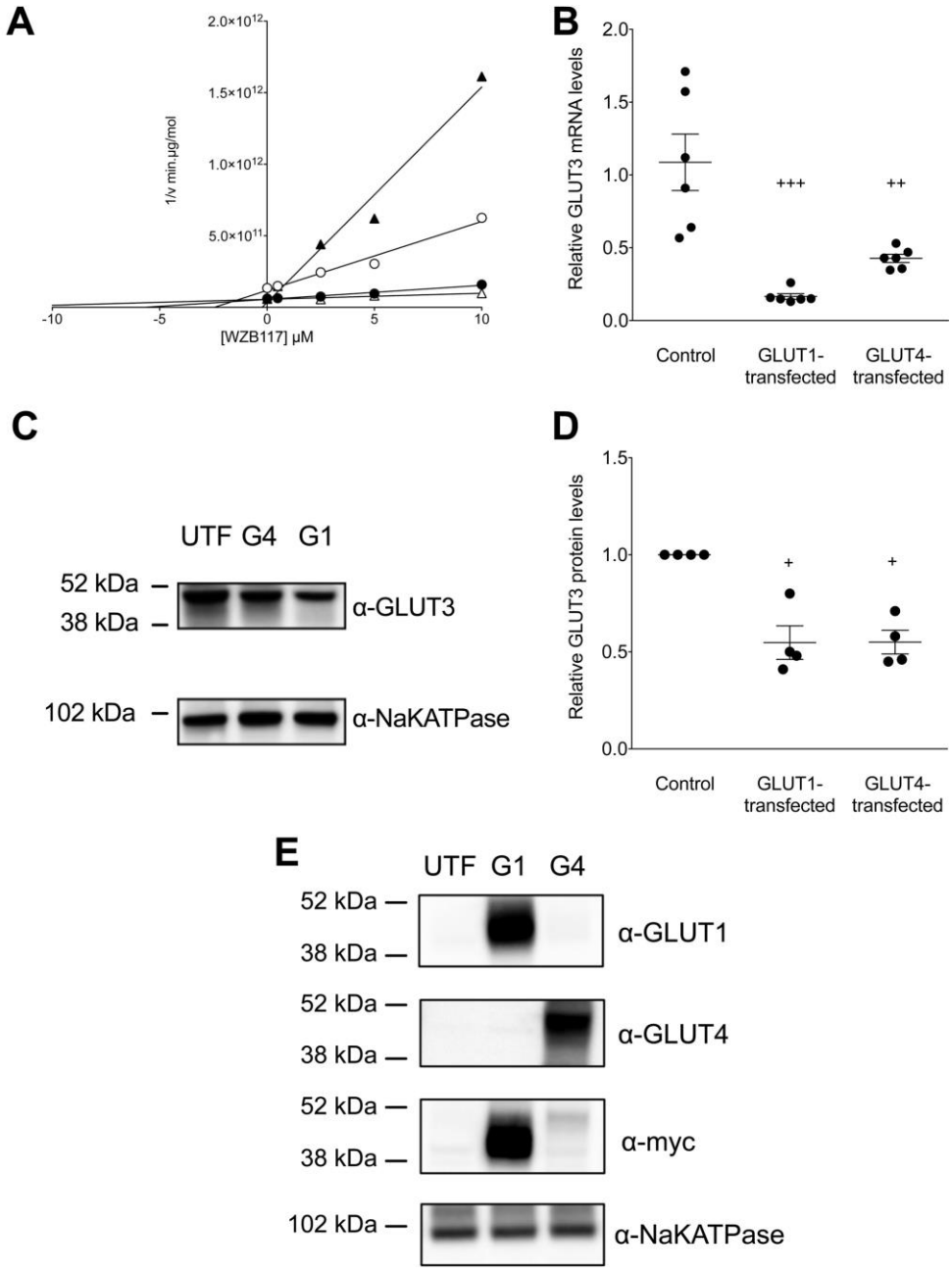

Figure 2.8: WZB117 inhibition of sugar transport is GLUT isoform-specific

A, Dixon plot of transport inhibition by WZB117 in untransfected HEK293 cells (○) and in cells transfected with and expressing hGLUT1 (●), hGLUT3 (△), or hGLUT4 (▲). *Ordinate*: 1/2DG uptake in min•µg protein/mol. *Abscissa*: WZB117 in µM. Lines drawn through the points were computed by linear regression and $K_{i(app)}$ for WZB117 inhibition of transport computed as *-x*-intercept. The results are: untransfected cells (○), $K_{i(app)}$ 2.45 ± 0.66 µM, R^2 = 0.975, standard error of regression = 3.66 x 10^{10}; hGLUT1-transfected cells (●), $K_{i(app)}$ = 5.71 ± 0.95 µM, R^2 = 0.974, standard error of regression = 7.59 x 10^9; hGLUT3-transfected cells (△), $K_{i(app)}$ = 13.32 ±

5.12 µM, R^2= 0.862, standard error of regression 8.82 x 10^9; hGLUT4-transfected cells (▲), $K_{i(app)}$ = 0.23 ± 0.47 µM, R^2 = 0.977, standard error of regression = 1.09 x 10^{11}. **B,** effect of heterologous GLUT1 or GLUT4 expression on parental GLUT3 mRNA levels as detected by qPCR. For each condition, the symbols (●) show the results of six separate measurements, and the *horizontal lines plus error bars* show their mean ± SEM. The conditions are untransfected (*Control*), GLUT1-transfected, and GLUT4-transfected cells. Results are normalized to one of the six GLUT3 message levels measured in untransfected cells. Ordinary one-way ANOVA shows that GLUT3 mRNA expression is significantly reduced in GLUT1-transfected and GLUT4-transfected cells relative to control cells (+++, p = 0.0001; ++, p = 0.0025). **C,** effect of heterologous GLUT1 or GLUT4 expression on parental GLUT3 expression. Results are shown for untransfected (*UTF*), GLUT1-transfected (*G1*), and GLUT4-transfected (*G4*) cells. Total GLUT3 and NaKATPase expression were assayed by obtaining whole cell lysates followed by SDS-PAGE of protein load-normalized samples and immunoblotting using protein-directed antibodies. Molecular mass markers are shown. **D,** quantitation of the effect of heterologous GLUT1 or GLUT4 expression on parental GLUT3 protein levels. Results (normalized to parental GLUT3 levels in untransfected cells as in figure 2.8C) are shown for untransfected (*Control*), GLUT1-transfected (*G1*) and GLUT4-transfected (*G3*) cells. For each condition, the symbols (●) show the results of four separate measurements, and the *horizontal lines plus error bars* show their mean ± SEM. Ordinary one-way ANOVA (+) shows that GLUT3 expression is significantly reduced in G1 and G4 cells relative to control cells (p = 0.0014). **E,** heterologous expression of GLUT1 and GLUT4 in HEK293 cells. Results are shown for untransfected (*UTF*), GLUT1-transfected (*G1*), and GLUT4-transfected (*G4*) cells. The GLUT1, GLUT4, and NaKATPase contents of protein load-normalized, whole cell lysates were assayed by immunoblot analysis using transporter specific (peptide-directed) antibodies (α-GLUT1, α-GLUT4, or α-NaKATPase IgGs) or with GLUT1 and GLUT4 by using-myc IgGs. Molecular mass markers are shown. Heterologous expression of GLUT1 increased HEK293 cell GLUT1 expression over untransfected cells by 47.5- and 30.8-fold using-fold α-GLUT1 and α-myc IgGs, respectively. Heterologous expression of GLUT4 increased HEK293 cell GLUT4 expression over untransfected cells by 58.7- and 3.6-fold using α-GLUT4 and α-myc IgGs, respectively.

Molecular Docking Studies

We undertook molecular docking studies of D-glucose, WZB117, and CB binding to a homology model of the exofacial (e2) open conformation of GLUT1 (hm-GLUT1-e2). We used the ligand-depleted chain A of the maltose-bound human GLUT3 (PDB code 4ZWC) structure (30) as the template to generate the homology model of the GLUT1-e2 (open) state. GLUT1 and GLUT3 share 65% sequence identity and 88% sequence similarity (194). ß-D-glucose docks at three high affinity sites in hm-GLUT1-e2 (figure 2.9a; figure 2.9, a–f). We term these sites peripheral, intermediate, and core based upon their location within the exofacial, interstitium–exposed cavity of the GLUT1-e2 conformer. Eighteen ß-D-glucose binding configurations were obtained at the core site. The affinity of binding (ΔG) ranged from –6 to –4kcal/mol. Of these 18 possibilities, only 4 match the known stereospecificity of sugar inhibition of GLUT1-mediated L-sorbose entry in human erythrocytes (87). We illustrate one such complex in figure 2.10 e and f. ß-D-glucose binding at this site is coordinated by hydrogen bonds to Gln161, Gln282, Asn317, and Glu380. Two additional ß-D-glucose binding sites were detected in the exofacial cavity. ß-D-glucose binding at the peripheral site (figure 2.10a and b) and at the intermediate site (figure 2.10c and d) presents fewer configurations, and in both instances C1 and its hydroxyl are solvent-exposed, whereas C6 and its hydroxyl are not. ß-D-glucose binding at the intermediate site is coordinated by hydrogen bonds to Thr30, Asn34, Val69, Ser73, and Asn415. This orientation of sugar is incompatible with the stereochemistry of L-sorbose uptake inhibition described by Barnett et al. (87).

WZB117 docking studies indicate that WZB117 can assume three positions in the exofacial cavity of hm-GLUT1-e2. When binding at its highest affinity site, WZB117

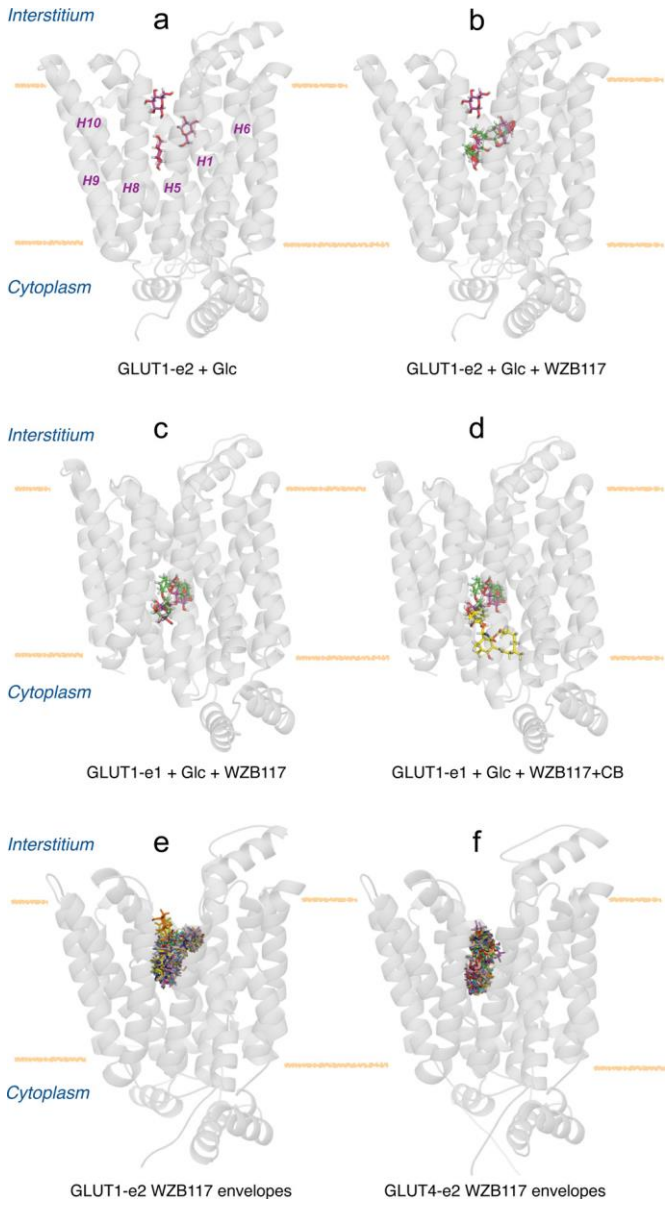

Figure 2.9: Molecular docking studies of ligand binding to hm-GLUT1 and hm-GLUT4.

a, hm-GLUT1-e2 complexed with peripheral, intermediate, and core -D-glucose molecules (red). GLUT1 is shown in transparent, schematic representation normal to the bilayer plane (horizontal yellow lines), membrane spanning -helices (H1, H5, H6, H8, H9, and H10) are indicated, and locations of the interstitium and cytoplasm are highlighted. **b,** hm-GLUT1-e2 complexed with ß-D-glucose molecules (red) and WZB117 (green). **c,** human GLUT1-e1 conformation complexed with intermediate and core ß-D-glucose molecules (red) and WZB117 (green). **d,** human GLUT1-e1 conformation complexed with ß-D-glucose molecules (red), WZB117 (green), and CB (yellow). **e,** hm-GLUT1-e2 conformation complexed with WZB117. The majority of computed binding sites (28 of 30) overlap with intermediate and core Glc binding sites. **f,** hm-GLUT4 e2 conformation complexed with WZB117. 30 potential binding sites are indicated; all overlap with peripheral and core Glc binding sites.

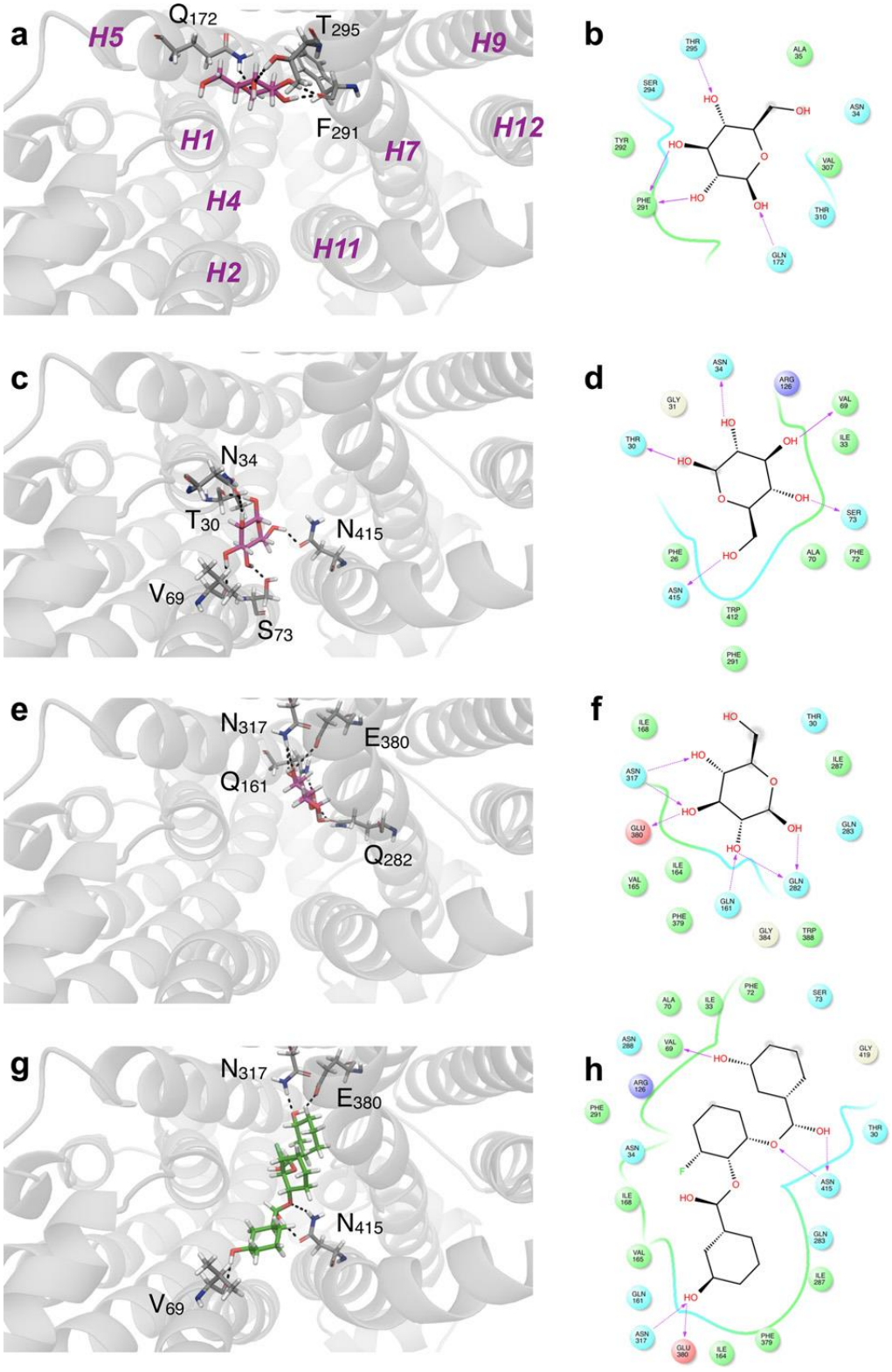

Figure 2.10: ß-D-glucose (a–f) and WZB117 (g and h) binding to hm-GLUT1-e2

The perspective is looking into the exofacial cavity of hm-GLUT1-e2 from the interstitium. The identities of several membrane spanning α helices (H1, H2, H4, H5, H7, H9, H11, and H12) are indicated in magenta in a. ß-D-glucose (in red) is shown docked to the peripheral (a and b), intermediate (c and d), and core (e and f) sites. Computed ∆G for ligand binding: peripheral, D-Glc binding site ∆G = – 5.1 kcal/mol; intermediate D-Glc binding site ∆G = –5.1 kcal/mol; core binding site = 4.9 kcal/mol. WZB117 is shown in green (g), and its docking site overlaps with intermediate and core-D-Glc binding sites. ∆G for WZB117 binding = –8.22 kcal/mol. Note that two additional configurations of WZB117-hm-GLUT1-e2 interactions were observed: one in which WZB117 interacts with and spans peripheral and core-D-glucose binding sites (∆G = –7.37 kcal/mol) and a second where WZB117interacts only with the peripheral and intermediate-D-glucose binding sites (∆G = –6.74 kcal/mol). Binding is shown as two representations: 1) three-dimensional in which GLUT1 is represented in transparent schematic format, Glc and WZB117 is in stick format, and H-bonds are represented as dashed lines (a, c, e, and g); 2) two-dimensional format in which Glc and WZB117 are shown as two-dimensional structures, coordinating GLUT1 residues are shown as circles, GLUT1 backbones are shown as ribbons, solvent-exposed regions of-D-Glc and WZB117 are indicated by gray-shaded circles, and H-bonds and their directionality are represented as red arrows (b, d, f, and h).

spanned the core and intermediate ß-D-glucose binding sites (figure 2.9b and figure 2.10g and h). Phenol ring 1 occupied the intermediate glucose binding site and was coordinated by hydrogen bonds to GLUT1 residues Val69 and Asn415. Phenol ring 2 occupied the core glucose binding site and was coordinated by hydrogen bonds to GLUT1 residues Asn317 and Glu380 (figure 2.10g and h). The two lower affinity WZB117 binding sites comprise one in which WZB117 docks to and spans the peripheral and core D-Glc binding sites and a second where WZB117 interacted with the peripheral

and intermediate D-Glc binding sites (not shown). CB did not dock at any high affinity sites in hm-GLUT1-e2 but did dock to the endofacial, GLUT1-e1 conformer (GLUT1-e1; figure 2.9d). The e1 GLUT1 conformation presented overlapping endofacial WZB117 and D-glucose sites that partially overlapped with the benzene ring of CB (figure 2.9c and d).

Discussion

WZB117, a prototypic anticancer drug, inhibited human erythrocyte sugar transport by acting as a competitive inhibitor of sugar uptake and as a noncompetitive inhibitor of sugar exit. This suggests that WZB117 and extracellular glucose compete for binding to the same site on the erythrocyte sugar transporter. Molecular docking and ligand binding studies support this hypothesis by showing that extracellular D-glucose and WZB117 binding sites comprise overlapping amino side chains distinct from those involved in binding CB, an inhibitor that acts at the endofacial sugar binding site.

Several studies have demonstrated (regardless of the assumed carrier model) that reversible transport inhibitors binding at the exofacial sugar binding site of the passive glucose transporters serve as competitive inhibitors of net sugar uptake and equilibrium

exchange transport and as noncompetitive inhibitors of net sugar exit (104,118,186). Conversely, reversible transport inhibitors binding at the endofacial sugar binding site are competitive inhibitors of net sugar exit and equilibrium exchange transport and are noncompetitive inhibitors of net sugar uptake (104,118,186). WZB117, therefore, fits the profile of a reversible inhibitor binding at the exofacial sugar binding site. CB behaves as a reversible inhibitor that binds at the endofacial sugar binding site, although the mixed-type inhibition of equilibrium exchange sugar transport and our molecular docking studies suggest that CB binding may involve more than a simple interaction with the endofacial sugar binding site.

Although several permutations of D-glucose and WZB117 binding sites were identified in GLUT1 docking studies, the highest affinity binding sites are consistent with the transport and ligand binding studies presented here and with previous studies of ligand binding to GLUT1 (30,62,86,116,118,208,209). Three exofacial D-glucose docking sites are present in the interstitium exposed exofacial cavity of hm-GLUT1-e2, peripheral, intermediate, and core. The stereochemistry of sugar binding at the peripheral and intermediate sites is incompatible with the findings of previous studies describing the stereochemistry of sugar transport inhibition by D-glucose analogs (87), whereas several configurations of sugar binding at the core site are compatible with the earlier studies. We, therefore, propose that the core D-glucose binding site may be the site at which hexose binding subsequently gives rise to sugar translocation.

WZB117 occupies three envelopes in GLUT1-e2. Envelope 1 comprises peripheral and core Glc binding sites, envelope 2 comprises intermediate and core Glc binding sites, and envelope 3 comprises peripheral and intermediate Glc sites. A majority (93%) of computed

WZB117:GLUT1 complexes correspond to WZB117 binding within envelope 2. The remaining 7% are equally distributed between envelopes 1 and 3. WZB117 geometry is fully extended (linear) in envelope 1 but is “L” shaped in envelopes 2 and 3. Although each envelope would leave one available Glc binding site available for extracellular hexose, it is easy to see how Glc and WZB117 would compete for binding to GLUT1.

CB does not dock to hm-GLUT1-e2 but can be docked with high affinity to GLUT1-e1. D-Glucose and WZB117 also dock to GLUT1-e1 but bind at overlapping (and presumably mutually exclusive) sites deeper within the e1 cavity. These sites do overlap with the CB binding site, and the observed competitions between sugar, intracellular WZB117, and CB for binding to GLUT1 suggest that mutually exclusive binding could result from steric hindrance.

GLUT1 and GLUT3 are inhibited by WZB117 with $K_{i(app)}$ of ~ 5–10 μM. GLUT4, the insulin-sensitive glucose transporter of fat and muscle cells (210-212), is inhibited by WZB117 with a 30 –100-fold greater potency.

The GLUT4-e2 conformer also presents peripheral, intermediate, and core Glc binding sites. However, the presence of Ile42 in GLUT4 transmembrane helix 1 (Thr30 in GLUT1 H1) leaves only linear envelope 1 (peripheral and core Glc sites) accessible to WZB117 (figure 2.9F). Molecular docking, therefore, suggests that WZB117 preferentially occupies envelope 2 in GLUT1-e2 and envelope 1 in GLUT4-e2. $K_{m(app)}$ for sugar transport and $K_{i(app)}$ for transport inhibition are products of multiple steps in the catalytic cycle regardless of the presumed mechanism of transport (118,213). It is not surprising, therefore, that WZB117 occupancy of different binding envelopes in two transporters characterized by

very different transport kinetics (97) would result in significantly different $K_{i(app)}$ for sugar transport inhibition.

Four observations in the present study impact our understanding of glucose transport mechanism, and are stated below. While the first 2 observations lend support for the simple carrier hypothesis, observation 3 negates the idea that exofacial and endofacial sugar binding sites cannot coexist. Our observations are as follows. 1) As is the case for extracellular maltose (118), extracellular WZB117 inhibits CB binding to GLUT1. Hence, the transporter's exofacial WZB117 binding site and the endofacial CB binding site are mutually exclusive. If CB binds only to the GLUT1-e1 conformer, which presents an endofacial sugar binding site, this behavior is consistent with the simple (alternating conformer) carrier model for sugar transport which predicts that inhibitor binding to the exofacial sugar binding site should competitively inhibit CB binding (95,105,214). 2) Extracellular WZB117 increases $K_{i(app)}$ for CB noncompetitive inhibition of sugar uptake. Again, this observation supports the simple (alternating conformer) carrier model for sugar transport (95,105,214). 3) Like extracellular maltose and intracellular CB (122,124), subsaturating extracellular WZB117 modestly stimulates sugar uptake. Transport stimulation by exofacial and endofacial transport inhibitors has been ascribed to cooperative interactions between co- existent exofacial and endofacial sugar binding sites present in the tetrameric GLUT1 transporter complex (122,124). The transporter is proposed to comprise four subunits (GLUT1 proteins) in which each subunit behaves as an alternating conformer carrier but where intersubunit cooperativity results in two subunits presenting exofacial (e2) orientations and 2 subunits presenting endofacial (e1) conformations at any instant (115,215). At subsaturating WZB117, there is a greater probability that only one of the two available GLUT1-e2 conformers is occupied by

WZB117, and its occupancy is proposed to allosterically activate sugar uptake via the remaining, inhibitor-free e2 subunit (124). As WZB117 is further increased, the probability that inhibitor occupies both e2 subunits increases and leads to sugar uptake inhibition. An alternative hypothesis is that exofacial ligand-induced allostery is an intra-subunit phenomenon in which occupancy of the exofacial cavity by polyphenolic WZB117 increases GLUT1 affinity for, or transport of, the transported sugar through the same GLUT1 subunit (216). 4) Molecular docking studies reveal three exofacial D-glucose binding sites in the hm-GLUT1-e2 cavity, peripheral, intermediate, and core. This is consistent with previous observations that GLUT1 binds ≥ 2 mol of transported sugar per mol GLUT1 (140). Each envelope would leave one Glc binding site available for substrate. The results of this docking analysis, therefore, do not permit resolution of the mechanism of exofacial allostery (i.e. inter- or intrasubunit interactions).

Although a promising strategy for cancer cell elimination, glucose transport inhibition using WZB117 could perturb organismal carbohydrate homeostasis in several important ways. Blood-brain and blood-tissue barrier GLUT1-dependent glucose transport will be depressed, perturbing peripheral and central neuro-metabolic function (127). Human, GLUT1-dependent, pancreatic beta cell insulin secretion in response to hyperglycemia will be diminished (217), and insulin-dependent, GLUT4-mediated skeletal muscle and adipose glucose transport will be prone to high affinity WZB117 inhibition thereby further compounding hyperglycemia. The net effects will include acute hyperglycemia and perturbations of neurometabolic function and insulin-dependent lipogenesis. These predictions are consistent with the reported hyperglycemia and lipodystrophy in mice after WZB117 treatment (165) and suggest that WZB117-treatment could induce metabolic syndrome/insulin resistance in individuals undergoing therapy.

The current study demonstrates that WZB117 inhibits facilitative sugar transport by competing with sugars for occupancy of the exofacial substrate binding site of the transporter. GLUT1, GLUT3, and GLUT4 are sensitive to transport inhibition, suggesting that sugar transport across the blood brain barrier in CNS astrocytes and neurons and in insulin-sensitive tissues is susceptible to inhibition (5). Most cancer cells rely on anaerobic glycolysis to generate the ATP and substrates required for cellular processes and proliferation (181). This contrasts with normal, differentiated cells, which mostly use mitochondrial oxidative phosphorylation to sustain cellular function (187). This could explain why sugar transport inhibition is a successful anticancer strategy in mice (165). However, human CNS development and function are especially dependent on glucose transport and metabolism (127), and the consequences of inhibition of glucose transport into and within the CNS could be catastrophic. We suggest, therefore, that a combination therapy of ketogenic diet (such as is used to manage GLUT1 deficiency; Refs. (189) and (218-220)) plus sugar transport inhibition might be more successful.

Chapter III

Preface

Chapter III of this dissertation will be submitted for publication as:

Ojelabi, O. A., Lloyd, K. P., De Zutter, J. K., and Carruthers, A. (2017) Red wine and green tea flavonoids act as cis-allosteric GLUT1 activators at low concentrations but are competitive inhibitors of glucose uptake at higher concentrations

Author contributions: OAO and AC designed experiments, analyzed results and co-wrote the manuscript. OAO conducted all experiments except isoform specificity of transport inhibition. KPL contributed to the molecular docking studies. JKD conducted experiments on the isoform specificity of transport inhibition

Red wine and green tea flavonoids act as cis-allosteric GLUT1 activators at low concentrations but are competitive inhibitors of glucose uptake at higher concentrations

Introduction

Moderate consumption of red wine or green tea is associated with protection against cancer, cardiovascular disease and diabetes (221-224). These benefits are hypothesized to result from the flavonoid-rich content of the beverages (225).

The flavonoids are a large group of polyphenolic secondary metabolites with over 4000 types identified in fruits, flowers, vegetables and leaves (225,226). The general structure of flavonoids is a flavan backbone consisting of 2 benzene rings linked together by a heterocyclic pyran ring (227). Substitutions in the flavan structure by hydroxyls, methyl groups and sugars creates the wide range of flavonoid derivatives (225). Quercetin, epigallocatechin gallate (EGCG) and epicatechin gallate (ECG) are present in red wine and green tea and are among the most extensively characterized flavonoids. Each cup of green tea is estimated to contain up to 300 mg EGCG, 49 mg ECG and 14 mg quercetin (228-230). Red wine contains 4–16 mg/L quercetin (231,232) and although EGCG and ECG are known to be present in red wine (229) their levels are not well defined. The health benefits of flavonoids have been attributed to their strong antioxidant capacity. Flavonoids chelate metal ions such as Fe^{3+}, and trap reactive species including singlet oxygen, superoxide radicals, nitric oxide, and peroxynitrite (225,233,234).

Some studies, however, have shown that the red wine and green tea flavonoids quercetin, EGCG and ECG inhibit GLUT1-mediated facilitative glucose transport (198,199,235-237)

raising the possibility that the interaction of these molecules with GLUT1 and their downstream effects on carbohydrate metabolism contribute to their impact on health. While this could make sense in cancer cells where GLUT1 expression and non-oxidative glucose metabolism are upregulated (238), it is harder to understand how glucose transport inhibition would ameliorate diabetes and cardiovascular disease.

Recent studies have suggested that GLUT1 functions as an oligomeric complex of interacting, allosteric, alternating access transporters (120) and that low concentrations of GLUT1 inhibitors acting at exofacial or endofacial sugar binding sites stimulate sugar transport (120,239). The present study explores the detailed structure/function relationships of flavonoid-GLUT1 interactions in an effort to explicate flavonoid action on cellular function. We find that the flavonoids act as heterotropic, cis-allosteric activators of sugar uptake at low concentrations and as competitive inhibitors of sugar uptake at higher concentrations. Low concentrations of flavonoids could, therefore, be protective against diabetes and Alzheimer's, by stimulating GLUT1-mediated glucose uptake while higher concentrations of, flavonoids could be anti-tumorigenic by inhibiting GLUT1.

Methods

Reagents

Tritium-labeled 3-O-methylglucose ([^{3}H]-3MG), 2-deoxy-D-glucose ([^{3}H]-2DG) cytochalasin B ([^{3}H]-CB) and quercetin ([^{3}H]-quercetin) were purchased from American Radiolabeled Chemicals (St. Louis, MO). Unlabeled 3MG, CB, quercetin, (-)-epigallocatechin gallate (EGCG), (-)-epicatechin gallate (ECG) and phloretin were purchased from Sigma-Aldrich (St. Louis, MO). Phosphate-buffered saline (PBS) was

purchased from Thermo Fisher Scientific (Waltham, MA). WZB117 was purchased from EMD Millipore (Billerica, MA).

Solutions

KCl medium comprised 150 mM KCl, 5 mM HEPES, 0.5 mM EDTA, pH 7.4. Stop solution comprised ice-cold KCl medium plus 50 µM WZB117 and 100 µM phloretin. Sugar uptake/exit medium was made up in KCl medium containing 0 – 20 mM 3MG ± inhibitors and contained [^{3}H]-3MG or [^{3}H]-quercetin as indicated. HEK293 solubilization buffer comprised KCl medium with 1% Triton X-100.

Cells

De-identified whole human blood was purchased from Biological Specialty Corporation (Colmar, PA). HEK293 cells were maintained in Dulbecco's modified Eagle's medium (DMEM) supplemented with 10% fetal bovine serum, 100 units/mL penicillin, and 100 µg/mL streptomycin in a 37 °C humidified 5% CO_2 incubator.

Heterologous Expression of GLUT Isoforms

Heterologous expression of hGLUT1, hGLUT3 and hGLUT4 in HEK293 cells was as previously described (97,123). Both hGLUT1 and hGLUT4 contain a myc-epitope in exofacial loop 1 (97), while the 13 C-terminal amino acids in hGLUT3 are replaced by the corresponding residues of hGLUT4 (123) to facilitate detection of heterologous expression.

Red blood Cell Transport Measurements

All human erythrocytes sugar transport experiments were performed at 4 ºC as previously described (205,239). Red blood cells were isolated from whole blood, and glucose-depleted as described previously (204,205). One volume of glucose-depleted RBCs was pre-incubated in 50 – 400 volumes of ice-cold KCl medium ± inhibitors at 4 ºC for 10 – 15 min, to ensure optimal equilibration of inhibitor with GLUT1 before performing transport measurements.

Zero-trans Uptake: Zero-trans [^{3}H]-3MG or [^{3}H]-quercetin uptake (uptake into cells lacking intracellular sugar or quercetin) was initiated by adding 10 volumes (100 µL) of uptake medium ± inhibitor to 1 volume (10 µL) of sugar-depleted, 50% hematocrit (Ht) red cells, and sugar uptake allowed to proceed for 30 – 60 seconds at 4 ºC. Uptake was stopped by adding 50 volumes (1 mL) of ice-cold stop solution containing 50 µM WZB117 and 100 µM phloretin. Cells were washed one more time in stop solution, lysed in 3% perchloric acid, and radioactivity assayed in clarified lysates using liquid scintillation counting. Radioactivity measurements were done in duplicates.

Zero-trans Exit: Glucose-depleted, packed RBCs were loaded with 10 mM 3MG by incubating 1 volume of cells with 20 volumes of 20 mM 3MG (containing 1 µCi [^{3}H]-3MG/mL of cold 3MG) for 1 hour at 37 ºC. Immediately following 3MG loading, cells were transferred to 4 ºC and pre-incubated with or without inhibitors for 10 – 15 min. Cell suspension were spun at 10,000 x g for 1 min, and supernatant discarded. One volume (0.5 mL) of sugar-loaded RBCs were added to 50 volumes of KCl medium ± inhibitor on a shaker with magnetic stirrer. Aliquots (0.5 mL) of the suspension were withdrawn at indicated time intervals, and immediately added to 1 mL ice-cold stop solution. Cells were

washed again in stop solution, lysed in 3% perchloric acid and assayed in duplicate for radioactivity.

HEK-293 Cell Sugar Uptake

All HEK293 cell sugar uptake measurements were performed at 37 ºC, using 100 µM 2-deoxyglucose (2DG plus [^{3}H]-2DG) as described previously (97,143).

Equilibrium CB Binding

CB binding to human red cells was performed as previously described (116,239). Briefly, 50 µL of sugar-depleted RBC (50% Ht) ± inhibitors were mixed with 50 µL of ice-cold KCl medium containing 40 nM [^{3}H]-CB and 10 µM cytochalasin D for 15 min at 4 ºC, with constant end-over-end rotation. Total [CB] was obtained from 2 x 10 µL of the cell suspension lysed in 100 µL of 3% perchloric acid, and radioactivity assayed for by liquid scintillation counting. To obtain free [CB], cell suspension was centrifuged at 10,000 x g for 30 s, and 2 x 10 µL of clarified supernatant were assayed for radioactivity. Bound [CB] was calculated as Total [CB] – Free [CB].

Homology Modeling

The homology models of the outward-open (e2) conformations of GLUT1 and GLUT4 were generated using the maltose-bound human GLUT3 structure (PDB code: 4ZWC) (30). Maltose was removed from the GLUT3 structure and chain A was used as the template for modeled structures. Sequence alignments were generated using ClustalX (240). Homology models were built using Modeller-9.9 (241) and analyzed using PROCHECK (242).

Stochastic docking

The crystal structure of outward-open hGLUT3-e2 (4ZWC) (30) was obtained from the protein databank (http://www.rcsb.org/pdb/home/home.do). The structures for β-D-Glucose, quercetin, EGCG and ECG were obtained from Pubchem (https://pubchem.ncbi.nlm.nih.gov). Docking was performed using the Schrodinger software suite. The protein structure was preprocessed with the Protein Preparation Wizard, bond orders were assigned, hydrogens added and the H-bond network was optimized. The system was energy minimized using the OPLS 2005 force field. Ligand structures were prepared with the LigPrep module and the pKa of the ligands was calculated using the Epik module. Molecular docking was performed by the GLIDE module in standard-precision (SP) mode and default values for grid generation. Cavities for docking were calculated using the CastP server (http://sts.bioe.uic.edu/castp/) and the grid was centered on the residues forming the cavity. No restraints were used during the docking.

Data analysis

Linear and nonlinear regression analysis of data sets and statistical tests were performed using GraphPad Prism (Version 7.0a; La Jolla, CA).

Michaelis-Menten inhibition of sugar transport is assumed to be described by:

$$V = V_c - \frac{V_c[I]}{K_{i(app)} + [I]} \qquad \text{(equation 3.1)}$$

where V_c is V measured in the absence of inhibitor I, [I] is the concentration of inhibitor and $K_{i(app)}$ is that [I] producing 50% inhibition of uptake.

Michaelis-Menten transport is assumed to be described by:

$$V = \frac{V_{max}[3MG]}{K_{m(app)} + [3MG]} \qquad \text{(equation 3.2)}$$

where V_{max} is the maximum rate of 3MG transport, [3MG] is the concentration of 3MG and $K_{m(app)}$ is the [3MG] where the rate of uptake is $V_{max}/2$. Sugar exit was analyzed by nonlinear regression analysis using Mathematica 10.4.1.0 (Wolfram Research) assuming that exit follows Michaelis-Menten kinetics and that the first derivative of the exit progress curve represents d[S]/dt at any given [S] (239).

Transport stimulation followed by inhibition by inhibitors was approximated first by normalizing all uptake to V_c and then using the following model:

$$\frac{V_i}{V_c} = \frac{Const_1 + [I](Const_2 + [I])}{Const_1 + [I](Const_3 + [I]Const_4)} \qquad \text{(equation 3.3)}$$

where V_c is uptake measured in the absence of inhibitor I, V_i is uptake measured in the presence of inhibitor, [I] is the concentration of inhibitor and $Const_1$ through $Const_4$ are model dependent (120).

Inhibition of [^{3}H]-CB binding to GLUT1 by ligands was analyzed by simple competitive inhibition using the model:

$$\frac{[CB]_b}{[CB]_f} = \frac{K_{i(app)}(K_{CB} + [CB])}{[I]K_{CB} + K_{i(app)}(K_{CB} + [CB])} \qquad \text{(equation 3.4)}$$

where $[CB]_b$ = bound [CB], $[CB]_f$ = free [CB], $K_{i(app)}$ is the apparent inhibitory constant for inhibition of CB binding by inhibitor, I, and K_{CB} is dissociation constant for CB binding to GLUT1.

CB binding was also analyzed using a variation of Michaelis-Menten equilibrium binding kinetics in which the transporter is allowed to bind more than one molecule of competing ligand, I

$$\frac{[CB]_{(b/f)i}}{[CB]_{(b/f)c}} = 1 - \frac{K[I]^n}{K_I + [I]^n} \qquad \text{(equation 3.5)}$$

where $[CB]_{(b/f)I}$ = the ratio of bound to free [CB] measure in the presence of inhibitor I, $[CB]_{(b/f)c}$ = the ratio of bound to free [CB] measure in the absence of inhibitor, K is a number where $0 \leq K \leq 1$, K_I is $K_{d(app)}$ for I binding to GLUT1 and n is the number of inhibitor binding sites.

Results

Dose-dependent inhibition of human erythrocyte sugar transport by dietary flavonoids

Dietary flavonoids are reported to impair cellular sugar transport to varying degrees in different cell types (199,236,243-246). Here we tested the effect of quercetin, EGCG and ECG on GLUT1-mediated zero-trans sugar uptake (uptake in the absence of intracellular sugar) in human red blood cells. Figure 3.1A–D shows the chemical structures of the quercetin, EGCG and ECG, as well as the general backbone (flavan nucleus) of all flavonoids. Quercetin, EGCG and ECG inhibit uptake of 0.1 mM 3-O-methylglucose (3MG) in a dose-dependent manner, with $K_{i(app)}$ = 1.882 ± 0.3324 μM, 9.631 ± 1.947 μM, and 1.902 ± 0.315 μM respectively (figure 3.1E).

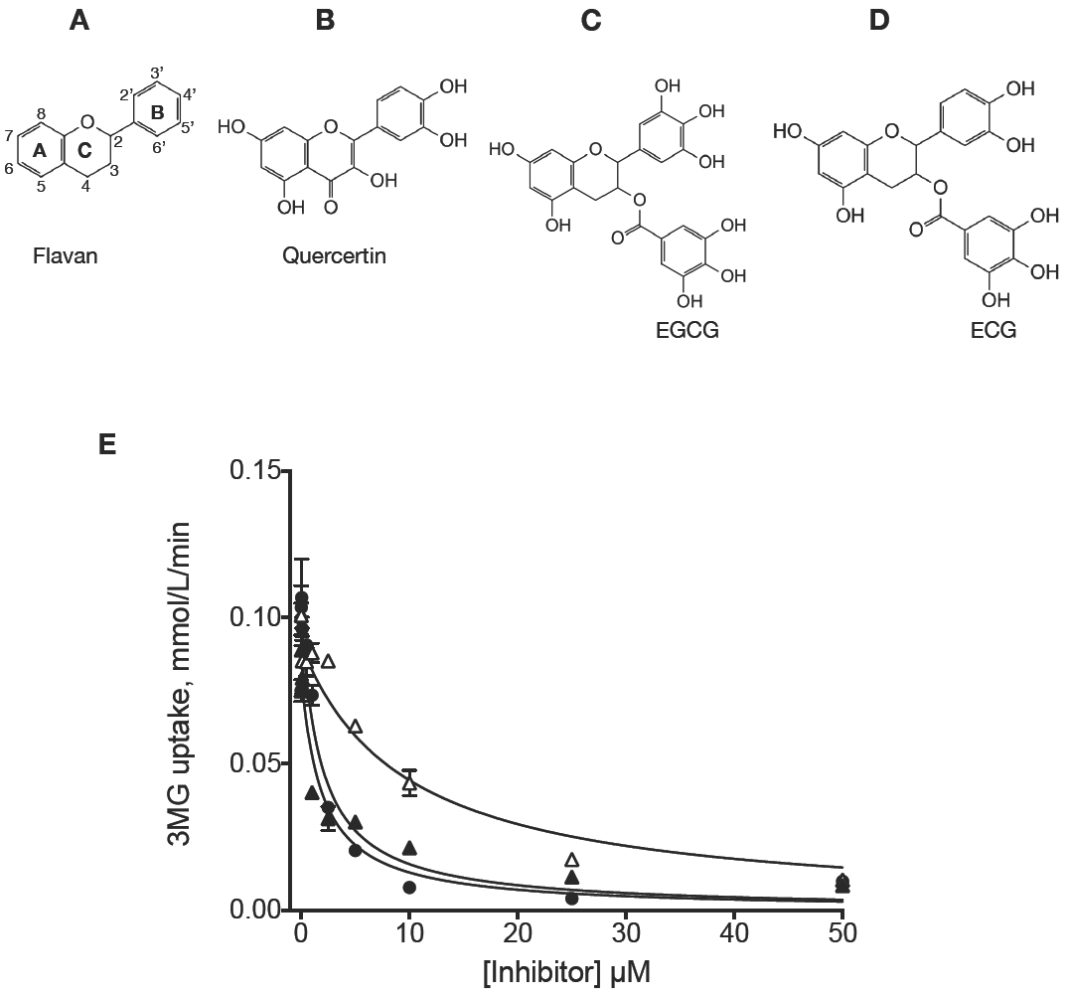

Figure 3.1: Chemical structures and dose-dependent inhibition of human erythrocytes zero-trans 3MG (0.1 mM) uptake by quercetin, EGCG and ECG

A, Flavan skeleton which provides the basic backbone for over 4000 identified flavonoids, including quercetin (**B**), epigallocatechin gallate (EGCG) (**C**), and epicatechin gallate (ECG) (**D**). **E,** Ordinate: 3MG uptake in mmol/L cell water/min; Abscissa: [Inhibitor] in µM. Results are shown for quercetin (●), EGCG (△), and ECG (▲). Each point represents the mean ± SEM of at least 3 duplicate measurements. The points were fitted by nonlinear regression assuming that uptake is completely inhibited by inhibitors in a dose-dependent manner (equation 3.1), with the following results: quercetin-treated cells (●): $K_{i(app)}$ = 1.882 ± 0.332 µM, R^2 = 0.915, standard error of regression = 0.012 mmol/L cell water/min; EGCG-treated cells (△): $K_{i(app)}$ = 9.631 ± 1.947 µM, R^2 = 0.873, standard error of regression = 0.012 mmol/L cell water/min; ECG-treated cells (▲): $K_{i(app)}$ = 1.902 ± 0.315 µM, R^2 = 0.929 standard error of regression = 0.008 mmol/L cell water/min.

Quercetin, EGCG and ECG competitively inhibit net sugar uptake, but are noncompetitive inhibitors of net sugar exit by human erythrocytes

We determined the sidedness of flavonoid action on GLUT1 by examining their effects on 2 modes of red cell sugar transport: 1) zero-trans 3MG uptake (influx into sugar-free cells), and 2) zero-trans 3MG exit (efflux from sugar-loaded cells into medium lacking sugar). Transport theory informs us (117,118) that a ligand competing with sugar for binding at the exofacial sugar binding site serves as a competitive inhibitor of sugar uptake and as a noncompetitive inhibitor of sugar exit. Conversely, a ligand competing with sugar for binding at the endofacial sugar binding site serves as a noncompetitive inhibitor of sugar uptake and as a competitive inhibitor of sugar exit.

The flavonoids increase $K_{m(app)}$ for sugar uptake from 2.39 ± 0.356 mM to 11.07 ± 5.03 mM (quercetin), 10.64 ± 2.63 mM (EGCG) and 7.14 ± 2.63 mM (ECG), without significantly affecting V_{max} for uptake (1.202 ± 0.082 mmol/L cell water/min; figure 3.2A). This suggests that quercetin, EGCG and ECG inhibit GLUT1-mediated sugar uptake by binding at the exofacial 3MG binding site or at a site whose occupancy is mutually exclusive with 3MG occupancy of the exofacial sugar binding site. Consistent with this idea, the flavonoids act as noncompetitive inhibitors of net 3MG exit: they are without effect on $K_{m(app)}$ (12.9 mM) for exit, but decrease V_{max} for exit by more than 2-fold from 2.03 mmol/L cell water/min to 0.89 (quercetin), 0.72 (EGCG), and 0.60 mmol/L cell water/min (ECG; figure 3.2B).

Subsaturating concentrations of Quercetin, EGCG, and ECG stimulate GLUT1-mediated sugar uptake in human red blood cells

We have previously shown that low concentrations of exofacial inhibitors (e.g. WZB117

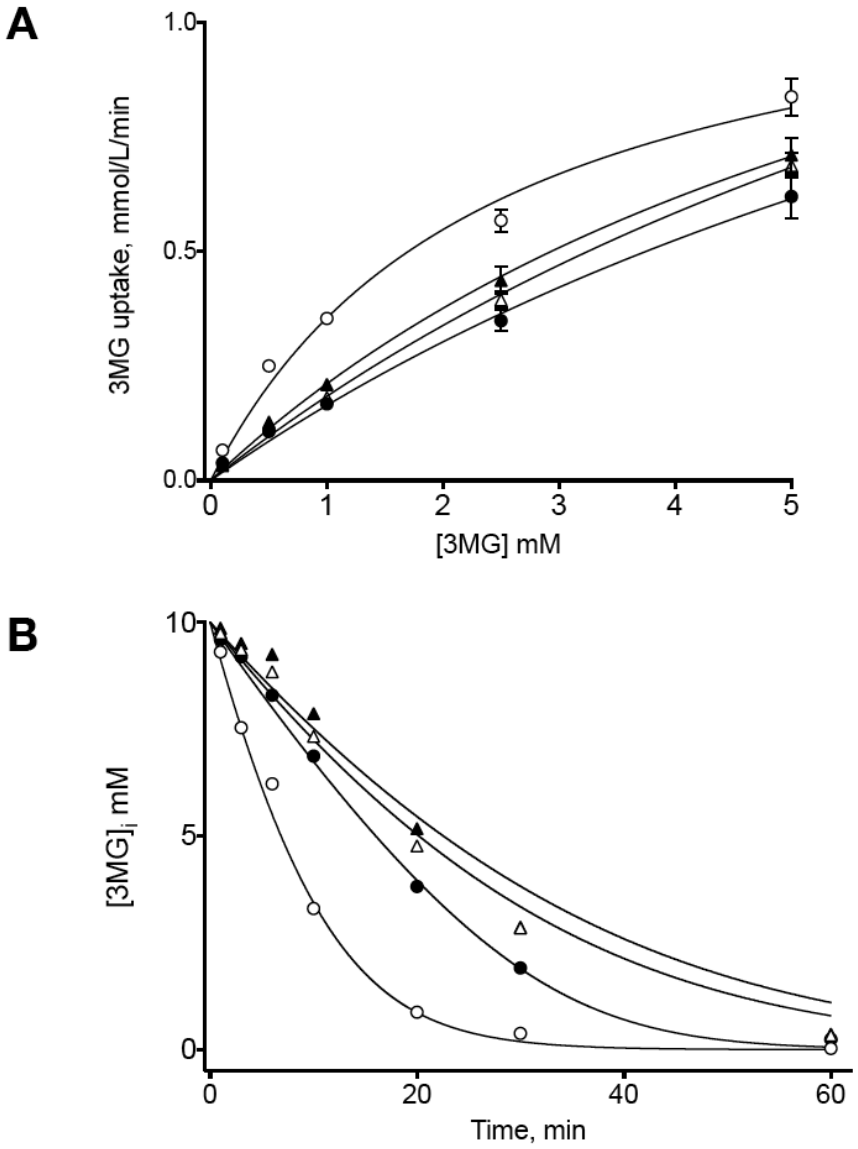

Figure 3.2: Effects of quercetin, EGCG and ECG on Michaelis-Menten kinetics of zero-trans 3MG uptake (A) and zero-trans 3MG exit (B)

Results are shown for control cells (○), quercetin-treated cells (●), EGCG-treated cells (△), and ECG-treated cells (▲). Each data point represents the mean ± SEM of at least 3 experiments measured in duplicates. **A,** Ordinate: 3MG uptake in mmol/L cell water/min; Abscissa: [3MG] in mM. Curves drawn through the points were computed by Michaelis-Menten uptake kinetics as in equation 3.2. The results are: Control cells (○): V_{max} = 1.202 ± 0.082 mmol/L cell water/min, $K_{m(app)}$ = 2.39 ± 0.36 mM, R^2 = 0.934, standard error of regression = 0.072; quercetin-treated cells (●): V_{max} = 1.976 ± 0.663 mmol/L cell water/min, $K_{m(app)}$ = 11.07 ± 5.03 mM, R^2 = 0.893, standard error of regression = 0.074; EGCG-treated cells (△): V_{max} = 2.137 ± 0.387 mmol/L cell water/min, $K_{m(app)}$ = 10.64 ± 2.63 mM, R^2 = 0.965, standard error of regression = 0.046; ECG-treated cells (▲): V_{max} = 1.717 ± 0.292 mmol/L cell water/min, $K_{m(app)}$

= 7.14 ± 1.85 mM, R^2 = 0.937, standard error of regression = 0.065. **B,** Ordinate: $[3MG]_i$ in mmol/L cell water; Abscissa: Time in minutes. Curves drawn through the points were computed by numerical integration and nonlinear regression assuming Michaelis-Menten exit kinetics (equation 3.2) with the following results: Control cells (○): V_{max} = 2.033 mmol/L cell water/min, $K_{m(app)}$ = 12.90 mM, R^2 = 0.999, standard error of regression = 0.014 mmol/L cell water/min; quercetin treatment (●): V_{max} = 0.894 mmol/L cell water/min, $K_{m(app)}$ = 12.10 mM, R^2 = 0.989, standard error of regression = 0.050; EGCG treatment (△): V_{max} = 0.720 mmol/L cell water/min, $K_{m(app)}$ = 12.30 mM, R^2 = 0.972, standard error of regression = 0.075; ECG treatment (▲): V_{max} = 0.600 mmol/L cell water/min, $K_{m(app)}$ = 12.10 mM, R^2 = 0.999, standard error of regression = 0.016.

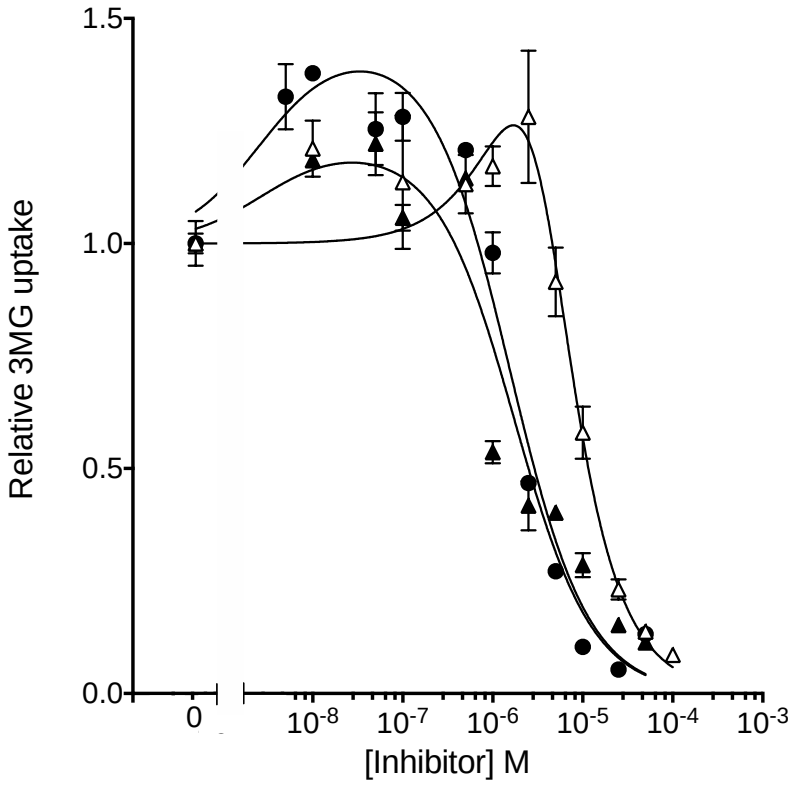

Figure 3.3: Subsaturating concentrations of quercetin, EGCG, and ECG stimulate 3MG uptake

Relative 3MG uptake. Abscissa: Concentration of inhibitors in M (expressed in log scale). Results are shown for cells treated with quercetin (●), EGCG (△), and ECG (▲). Each data point represents the mean ± SEM of at least 3 duplicate measurements. The curves drawn through the data points were computed by nonlinear regression using equation 3.3 and have the following constants: quercetin treatment (●): $Const_1 = 4.69 \times 10^{-5} \pm 2.05 \times 10^4$, $Const_2 = 2.59 \times 10^4 \pm 1.13 \times 10^{13}$, $Const_3 = 1.80 \times 10^4 \pm 7.83 \times 10^{12}$, $Const_4 = 1.17 \times 10^{10} \pm 5.08 \times 10^{18}$, $R^2 = 0.966$, standard error of regression = 0.101; EGCG treatment (△): $Const_1 = 3.02 \times 10^2 \pm 5.13 \times 10^6$, $Const_2 = 1.27 \times 10^4 \pm 2.14 \times 10^{12}$, $Const_3 = 2.60 \times 10^3 \pm 4.40 \times 10^{11}$, $Const_4 = 2.19 \times 10^9 \pm 3.71 \times 10^{17}$, $R^2 = 0.923$, standard error of regression = 0.135; ECG treatment (▲): $Const_1 = 4.44 \times 10^2 \pm 9.49 \times 10^7$, $Const_2 = 9.86 \times 10^2 \pm 2.11 \times 10^{12}$, $Const_3 = 1.74 \times 10^4 \pm 3.72 \times 10^{13}$, $Const_4 = -4.46 \times 10^7 \pm 9.53 \times 10^{16}$, $R^2 = 0.866$, standard error of regression = 0.167.

and maltose) or endofacial inhibitors (e.g cytochalasin B) of GLUT1-mediated sugar transport modestly stimulate red cell sugar uptake (122,124,239). Consistent with these reports, quercetin (≤ 0.5 μM), EGCG (≤ 2.5 μM) and ECG (≤ 0.5 μM) reproducibly stimulate erythrocyte zero-trans 3MG uptake by up to 35% ($p < 0.05$; figure 3.3). These results suggest that GLUT1 presents at least 2 exofacial flavonoid binding sites – one that stimulates sugar uptake and a second site that inhibits uptake (120).

Quercetin, EGCG and ECG interfere with cytochalasin B (CB) binding to human erythrocytes

CB is a membrane-permeant, GLUT1 inhibitor which binds to the endofacial glucose binding site (117,118). Extracellular maltose, but not glucose, inhibits equilibrium binding of the CB to the endofacial glucose binding site of GLUT1 (124,247). We asked if exofacial binding of quercetin, EGCG, or ECG interfere with equilibrium binding of ^{3}H-CB to GLUT1. Quercetin, EGCG, ECG, and nonradioactive CB inhibit [^{3}H]-CB binding to GLUT1 with $K_{i(app)}$ of 0.637 ± 0.071 μM, 6.097 ± 0.726 μM, 0.871 ± 0.103 μM, and 0.064 ± 0.003 μM respectively (figure. 3.4A). While these curve fits produce good correlation coefficients (R^2 > 0.91 in all cases), the standard deviation of residuals of the fit (0.09) is greater than 20% of the standard deviation of the y values suggesting that the fit is poor.

Closer examination reveals that inhibition by quercetin and EGCG increases more steeply while inhibition produced by ECG increases less steeply than is expected for simple Michaelis-Menten inhibition. Inhibition of radiolabeled CB binding by unlabeled CB is well-described by simple Michaelis-Menten inhibition. We therefore asked if the quercetin, EGCG and ECG data are better approximated by inhibition involving multiple, cooperative ligand binding sites and applied a simple, Hill-type model to analyze these results (figure

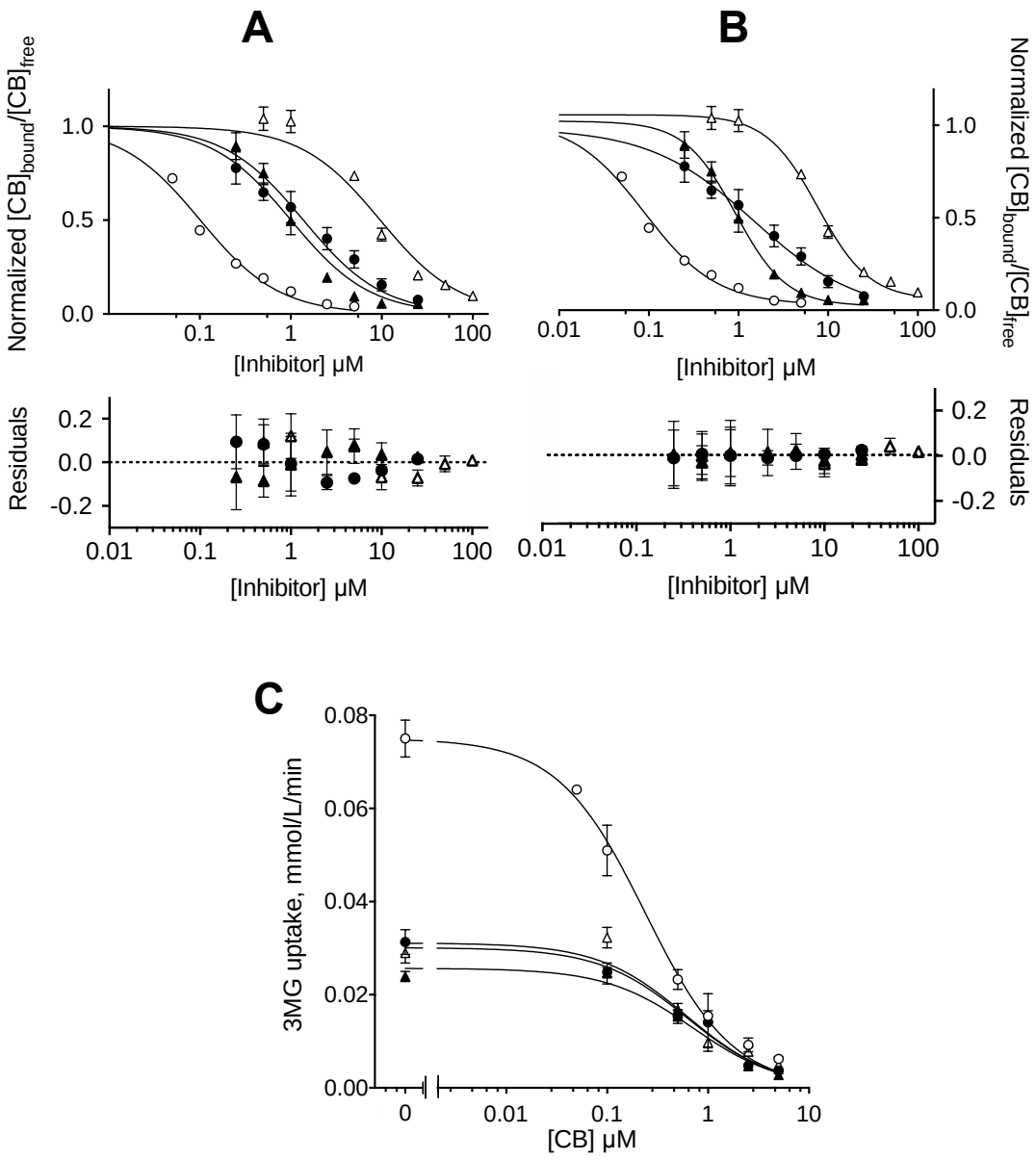

Figure 3.4: Exofacial interaction of flavonoids with GLUT1 interfere with CB binding to human red blood cells

A, Inhibition of [^{3}H]-CB binding to human RBCs. Ordinate: Normalized ratio of bound [^{3}H]-CB to free [^{3}H]-CB. Abscissa: Concentration of inhibitors in µM (expressed in log scale). Results are shown for cells treated with quercetin (●), EGCG (△), ECG (▲) and non-radioactive CB (○). Each data point represents the mean ± SEM of duplicate measurements of 3 separate experiments. The curves drawn through the data points were computed by nonlinear regression using equation 3.4, with the following results: quercetin treatment (●): $K_{i(app)}$ = 0.637 ± 0.071 µM, R^2 = 0.948, standard error of regression = 0.087; EGCG treatment (△): $K_{i(app)}$ = 6.097± 0.726 µM, R^2 = 0.949, standard error of regression = 0.089; ECG treatment (▲): $K_{i(app)}$ = 0.871

± 0.103 μM, R^2 = 0.910, standard error of regression = 0.094; nonradioactive CB treatment (○): $K_{i(app)}$ = 0.064 ± 0.003 μM, R^2 = 0.988, standard error of regression = 0.036. The residuals of the fits (for quercetin, EGCG and ECG data) are plotted beneath the inhibition plot. **B,** Reanalysis of the same data set assuming multiple binding sites for competing ligand using the Hill-equation (equation 3.5). The results are: quercetin treatment (●): $K_{i(app)}$ = 0.89 ± 0.14 μM, n = 1.53 ± 0.14, R^2 = 0.974, standard error of regression = 0.064; EGCG treatment (△): $K_{i(app)}$ = 21.75 ± 7.80 μM, n = 1.51 ± 0.16, R^2 = 0.976, standard error of regression = 0.063; ECG treatment (▲): $K_{i(app)}$ = 1.34 ± 0.30 μM, n = 0.75 ± 0.08, R^2 = 0.94, standard error of regression = 0.083; nonradioactive CB treatment (○): $K_{i(app)}$ = 0.074 ± 0.014 μM, n = 1.08 ± 0.07, R^2 = 0.991, standard error of regression = 0.034. The residuals of the fits (for quercetin, EGCG and ECG data) are plotted beneath the inhibition plot. **C,** Ordinate: 3MG uptake in mmol/L cell water/min. Abscissa: Concentration of inhibitors in μM (expressed in log scale). Results are shown for CB-treated cells (○), and CB-treated cells plus 2 μM quercetin (●), 20 μM EGCG (△), or 5 μM ECG (▲). Each data point represents the mean ± SEM of at least 3 duplicate measurements. The curves drawn through the data points were computed by nonlinear regression using equation 3.1 and have the following results: CB only treatment (○): $K_{i(app)}$ = 0.240 ± 0.003 μM, R^2 = 0.936, standard error of regression = 0.007; CB + 2 μM quercetin treatment (●): $K_{i(app)}$ = 0.619 ± 0.175 μM, R^2 = 0.831, standard error of regression = 0.004; CB + 20 μM EGCG treatment (△): $K_{i(app)}$ = 0.619± 0.123 μM, R^2 = 0.897, standard error of regression = 0.004; CB + 5 μM ECG treatment (▲): $K_{i(app)}$ = 0.713 ± 0.119 μM, R^2 = 0.941, standard error of regression = 0.002.

3.4B). The analysis produces better fits with residuals that do not deviate from zero and the standard error of the residuals is significantly reduced. The analysis indicates that quercetin, EGCG, ECG and CB interact with 1.53 ± 0.14, 1.51 ± 0.16, 0.75 ± 0.08 and 1.08 ± 0.07 sites per CB binding site respectively with inhibitory constants of 0.89 ± 0.14, 21.75 ± 7.80, 1.34 ± 0.30 and 0.17 ± 0.02 μM respectively (figure 3.4B).

To further test the effects of flavonoids on CB binding to erythrocyte GLUT1, we measured the concentration dependence of CB inhibition of 3MG (0.1 mM) uptake ± flavonoids in human red cells. The presence of quercetin (2 μM), EGCG (20 μM) or ECG (5 μM) increases the $K_{i(app)}$ for CB inhibition of 3MG uptake by at least 2.5-fold (figure 3.4C). Assuming simple competition between the flavonoids and CB for binding to GLUT1 (but see figure 3.4B), the computed $K_{i(app)}$ for quercetin (2 μM), EGCG (20 μM) and ECG (5 μM) inhibition of CB inhibition ($K_{i(app)}$ = 0.24 ± 0.03 μM) of transport are 1.88 ± 0.33, 9.63 ± 1.95 and 1.90 ± 0.32 μM respectively. These results indicate that exofacial inhibitors impair CB binding to the GLUT1 endofacial sugar binding site and thereby reduce the potency of CB inhibition of sugar transport.

Quercetin does not cross the cell membrane via a GLUT1-dependent pathway

To act as potent cytoplasmic antioxidants, the flavonoids must first cross the cell membrane. Previous studies have suggested that dietary flavonoids permeate cell membranes both by protein-independent transbilayer diffusion (248,249), and via carrier proteins, including GLUT1, GLUT4, SGLT1 and MCT (198,235,250-252). If GLUT1 transports quercetin, as suggested by Cunningham et al (198), [^{3}H]-quercetin uptake by human erythrocytes should be inhibited by high concentrations of CB (figure 3.5A). CB (20 μM) almost completely inhibits [^{3}H]-3MG uptake, but is without effect on [^{3}H]-quercetin

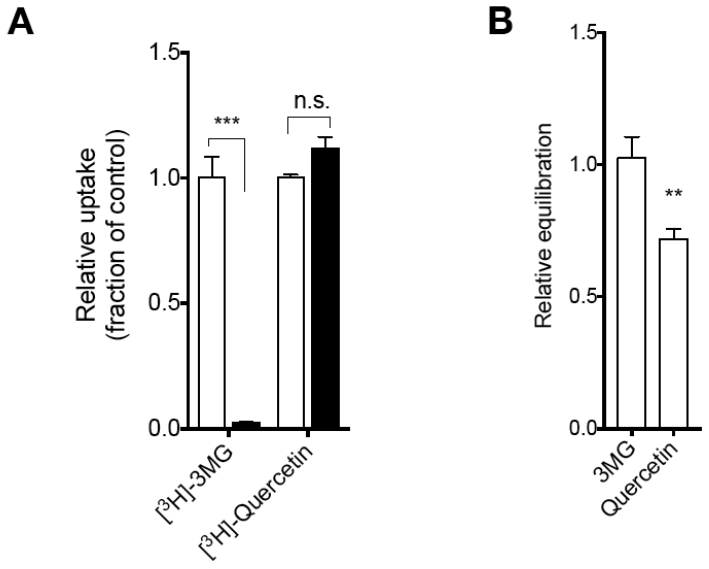

Figure 3.5: Quercetin is not transported by GLUT1

A, Effect of CB on [^{3}H]-quercetin and [^{3}H]-3MG uptake by human erythrocytes. Ordinate: Relative substrate uptake. Abscissa: Radiolabeled substrate. Results are shown for control (□) and 20 µM CB-treated cells (■). Each bar represents the mean ± S.E.M of 3 separate experiments measured in duplicates. Analysis by unpaired t test indicates: ***, significant [^{3}H]-3MG uptake inhibition by CB ($p < 0.0005$), n.s., no significant difference in [^{3}H]-quercetin uptake with or without CB treatment ($p > 0.05$). **B,** Relative [^{3}H]-3MG and [^{3}H]-quercetin spaces of RBCs. Ordinate Equilibration relative to the equilibrated 3MG space of the cell. Time course analysis indicates that [^{3}H]-quercetin achieves equilibrium uptake within 5 minutes of exposure to cells. Each bar represents the mean ± S.E.M of 3 separate experiments measured in duplicates. Analysis by unpaired t test indicates: **, significant difference between the 3MG and quercetin cell volume ($p = 0.0044$).

influx into human RBCs (figure 3.5A). Analysis of [^{3}H]-quercetin binding normalized to the RBC equilibrium 3MG space (i.e. accessible cell water) reveals that quercetin achieves up to 70% equilibration with human RBC cell water (figure 3.5B).

Molecular docking of quercetin, EGCG and ECG to GLUT1

We investigated potential interactions of ß-D-glucose, quercetin, EGCG and ECG with the exofacial sugar binding site by molecular docking using a homology modeled GLUT1 outward-open (GLUT1e2) structure (120). The exofacial, interstitium-exposed cavity of GLUT1e2 presents 3 potential ß-D-glucose docking sites – peripheral, intermediate and core (120,239). Benzene ring A (figure 3.1A–D) in quercetin, EGCG and ECG overlaps with the proposed core ß-D-glucose docking site (ref. (239); and figure 3.6A–D) while benzene ring B in quercetin interacts with intermediate and peripheral sites via hydrogen bonding and/or hydrophobic interactions (figure 3.6B). In EGCG and ECG, benzene ring B is flipped 45º, and makes additional interactions with core ß-D-glucose docking site, while their gallate group overlaps with the intermediate ß-D-glucose docking site (figure 3.6C & D).

The residues contributing to ß-D-glucose docking at core, intermediate, and peripheral ß-D-glucose have been previously described (239). Figure 3.6E–H illustrates the putative hydrogen bond and hydrophobic contacts of core ß-D-glucose, quercetin, EGCG and ECG with GLUT1-e2. All ligands form 5 common hydrophobic interactions (Ile164, Val165, Ile168, Phe291 & Phe379), and 1 hydrogen bond interaction at Glu380 (figure 3.6E-H). Additionally, each inhibitor forms hydrogen bonds with Asn34 and Gln283 (figure 3.6F–H), but quercetin forms 3 additional hydrogen bonds (Gln283, Glu380 and Asn415; figure 3.6F). EGCG and ECG form more hydrophobic contacts with GLUT1-e2 than does

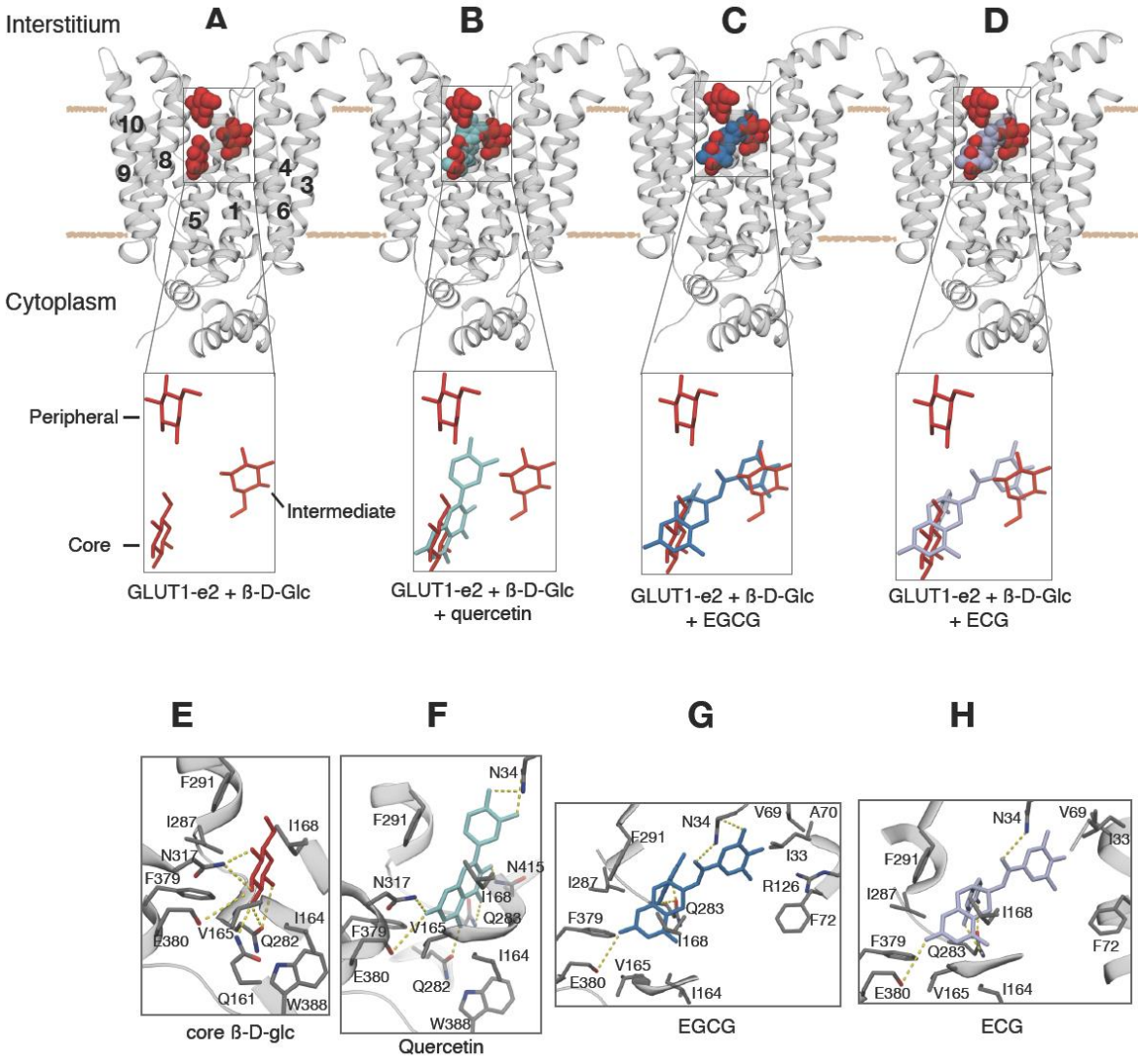

Figure 3.6: Molecular docking of ß-D-glucose, quercetin, EGCG and ECG to homology-modeled exofacial GLUT1 conformation

A–D, Homology-modeled exofacial GLUT1 (hm-GLUT1-e2) is shown in cartoon representation, and membrane spanning helixes are indicated. Ligands – peripheral, intermediate and ß-D-glucose (red); quercetin (cyan); EGCG (sky blue); ECG (light blue) – are shown as spheres complexed with hm-GLUT1-e2, and as sticks in the zoomed in sections. **E–G,** Interactions between ligands and hm-GLUT1-e2, showing residues that form hydrogen bonds and hydrophobic interactions. Color scheme is the same as in A–D, and hydrogen bonds are represented by yellow dashed lines.

quercetin (figure 3.6G & H).

Isoform specificity of transport inhibition

Neuronal GLUT3, and the insulin-sensitive GLUT4 share 93% and 85% sequence similarity with GLUT1 respectively (29). We therefore asked if $K_{i(app)}$ for quercetin, EGCG and ECG inhibition of GLUT3 and GLUT4 resemble $K_{i(app)}$ for their inhibition of GLUT1 or if they present an unanticipated selectivity towards these proteins. We stably expressed hGLUT1, hGLUT3 or hGLUT4 into HEK293 cells and assayed for the dose-dependent inhibition of 100 μM 2-deoxy-D-glucose uptake (2DG) at 37 ºC. Quercetin, EGCG and ECG inhibit GLUT1-, GLUT3- and GLUT4-mediated 2DG uptake in HEK-293 cells (figure 3.7A–C). $K_{i(app)}$ for quercetin-inhibition of GLUT1, GLUT3 and GLUT4 are 2.00 ± 0.98, 17.68 ± 1.71 and 1.70 ± 0.25 μM respectively, suggesting that quercetin may have reduced affinity for GLUT3 relative to GLUTs 1 and 4. $K_{i(app)}$ for EGCG-inhibition of GLUT1, GLUT3 and GLUT4 are 9.09 ± 4.99, 14.44 ± 8.19 and 8.45 ± 5.47 μM respectively, suggesting that EGCG may interact with GLUTs 1, 3 and 4 with similar affinities. Analysis of ECG inhibition of transport does not converge as successfully because these experiments demonstrate significant allosteric activation of transport at subsaturating inhibitor concentration. Assuming simple saturable inhibition of transport, $K_{i(app)}$ for ECG-inhibition of GLUT1, GLUT3 and GLUT4 are 22.7 ± 17.3, 199.4 ± 333.4 and 126.2 ± 106.3 μM respectively. The large errors associated with these estimates indicate that additional measurements are needed to confirm any suggested isoform-specific differences in affinity for ECG.

Docking of quercetin, EGCG and ECG to exofacial GLUT3 and GLUT4 reveal that these ligands coordinate with equivalent residues when docked to the same GLUT isoform, but

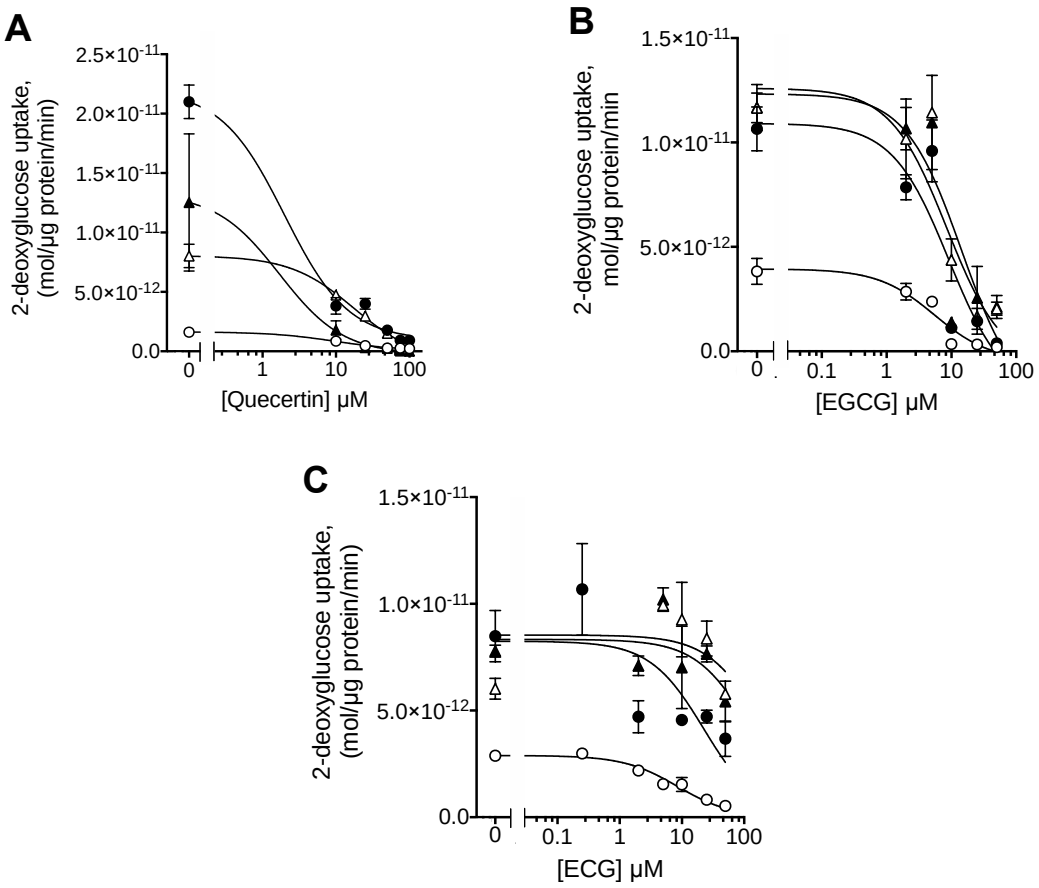

Figure 3.7: Isoform specificity of sugar transport inhibition by quercetin, EGCG and ECG

Results are shown for transport inhibition by quercetin (**A**), EGCG (**B**) and ECG (**C**), in untransfected (○), and in transfected HEK293 cell stably expressing hGLUT1 (●), hGLUT3 (△), or hGLUT4 (▲). Ordinate: 2–deoxyglucose uptake in mol/µg protein/min; Abscissa: inhibitor concentration in µM (axis shown in log scale). The curves drawn through the data points were computed by nonlinear regression using equation 3.1, with results shown in table 3.1.

Table 3.1: Inhibition of GLUT1-, GLUT3- and GLUT4-mediated 2DG uptake in HEK293 cells by quercetin, EGCG and ECG

R^2 for quercetin and EGCG fits was ≥ 0.729, while R^2 for ECG was 0.200 – 0.976. Standard error of regression for all fits was ≥ 4.25×10^{-14}

	$K_{i(app)}$, µM			
Inhibitor	**UTF**	**GLUT1**	**GLUT3**	**GLUT4**
Quercetin	9.59 ± 1.42	2.00 ± 0.99	17.68 ± 1.71	1.70 ± 0.25
EGCG	5.49 ± 1.86	9.09± 4.99	14.44 ± 8.19	8.45 ± 5.47
ECG	5.52 ± 1.84	22.7 ± 17.3	199.4 ± 333.4	126.2 ± 106.3

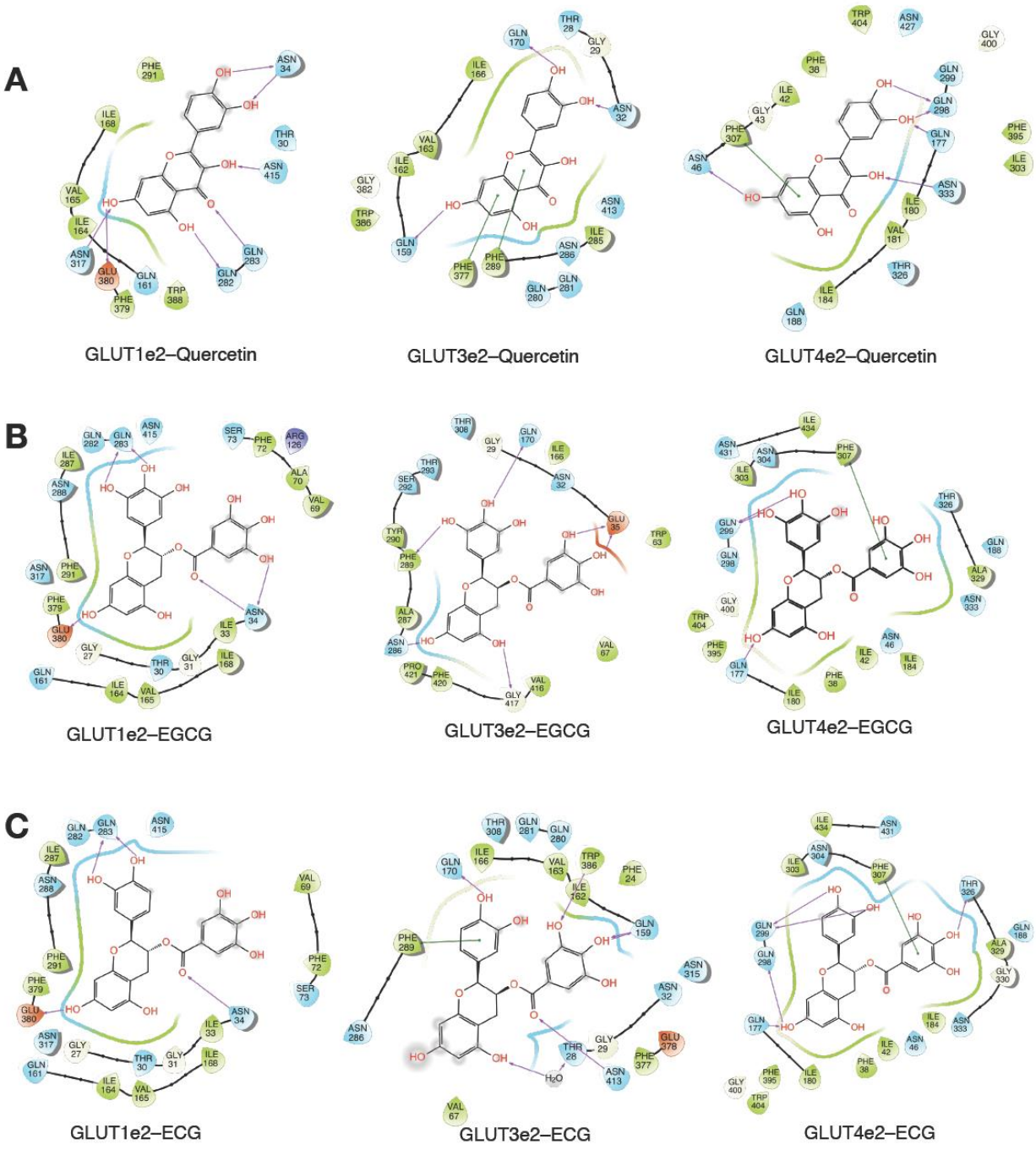

Figure 3.8: 2-dimensional representation of ligands interactions with hm-GLUT1-e2, GLUT3-e2 and hm-GLUT4-e2 interactions

Residues within 4Å distance to docking ligand are shown for quercetin (**A**), EGCG (**B**) and ECG (**C**). Residues and contacts are shown in the following color codes: Polar, blue; hydrophobic, green; negatively charged, orange; positively charged, violet; hydrogen bond; purple arrow.

differ significantly when their interactions are compared across GLUT1, GLUT3 and GLUT4 (figure 3.8).

Discussion

The major dietary flavonoids in red wine and green tea inhibit the facilitative glucose transporter, GLUT1, by interacting with its exofacial sugar binding site. Quercetin, EGCG and ECG competitively inhibit net sugar uptake by human erythrocytes but are noncompetitive inhibitors of sugar exit from cells. This finding is supported by homology modeling and molecular docking studies which reveal that quercetin, EGCG and ECG overlap with extracellular D-glucose for binding to GLUT1. Additionally, we show that quercetin does not cross cell membranes via a GLUT1-dependent pathway.

Our data on the sidedness of action of quercetin, EGCG and ECG are consistent with previous reports suggesting that quercetin (236,246), and EGCG (199) compete with extracellular glucose for binding to the exofacial sugar binding site of GLUT1. Consistent with this conclusion, quercetin, EGCG and ECG all dock within the same binding pocket in the central cavity of GLUT1-e2 overlapping with the previously defined core ß-D-glucose docking site ((239), and figure 3.6), and form hydrogen bonds and/or hydrophobic interactions with the intermediate and peripheral ß-D-glucose docking sites. ß-D-glucose coordination by our homology model of GLUT1-e2 involves the same residues as those reported in the ß-D-glucose-bound human GLUT3-e2 crystal structure (30), lending further support to the present molecular docking analyses. Core ß-D-glucose, quercetin, EGCG and ECG all form hydrophobic interactions with Ile164, Val165, Ile168, Phe291 and Phe379; and hydrogen bonds with Glu380, suggesting that these residues are important for exofacial ligand binding to GLUT1.

Quercetin and ECG inhibit GLUT1 with a $K_{i(app)}$ of ~ 2 µM but EGCG ($K_{i(app)}$ ~ 10 µM) has a 5-fold lower inhibitory potency. There are no striking differences in the docking of EGCG and ECG to GLUT1-e2 that explain the difference in potency. It is not surprising that EGCG and ECG interact with the same residues in GLUT1-e2, since their chemical structures are almost identical (the only difference is the presence of a hydroxyl group at C3' in EGCG, which is absent in ECG). According to our docking analysis, C3'–OH is not involved in EGCG interaction with GLUT1. The similarity in computed ECG–GLUT1 and EGCG–GLUT1 interactions stands in contrast to the 5-fold greater transport inhibitory potency of ECG versus EGCG (figure 3.1E) and serves to emphasize the current limitations of docking analysis.

Consistent with previous equilibrium CB binding studies exploring the effects of extracellular maltose on CB binding (118,124), exofacial quercetin, EGCG or ECG, inhibit intracellular binding of CB to GLUT1. $K_{i(app)}$ for inhibition of CB binding is 1.6 – 3 fold lower than $K_{i(app)}$ for transport inhibition. This is not explained by competition between inhibitor and transported sugar for binding to the exofacial site because saturation of GLUT1 by 0.1 mM 3MG is less than 5% ($K_{m(app)}$ for 3MG = 2.4 mM; see figure 3.2A). Curve fit analysis indicates that Sy.x (square root of the sum of the squared residuals, divided by the number of measurements-number of fitted parameters) for nonlinear fits to equation 3.4 are poor (0.04 - 0.1). Fitting the data to a model comprising multiple cooperative binding sites (equation 3.5) produces significantly better fits (figure 3.4B; Sy.x = 0.03 - 0.08). These results suggest that GLUT1 presents at least 2 positively cooperative binding sites each for quercetin and EGCG and, because Hill analysis revealed $n < 1$ for ECG, two or more negatively cooperative binding sites for ECG. Our docking analyses do not reveal the possibility of a second binding site for these ligands in GLUT1-e2, suggesting that the

cooperativity effects observed with these ligands is due to GLUT1 oligomerization.

We considered the possibility that the flavonoids also compete directly with CB for binding at the endofacial sugar binding site. This would explain their competitive displacement of CB from GLUT1 and would also be consistent with previous demonstrations of cooperativity between endofacial ligand binding sites present on adjacent GLUT1 subunits forming the membrane-resident GLUT1 tetramer (115,121,122,124). Molecular docking of CB and quercetin to the endofacial orientation of GLUT1 (GLUT1-e1; (28)) supports the hypothesis that CB and quercetin could compete for high affinity binding to GLUT1 (not shown). However, inhibition of transport by a molecule that can bind with equal avidity to both exo- and endofacial sugar binding sites should produce noncompetitive inhibition of both net uptake or net exit (reduced V_{max}) and competitive inhibition of equilibrium-exchange transport (117,118). Flavonoid inhibition of net uptake is, however, observed to be competitive (figure 3.2A). If such an inhibitor were to bind with 500-fold lower affinity to the endofacial binding site versus the exofacial site, it would increase $K_{m(app)}$ for net sugar uptake but V_{max} for uptake would also be reduced by > 65% (117,118) and this is not observed. This complex cooperativity (positive and negative) in flavonoid inhibition of CB binding to GLUT1 reinforces the conclusion that analyses of ligand binding to GLUT1 which assume simple, saturable equilibrium binding represent a significant oversimplification of the behavior.

The actions of the flavonoids on GLUT1-mediated sugar transport demonstrate an additional form of cooperativity which we have termed cis-allostery (120). Quercetin, EGCG and ECG, like other exofacial GLUT1 inhibitors (e.g WZB117; (239) and maltose (122)), stimulate GLUT1-mediated sugar uptake at low inhibitor concentrations then inhibit

transport as their concentration is raised further. This observation reinforces the idea that GLUT1 presents at least 2 exofacial ligand binding sites at any given time (122,124). Binding of ligand at a high affinity site stimulates glucose uptake via a catalytic sugar binding site. As ligand concentration is then raised further, ligand and sugar now compete for binding at the active site and transport is inhibited.

Inhibition of GLUT1 by high flavonoid concentrations ($\geq$ 2 µM for quercetin and ECG; $\geq$ 10 µM for EGCG) could explain, at least in part, the anticancer action of flavonoids. GLUT1 inhibition studies have demonstrated that small molecule inhibition of GLUT1 results in a cascade of downstream events including downregulation of glycolytic enzymes, cell cycle arrest, and ultimately, cell death (165). Whereas, stimulation of GLUT1-mediated glucose uptake by low concentrations of flavonoids ($\leq$ 0.5 µM for quercetin and ECG; $\leq$ 2.5 µM for EGCG), could explain the protective effects of flavonoids against diseases, such as diabetes (253-255) and neurodegenerative diseases (256-259), where enhanced glucose uptake from the blood could be ameliorative.

Flavonoids have been shown to modulate several cellular targets including MAP kinase, CDKs, HIF-1α, and vimentin (260). Whether flavonoids interact directly or indirectly with their cytoplasmic targets is still unclear. There are suggestions, however, that flavonoids may not readily cross the plasma membrane, with studies showing that less than 1% of orally-ingested flavonoids make it into the bloodstream (261). It has been proposed that flavonoids are transported into cells by carrier proteins including SGLT1(251,252,262,263), MCT(250), GLUT1(198) and GLUT4 (235), while others have suggested that flavonoids interact with membrane phospholipids to cross cell membranes (248,249). This current study indicates that, while quercetin may cross the plasma

membrane, it does so via a GLUT1-independent pathway. This is contrary to the conclusion by Cunningham *et. al.* (198) that quercetin is transported into cells by GLUT1, but is consistent with the failure of GLUT1 inhibitors, phloretin (in their study; (198)), and CB (figure 3.5A) to inhibit quercetin uptake.

Our isoform specificity data reveal that quercetin, EGCG and ECG also inhibit GLUT3 and GLUT4. Quercetin inhibits GLUT1 and GLUT4 with similar avidity but is up to 9-fold less potent against GLUT3. EGCG shows similar inhibitory potency towards GLUT1, GLUT3 and GLUT4. The inhibitory concentrations obtained for quercetin and EGCG inhibition of GLUT1 in HEK293 cells are identical to those observed in human erythrocytes. ECG, however, inhibits sugar uptake in GLUT1-expressing HEK293 cells with a $K_{i(app)}$ that is 10-fold greater than that observed in human erythrocytes, and is 5 – 8 times less potent against GLUT3 and GLUT4 expressed in HEK293 cells. The disparity between the $K_{i(app)}$ for ECG inhibition of GLUT1 in human red blood cells versus HEK293 suggests a reduction in the effective concentration of ECG available for inhibiting GLUT1 in HEK293 cells probably because ECG interacts with other unknown targets more readily than GLUT1. Molecular docking supports the hypothesis that the flavonoids interact with equivalent amino acid residues when docked to the same GLUT isoform. However, when the docking of each ligand is compared across GLUT1, GLUT3 and GLUT4, there are significant differences in the interacting residues, which may account for the different inhibitory potencies observed, at least, for quercetin and ECG.

In addition to uncovering the mechanisms of dietary flavonoids inhibition of GLUT1, this study provides valuable insights into the mechanisms of GLUT1-mediated sugar transport. The two main mechanisms for proposed for how GLUT1 functions are: 1) the simple,

alternating access transporter (AAT) model, and 2) the fixed site transporter (FST) model. The AAT model argues that GLUT1 alternately presents exofacial and endofacial sugar binding sites but cannot present both simultaneously. The AAT model is supported by the recent crystal structures of human GLUT1 and GLUT3 which have captured monomeric GLUTs in the inward-open, outward-open, or outward-occluded conformations, clearly showing that these carriers alternate between the outward-facing and inward-facing conformations. Sugar transport studies, however, show that GLUT1 functions as a more complex transporter than is predicted by the AAT model, with the ability to simultaneously present exofacial and endofacial sugar binding sites, as predicted by the FST model (116,118,121,122,124,205,264,265).

A current model proposed by our group (120,239,266) reconciles the structural data (supporting the AAT model) and biochemical and sugar transport studies (which support the FST model), and views GLUT1 as an oligomeric complex of allosteric alternating access subunits. This idea is supported by the following observations made in this study: 1) Cis-allostery: as with other exofacial GLUT1 inhibitors such as maltose and WZB117, low concentrations quercetin, EGCG and ECG stimulate human erythrocyte sugar uptake, followed by sugar transport inhibition as inhibitor concentration increases. 2) Trans-allostery: the inhibition of CB binding and CB inhibition of sugar transport by these agents suggest inter-subunit interactions in GLUT1 where the binding of exofacial ligands at the cis side interfere with the binding of endofacial CB at the trans side of the membrane. This trans-allostery observation is consistent with previous studies that show that low concentrations of the exofacial inhibitors, maltose and ethylidene glucose, stimulate CB binding at the endofacial sugar binding site of human erythrocytes but higher concentration inhibit CB binding (116,124). These results, however, could also be

interpreted to support the monomeric AAT model, by arguing that quercetin, EGCG, and ECG, by trapping GLUT1 in the exofacial, outward conformation, competitively inhibit CB binding to the endofacial, inward-conformation. This interpretation is, however, improbable for several reasons. 1) We observe multiple cooperative binding sites for flavonoids as evidenced by transport stimulation followed by transport inhibition and, 2) Multiple cooperative, flavonoid binding sites are also evidenced by inhibition of CB binding where quercetin and EGCG binding to GLUT1 displays positive cooperativity whereas ECG and WZB117 binding displays negative cooperativity. Another interpretation of these findings is that quercetin, EGCG and ECG inhibit sugar transport and CB binding by entering the cell and interacting with the GLUT1 endofacial sugar binding site. If this were true, these ligands should function as noncompetitive inhibitors of zero-trans sugar uptake and as competitive inhibitors of sugar exit from cells. Future experiments should extend these dose response studies of cytochalasin B binding to much lower concentrations of quercetin, EGCG and ECG to determine whether subsaturating levels of these exofacial ligands, as with the exofacial ligand maltose (124,247) and the endofacial ligand families of cytochalasins and forskolins (121,122), enhance cytochalasin B binding to GLUT1.

Chapter IV

Preface

Chapter IV of this dissertation will be submitted for publication as:

Ojelabi, O. A., Lloyd, K. P., De Zutter, J. K., and Carruthers, A. (2017) Highly potent GLUT1 inhibitors, BAY-876 and NV-5440, inhibit human erythrocyte glucose transport by binding at the GLUT1 endofacial glucose binding site

Author contributions: OAO and AC designed experiments, analyzed results and co-wrote the manuscript. OAO conducted all experiments except isoform specificity of transport inhibition. KPL contributed to the molecular docking studies. JKD conducted experiments on the isoform specificity of transport inhibition

Navitor Pharmaceuticals provided the Navitor compounds (NV-5440, NV-5770, NV-5902, NV-5981, NV-6091 and NV-6346), and funded the Navitor compounds project. I would especially like to acknowledge Drs. Sengupta, Saiah and Vlasuk for their support and encouragement.

Highly potent GLUT1 inhibitors, BAY-876 and NV-5440, inhibit human erythrocyte glucose transport by binding at the GLUT1 endofacial glucose binding site

Introduction

Altered glucose metabolism is a hallmark of cancer, manifesting as abnormally elevated expression of the glucose transporter (GLUT) proteins and accelerated aerobic glycolysis (267,268). The reprograming of glucose metabolism to favor aerobic glycolysis over mitochondrial oxidative phosphorylation (Warburg effect) in cancer cells was first reported by Warburg more than 90 years ago (188,269). Warburg was convinced that this effect resulted from dysfunctional mitochondria in cancer cells, and that this underlies the generation of tumors. However, it is becoming increasingly clear that the Warburg effect, rather than being the cause, is in fact a consequence of cancer.

Cancer cells rely heavily on glucose transport, not only for ATP production, but also to generate biomass, including amino acids, DNA and RNA precursors, as well as NADPH, needed to support the rapidly proliferating tumor cells (270,271). Unlike cancer cells, normal cells, in the presence of oxygen, catabolize glucose by glycolysis and oxidative phosphorylation to produce a net total of 36 molecules of ATP compared to 2 ATP molecules generated in cancer cells through aerobic glycolysis. While completely breaking down glucose to CO_2 and water appears to be the most efficient way to generate energy from glucose, this process burns up the carbons in glucose which is critical for metabolite synthesis in rapidly proliferating cancer cells (7). To compensate for diminished ATP production, cancer cells upregulate the expression of glucose transporters, especially GLUT1, as well as the glycolytic enzymes (268). Consequently, cancer cells are more

sensitive to glucose deprivation than normal cells, and restricting glucose supply will force tumor cells to halt proliferation and ultimately die.

An emerging anticancer strategy is to develop therapeutics targeting glycolysis and glucose transport. Several inhibitors of glycolytic enzymes have been reported (reviewed in (268)). Similarly, many structurally unrelated compounds have been reported to inhibit GLUT1. These include: WZB117 (165) (an exofacial inhibitor of GLUT1 (239)), STF-31 (166), GLUT-i1 and GLUT-i2 (29) (endofacial GLUT1 inhibitors (29)) and BAY-876 (167). Most recently, Navitor Pharmaceuticals developed a novel class of GLUT1 inhibitors, referred to here as NV-5440 series. BAY-876 and NV-5440 as well as its analogs, are benzonitrile-containing compounds, whose mechanisms of GLUT1 inhibition have not been reported.

A vital part of the on-going development of these anticancer agents, is to understand how they interact with, and inhibit GLUT1, as this will ultimately aid in optimizing drug design and delivery. This present study explores how BAY-876 and NV-5440 inhibit GLUT1-mediated glucose transport.

We show that BAY-876 and NV-5440 inhibit GLUT1 by interfering with glucose binding to the endofacial sugar binding site. They, thus act as competitive inhibitors of glucose exit from cells, but are noncompetitive inhibitors of net glucose uptake. Additionally, we show that benzonitrile groups in BAY-876 as well as in NV-5440 and its analogs confers more inhibitory potency to these compounds as compared to their analogs lacking the nitrile unit.

Methods

Reagents

Tritium-labeled 2-deoxy-D-glucose ([^{3}H]-2DG), 3-O-methylglucose ([^{3}H]-3MG) and cytochalasin B ([^{3}H]-CB) were obtained from American Radiolabeled Chemicals (St. Louis, MO). Unlabeled 3MG, CB, BAY-876, BAY-588 and phloretin were purchased from Sigma-Aldrich (St. Louis, MO). WZB117 was purchased from EMD Millipore (Billerica, MA). NV-5440 and its analogs were provided by Navitor Pharmaceuticals (Cambridge, MA).

Solutions

KCl medium contained 150 mM KCl, 5 mM HEPES, 0.5 mM EDTA, pH 7.4. Sugar transport stop solution contained 50 µM WZB117 and 100 µM phloretin in ice-cold KCl medium. RBC sugar uptake/exit medium contained 0 – 20 mM 3MG, [^{3}H]-3MG ± inhibitors. [^{3}H]-CB–binding medium contained 40 nM [^{3}H]-CB and 10 µM cytochalasin D in KCl medium.

Cells

De-identified whole human blood was purchased from Biological Specialty Corporation (Colmar, PA). HEK293 cells heterologously expressing human GLUT1, GLUT3 or GLUT4 were made as previously described (97,123). HEK293 cells were maintained in Dulbecco's modified Eagle's medium (DMEM) supplemented with 10% fetal bovine serum, 100 units/mL penicillin, and 100 µg/mL streptomycin in a 37 °C humidified 5% CO_2 incubator.

Red blood Cell Sugar Transport and Ligand Binding Measurements

All human RBC sugar transport and ligand binding experiments were performed at 4 ºC as previously described (204,205,239). Glucose-depleted RBCs were incubated in 37.5 – 400 volumes of ice-cold KCl medium ± inhibitors at 4 ºC for 15 minutes before measurements.

Zero-trans Uptake: Zero-trans glucose–depleted RBCs were incubated in 400 volumes of ice-cold KCl medium ± inhibitors for 15 minutes. [^{3}H]-3MG uptake into sugar–lacking cells was performed by adding 100 µL of uptake medium ± inhibitor to 10 µL of sugar-depleted, 50% hematocrit (Ht) red cells, for 30 seconds at 4 ºC. Uptake was stopped by adding 1 mL of ice-cold stop solution. Cells were washed in stop solution, lysed in 3% perchloric acid, and radioactivity was measured in clarified lysates by liquid scintillation counting.

Zero-trans Exit: Glucose-depleted, packed RBCs were loaded with 10 mM 3MG (containing 1 µCi [^{3}H]-3MG/mL of cold 3MG) at 37 ºC as previously described (239). 3MG–loaded cells were transferred to 4 ºC and incubated with or without inhibitors for 15 minutes. Cell suspension was spun at 10,000 x g for 1 min, and supernatant discarded. 500 µL of sugar-loaded RBCs were added to 25 mL of KCl medium ± inhibitor on a shaker with magnetic stirrer. 2 x 500 µL aliquots of the suspension were withdrawn at indicated time intervals, and immediately added to 1 mL ice-cold stop solution. Cells were washed again in stop solution, lysed in 3% perchloric acid and radioactivity was measured in clarified lysates in duplicates.

Equilibrium CB Binding: CB binding to human erythrocytes was performed as previously described with slight modifications (116,239). Briefly, 1 volume of sugar-depleted packed

RBCs was incubated with 400 volumes of ice-cold KCl medium ± 2x of desired [inhibitor] for 15 minutes. Cells were spun at 10,000 x g for 1 min and 1 volume of cells was resuspended in 2x of desired [inhibitor], to make 50% hematocrit (Ht) red cells. 1 volumes of 50% hematocrit (Ht) red cells was mixed with 1 volume of ice-cold [^{3}H]-CB–binding medium and incubated at 4 ºC for 15 minutes, with constant mixing. For Total [CB] 2 x 10 µL of the cell suspension were withdrawn from tube and lysed in 100 µL of 3% perchloric acid, and radioactivity measured in duplicates. For free [CB], cell suspension was centrifuged at 20,000 x g for 1 minute, and 2 x 10 µL of clarified supernatant were assayed for radioactivity. Bound [CB] was estimated as Total [CB] – Free [CB].

HEK-293 Cell Sugar Uptake

All HEK293 cell sugar uptake measurements were performed at 37 ºC, using 100 µM 2-deoxyglucose (2DG plus [^{3}H]-2DG) as described previously (97,143).

Homology Modeling

The crystal structure of inward-open (e1) human GLUT1 (hGLUT1-e1; 4PYP) (28) was obtained from the RCSB protein databank (http://www.rcsb.org/pdb/home/home.do). Homology models of the e1 conformations of GLUT3 and GLUT4 were generated based on the crystal structure of hGLUT1-e1. Sequence alignments were generated using ClustalX (240). Homology models were built using Modeller-9.9 (241) and analyzed using PROCHECK (242).

Stochastic docking

Docking was performed using the Schrodinger software suite. Chemical structure for β-D-

glucose, BAY-876, BAY-588, NV-5440 (and its analogs) were drawn using the 2D sketcher of the Schrodinger software suite. Protein structures were preprocessed with the Protein Preparation Wizard, using default settings, and the system was energy minimized using the OPLS 2005 force field. Ligand structures were prepared with the LigPrep module and the pKa of the ligands was calculated using the Epik module. Grids for docking were mapped using the CastP server (http://sts.bioe.uic.edu/castp/) and the grid generation feature of the Schrodinger suite. Molecular docking was performed by the GLIDE module in standard-precision (SP) mode using default settings with no restraints.

Data analysis

Analyses of data and statistical tests were performed using GraphPad Prism (Version 7.0c; La Jolla, CA).

Michaelis-Menten inhibition of sugar transport is described by:

$$V = V_c - \frac{V_c[I]}{K_{i(app)} + [I]} \qquad \text{(equation 4.1)}$$

where V_c is V measured in the absence of inhibitor I, [I] is the concentration of inhibitor and $K_{i(app)}$ is that [I] producing 50% inhibition of uptake.

Sugar transport inhibition by analogs of BAY-876 and NV-5440 was estimated by:

$$Rel\ K_{i(app)} = \frac{(V_i/V_c)[I]}{1 - (V_i/V_c)} \qquad \text{(equation 4.2)}$$

where Rel $K_{i(app)}$ is the $K_{i(app)}$ of inhibitor relative to BAY-876 or NV-5440, V_c is V measured in the absence of inhibitor [I] and V_i is V measured in the presence of inhibitor

Michaelis-Menten sugar uptake is assumed to be described by:

$$V = \frac{V_{max}[3MG]}{K_{m(app)} + [3MG]} \qquad \text{(equation 4.3)}$$

where V_{max} is the maximum rate of 3MG transport, [3MG] is the concentration of 3MG and $K_{m(app)}$ is the [3MG] where the rate of uptake is $V_{max}/2$.

Sugar exit was analyzed by nonlinear regression analysis using Mathematica 10.4.1.0 (Wolfram Research) with the assumption that exit follows Michaelis-Menten kinetics and that the first derivative of the exit progress curve represents d[S]/dt at any given [S] (239).

Transport stimulation followed by inhibition by inhibitors was approximated first by normalizing all uptake to V_c and then using the following model:

$$\frac{V_i}{V_c} = \frac{K_1 + [I](K_2 + [I])}{K_1 + [I](K_3 + [I]K_4)} \qquad \text{(equation 4.4)}$$

where V_c is uptake measured in the absence of inhibitor I, V_i is uptake measured in the presence of inhibitor, [I] is the concentration of inhibitor and K_1 – K_4 are model dependent (120).

Inhibition of [^{3}H]-CB binding to GLUT1 by ligands was analyzed by simple competitive inhibition using the model:

$$\frac{[CB]_b}{[CB]_f} = \frac{K_{i(app)}(K_{CB} + [CB])}{[I]K_{CB} + K_{i(app)}(K_{CB} + [CB])} \qquad \text{(equation 4.5)}$$

where $[CB]_b$ = bound [CB], $[CB]_f$ = free [CB], $K_{i(app)}$ is the apparent inhibitory constant for inhibition of CB binding by inhibitor, I, and K_{CB} is dissociation constant for CB binding to GLUT1.

CB binding was also analyzed using a variation of Michaelis-Menten equilibrium binding kinetics in which the transporter is allowed to bind more than one molecule of competing ligand, I

$$\frac{[CB]_{(b/f)i}}{[CB]_{(b/f)c}} = 1 - \frac{K[I]^n}{K_I + [I]^n} \qquad \text{(equation 4.6)}$$

where $[CB]_{(b/f)I}$ = the ratio of bound to free [CB] measure in the presence of inhibitor I, $[CB]_{(b/f)c}$ = the ratio of bound to free [CB] measure in the absence of inhibitor, K is a number where $0 \leq K \leq 1$, K_I is $K_{d(app)}$ for I binding to GLUT1 and n is the number of inhibitor binding sites.

Results

Sensitivity of human erythrocyte sugar transport to BAY-876, NV-5440, and their analogs

GLUT1 is the quantitatively most abundant and sole significant glucose transport protein of the human erythrocyte, accounting for 10 – 20% of total plasma membrane protein content (197,272). To assess BAY-876 and NV-5440 as GLUT1 inhibitors, we tested their effects on zero-trans sugar uptake (influx into sugar-free cells) in freshly isolated human red blood cells. BAY-876 and NV-5440 inhibit the zero-trans uptake of 3MG (0.1 mM) by human erythrocytes in a dose-dependent manner with $K_{i(app)}$ of 13.15 ± 1.31 nM, and 12.74 ± 1.60 nM respectively (figure 4.1A). BAY-588, an analog of BAY-876, is marketed as an inactive control for BAY-876, for its purported lack of inhibition of GLUT1. However, figure 4.1B shows that BAY-588 inhibit GLUT1-mediated sugar uptake, although with ~ 50-fold less potency than BAY-876. We also tested the effects of 5 analogs of NV-5440 (NV-5770, NV-5902, NV-5981, NV-6091, and NV-6346) on 3MG uptake by human RBCs (figure

4.1C). $K_{i(app)}$ for NV-5440 analogs containing a benzonitrile group (just like NV-5440) ranged from 4.35 – 15.73 nM (figure 4.1C). However, replacing the benzyonitrile group by a benzaldehyde in NV-5981 increases its relative $K_{i(app)}$ by > 220-fold (figure 4.1C). Although BAY-588 ($K_{i(app)}$ = 0.58 µM) and NV-5981 ($K_{i(app)}$ = 2.9 µM) are much less potent than their respective parent analogs, they are still relatively decent inhibitors of GLUT1 as compared to other commercially available inhibitors of GLUT1 (e.g. cytochalasin B, $K_{i(app)}$ = 0.1 – 0.3 µM (117); WZB117, $K_{i(app)}$ = 0.23 – 10 µM (165,239)).

BAY-876 and NV-5440 are endofacial inhibitors of GLUT1

GLUT1 presents endofacial (e1) and exofacial (e2) sugar binding sites. Most known inhibitors of GLUT1 inhibit GLUT1-mediated glucose transport by competing with glucose for binding at either the e1 or e2 sugar binding site. We term ligands that bind GLUT1 at the e2 sugar binding site exofacial GLUT1 inhibitors, and ligands interacting at the e1 sugar binding site, endofacial GLUT1 inhibitors. The effects of exofacial and endofacial GLUT1 inhibitors on Michaelis-Menten kinetics of zero-trans sugar uptake (sugar influx into sugar-lacking cells) and zero trans sugar exit (sugar efflux into sugar-lacking medium) by human erythrocytes are well documented (104,117,118). Exofacial GLUT1 inhibitors increase the $K_{m(app)}$ for zero trans glucose uptake without affecting V_{max} for uptake, while endofacial inhibitors reduce V_{max} for uptake and are without effect on $K_{m(app)}$ for uptake. For zero trans glucose exit, exofacial GLUT1 inhibitors reduce Vmax with no change in $K_{m(app)}$, whereas endofacial inhibitors increase $K_{m(app)}$ for sugar exit without changing V_{max}. BAY-876 and NV-5440 reduce the V_{max} for zero trans 3MG uptake from 0.939 ± 0.044 mmol/L cell water/min (control) to 0.394 ± 0.029 mmol/L cell water/min (BAY-876) and

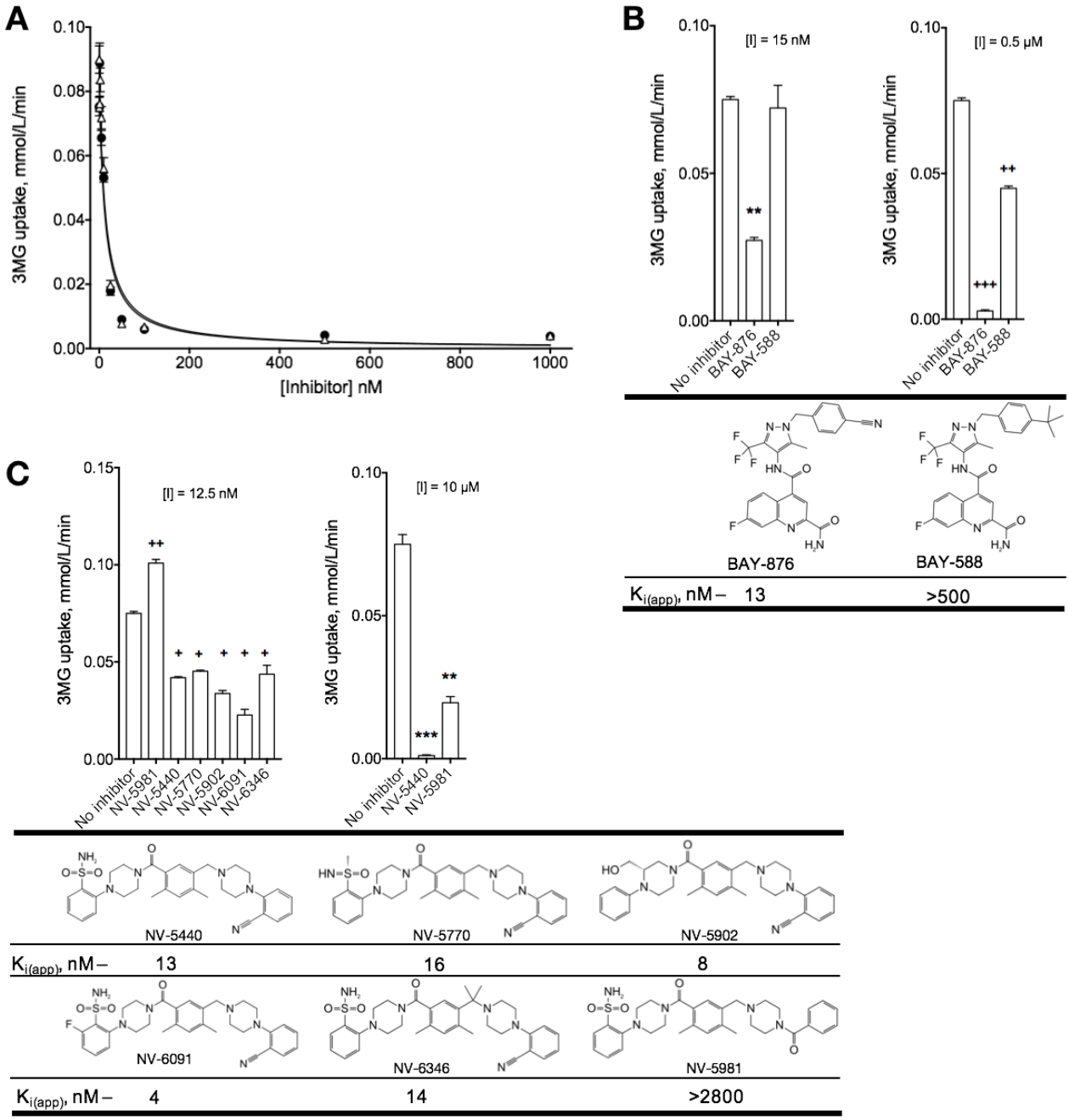

Figure 4.1: Sensitivity of human erythrocytes sugar transport to BAY-876, NV-5440, and their analogs

A, Concentration dependence of BAY-876 (△) and NV-5440 (●) inhibition of zero-trans 3MG (100 µM) uptake by human red blood cells. Ordinate: 3MG uptake in mmol/L cell water/min; Abscissa: [inhibitor] in nM. Each data point represents the mean ± SEM of duplicate measurements of at least 3 separate experiments. The curves drawn through the points were computed by nonlinear regression using equation 4.1, and with the assumption that sugar uptake is completely inhibited in a dose-dependent manner. The results are: BAY-876–treated cells (△): $K_{i(app)}$ = 13.15 ± 1.31 nM, R^2 = 0.905, standard error of mean = 0.011; NV-5440–treated cells (●): $K_{i(app)}$ =

12.74 ± 1.60 nM, R^2 = 0.926, standard error of mean = 0.009. **B & C,** Inhibition of human erythrocytes 3MG uptake by analogs of BAY-876 or NV-5440. Ordinate: 3MG uptake in mmol/L cell water/min; Abscissa: Inhibitors applied to cells. Each data point represents the mean ± SEM of 3 duplicate measurements. Relative $K_{i(app)}$, were calculated using equation 4.2. Relative $K_{i(app)}$ and chemical structures are shown for BAY-876 and its analog, BAY-588 (**B**), and NV-5440, and its analogs: NV-5770, NV-5902, NV-5982, NV-6091 and NV-6346 (**C**). Analysis was done by ordinary one-way ANOVA. **B,** Compared to control, **– significantly different at p = 0.0007; ++ & +++ – significantly different at p < 0.001. **C,** Compared to control, + – significantly inhibited uptake at p < 0.0001, ++ – significantly simulated uptake at p < 0.0001; ** & *** – significantly different at p < 0.0001.

0.544 ± 0.037 mmol/L cell water/min (NV-5440), but do not significantly affect $K_{m(app)}$ for uptake (figure 4.2A). Additionally, BAY-876, and NV-5440 increase $K_{m(app)}$ for exit from 14.3 mM (control) to 39.7 mM and 59.8 mM respectively, but are without effect on V_{max} for exit (figure 4.2B). These results support the hypothesis that BAY-876 and NV-5440 act as endofacial inhibitors of GLUT1.

Subsaturating concentrations of BAY-876, BAY-588 and NV-5440 stimulate sugar uptake by human erythrocytes

Previous studies have shown that both exofacial and endofacial inhibitors of GLUT1 stimulate erythrocyte sugar uptake at subsaturating concentrations, followed by inhibition of sugar uptake as inhibitor concentration is raised (120,122,124,239). In agreement with this observation, low concentrations of BAY-876 (0.01 nM), BAY-588 (≥ 0.1 μM), and NV-5440 (0.1 nM) significantly stimulate zero-trans 3MG uptake in red cells by up to 20% above untreated control cells ($p < 0.05$; figure 4.3). The ability of an endofacial GLUT1 ligand to stimulate, and then inhibit GLUT1-mediated sugar uptake strongly supports the idea that GLUT1 functions as an allosteric oligomeric carrier, simultaneously exposing 2 endofacial, and 2 exofacial ligand binding sites (120,122,124,239).

Molecular docking of ligands to endofacial GLUT1

Our sugar transport data revealed that BAY-876 and NV-5440 are 50 – 200 fold more potent than their respective analogs (BAY-588 and NV-5981) lacking the benzonitrile group. We docked these ligands to the crystal structure of the inward-open (e1) conformation of hGLUT1 (GLUT1-e1) (PDB code: 4PYP), to test if their interactions with GLUT1 would explain their different inhibitory potencies.

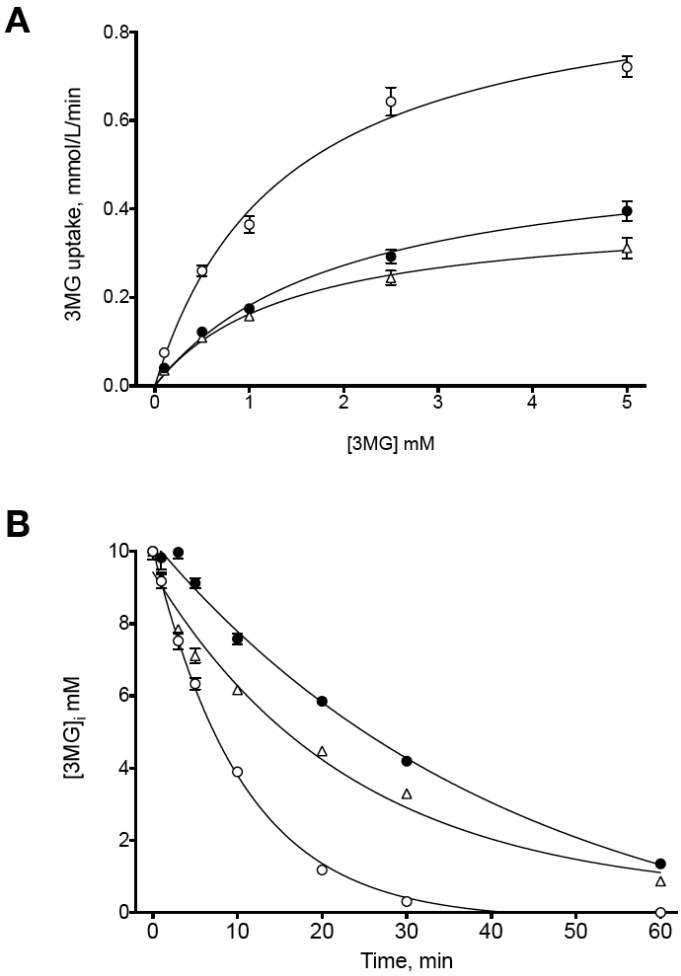

Figure 4.2: Effects of BAY-876 and NV-5440 on Michaelis-Menten kinetics of zero-trans 3MG uptake (A) and exit (B)

Results are shown for untreated control cells (○), BAY-876–treated cells (△) and NV-5440–treated cells (●). Each data point represents mean ± SEM of duplicate measurements of more than 3 separate experiments. **A,** Ordinate: 3MG uptake in mmol/L cell water/min; Abscissa: increasing concentration of 3MG in mM. Curves drawn through data points were computed by Michaelis-Menten uptake kinetics (equation 4.3), with the following results: Control (○): V_{max} = 0.939 ± 0.044 mmol/L cell water/min, $K_{m(app)}$ = 1.620 ± 0.198 mM, R^2 = 0.943, standard error of mean = 0.058; BAY-876 treatment (△): V_{max} = 0.394 ± 0.029 mmol/L cell water/min, $K_{m(app)}$ = 1.432 ± 0.276 mM, R^2 = 0.868, standard error of mean = 0.039; NV-5440 treatment (●): V_{max} = 0.544 ± 0.037 mmol/L cell water/min, $K_{m(app)}$ = 1.995 ± 0.305 mM, R^2 = 0.916, standard error of mean = 0.039. **B,** Ordinate: Concentration of intracellular 3MG in mM; Abscissa: 3MG exit time in minutes. Curves drawn through data points were computed by nonlinear regression and numerical integration assuming Michaelis-Menten exit kinetics as in equation 4.3. The results are: Control (○): V_{max} = 2.0 mmol/L cell water/min, $K_{m(app)}$ = 14.3 mM; BAY-876 treatment (△): V_{max} = 2.0 mmol/L cell water/min, $K_{m(app)}$ = 39.7 mM; NV-5440 treatment (●): V_{max} = 2 mmol/L cell water/min, $K_{m(app)}$ = 59.8 mM.

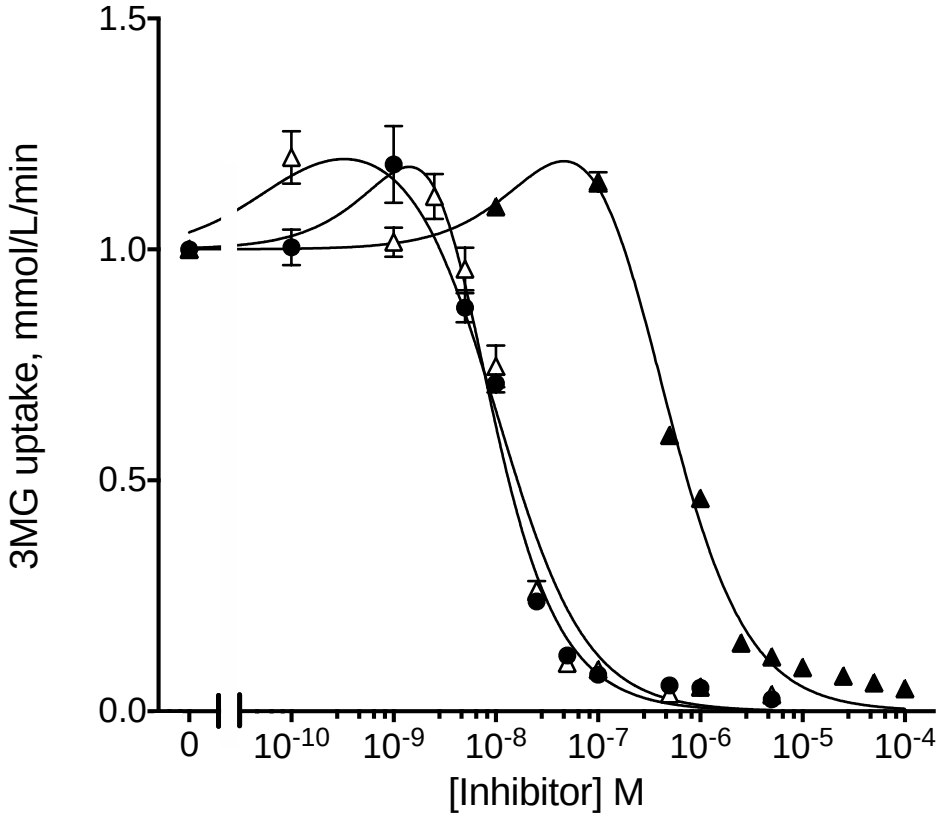

Figure 4.3: Low concentrations of BAY-876, BAY-588 and NV-5440 stimulate 3MG uptake

Ordinate: 3MG uptake in mmol/L cell water/min; Abscissa: [Inhibitor] in M, axis expressed in log scale. Results are shown for cells treated with increasing concentration of BAY-876 (△), BAY-588 (▲) and NV-5440 (●). Each data point represents mean ± SEM of duplicate measurements of 3 experiments. Data points were fitted by nonlinear regression using equation 4.4, and with the following constants: BAY-876–treated cells (△): K1 = 5.88 x 10^{-6} ± 3.98 x 10^{-6}, K2 = 1.19 x 10^{5} ± 6.16 x 10^{14}, K3 = 9.39 x 10^{4} ± 5.28 x 10^{14}, K4 = 8.95 x 10^{12} ± 3.34 x 10^{22}, R^2 = 0.922, standard error of regression = 0.134; BAY-588–treated cells (▲): K1 = 2.65 x 10^{-3} ± 8.12 x 10^{6}, K2 = 1.09 x 10^{5} ± 3.35 x 10^{14}, K3 = 7.34 x 10^{4} ± 2.25 x 10^{14}, K4 = 1.99 x 10^{11} ± 6.11 x 10^{20}, R^2 = 0.991, standard error of regression = 0.044; NV-5440–treated cells (●): K1 = 3.06 x 10^{-4} ± 1.11 x 10^{-4}, K2 = 1.89 x 10^{5} ± 7.43 x 10^{14}, K3 = 9.50 x 10^{4} ± 5.71 x 10^{14}, K4 = 2.30 x 10^{13} ± 5.67 x 10^{22}, R^2 = 0.967, standard error of regression = 0.085.

Our docking studies identified 3 high affinity sites for ß-D-glucose – 1 distinct intermediate docking site, and 2 overlapping site core 1 and core 2 (figure 4.4A). We obtained a total of 27 docking configurations for ß-D-glucose, with glide scores of –5.6 to –4.0 kcal/mol. Six of these correspond to the intermediate docking site, 18 correspond to core 1 site, and 3 correspond to core 2 site. We selected the docking pose in each configuration with the least glide score (GS), and whose hydroxyl groups of C3, C4 and/or C6 form hydrogen bonds with GLUT1-e1 (figure 4.4B), consistent with the experimentally demonstrated stereospecificity of GLUT1-e1 interaction with cytoplasmic sugars (86). BAY-876, NV-5440, and NV-5981 sterically clash with all 3 ß-D-glucose docking sites, while BAY-588 overlaps with the 2 core glucose sites, but not with the intermediate site (figure 4.4C). These docking analyses, together with experimental data in human erythrocytes, show how BAY-876, NV-5440, and their analogs could compete with glucose for binding at the endofacial sugar binding site. Figure 4.4D shows the GLUT1 amino acids residues predicted to interact with BAY-876, BAY-588, NV-5440 and NV-5981. Common contact residues that appear to be required for inhibitor binding include: Phe379, Trp388, Ile164. Although our experimental data show that the presence the benzonitrile group confers more inhibitory potency on the endofacial GLUT1 ligand, molecular docking reveal that the benzonitrile group does not orient the inhibitors to interact with GLUT1 in a similar fashion. The benzonitrile group in BAY-876 is oriented towards the intermediate ß-D-glucose docking site where it interacts with Pro141 and M142. Whereas, benzonitrile group in NV-5440, is oriented towards the core 1 and core 2 ß-D-glucose docking sites where it forms hydrogen bonds with Gln282 and Trp388, and hydrophobic interactions with Val165.

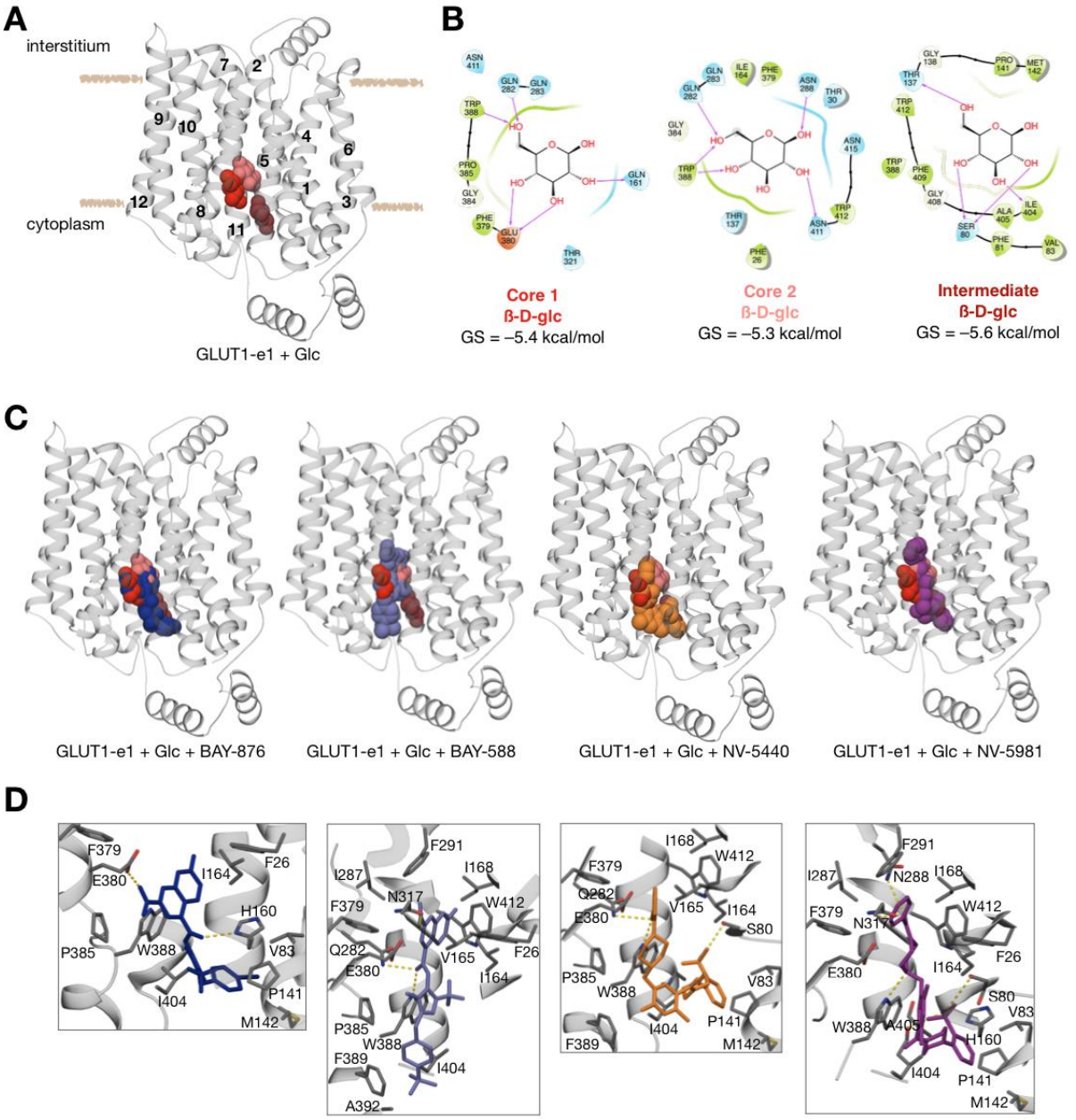

Figure 4.4: Ligand docking to endofacial GLUT1 (GLUT1-e1)

A, GLUT1-e1 (semitransparent grey cartoon) complexed with core 1 (red), core 2 (deep salmon), and intermediate (ruby) ß-D-glucose, shown as spheres. **B,** 2-dimensional representations of GLUT1-e1–ß-D-glucose interactions. Residues and contacts are shown as: hydrophobic (green); polar (blue); negatively charged (orange); hydrogen bond (magenta arrow). **C,** BAY-876 (blue), BAY-588 (light blue), NV-5440 (orange), and NV-5981 (purple) docking to GLUT1-e1–ß-D-glucose. **D,** 3-dimensional representation of GLUT1-e1–ligand contact residues and interactions (color code as in C). Viewing perspective is zoomed-in orientation as in C.

BAY-876 and NV-5440 interfere with cytochalasin B (CB) inhibition of GLUT1

CB is a well characterized membrane permeable endofacial inhibitor of GLUT1, which as acts a noncompetitive inhibitor of sugar uptake but competitively inhibits net sugar exit from cells (117). To further validate BAY-876 and NV-5440 as endofacial GLUT1 inhibitors, we tested their effects on CB binding to GLUT1 and CB inhibition of sugar uptake in human red blood cells. BAY-876, NV-5440 and nonradioactive CB inhibit the binding of [^{3}H]-CB to human RBCs in a dose-dependent manner (figure 4.5A). As with inhibition of CB binding by the flavonoids, our results suggest that inhibition by BAY-876 and NV-5440 but not by CB increases more steeply with increasing [inhibitor] than is predicted by simple Michaelis-Menten inhibition. We therefore reanalyzed these data using a Hill equation and found that the data fits are significantly improved (figure 4.5B). The number of BAY-876, NV-5440 and CB binding sites contributing to inhibition of CB binding are 1.50 ± 0.12, 1.82 ± 0.13 and 1.07 ± 0.07 respectively.

Docking analysis indicates that BAY-876 and NV-5440 both overlap with cytochalasin B (CB) for binding to GLUT1-e1 (figure 4.5C). This suggests that CB and BAY-876 or CB and NV-5440 cannot simultaneously occupy the same GLUT1 molecule. Cooperative inhibition of CB binding by BAY-876 and NV-5440 must, therefore, require their interaction with multiple, interacting GLUT1 molecules.

BAY-876 (15 nM) modulates CB inhibition of 3MG uptake by human erythrocytes, by doubling $K_{i(app)}$ for CB inhibition of uptake (figure 4.5D). This inhibition is two-fold less than that expected on the basis of BAY-876 inhibition of CB binding ($1+[\text{BAY-876}]/K_{i(app)}$ where [BAY-876] = 15 nM and $K_{i(app)}$ = 6 nM see figure 4.5A). Together, these results reveal that

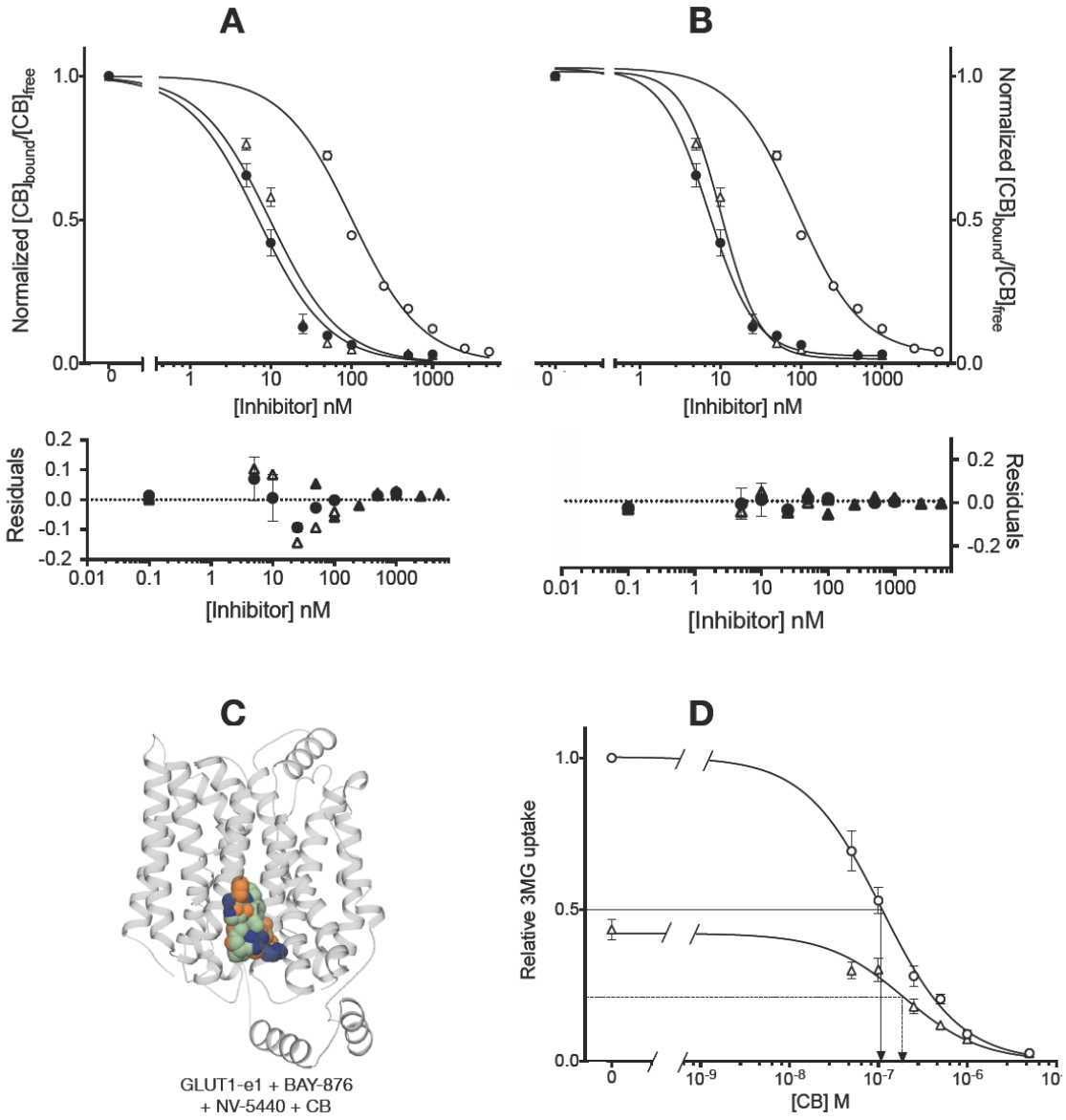

Figure 4.5: BAY-876 and NV-5440 overlap with cytochalasin B (CB) for binding to GLUT1e1

A, BAY-876, NV-5440 and nonradioactive CB inhibits [^{3}H]-CB binding to human RBCs. Ordinate: Normalized $[CB]_{bound}/[CB]_{free}$; Abscissa: [inhibitor] in nM (axis expressed in log scale). Each data point represents mean ± SEM of at least 3 duplicate measurements. Results are shown for BAY-876–treated cells (△), NV-5440–treated cells (●) and nonradioactive CB–treated cells (○). The curves drawn through data points were computed by nonlinear regression assuming simple competitive inhibition (equation 4.5), with the following results: BAY-876 treatment (△): $K_{i(app)}$ = 6.17 ± 0.71 nM, R^2 = 0.949, standard error of regression = 0.084; NV-5440 treatment (●): $K_{i(app)}$ = 4.46 ± 0.35 nM, R^2 = 0.975, standard error of regression = 0.055; nonradioactive CB treatment (○): $K_{i(app)}$ = 64.06 ± 3.09 n M, R^2 = 0.988, standard error of regression = 0.036. The residuals of the fits (for BAY-876, NV-5440 and CB data) are plotted beneath the inhibition plot. **B,** Reanalysis of the same data set assuming multiple binding sites for competing ligand using the Hill-equation (equation 4.6). The results are: BAY-876 treatment (△): $K_{i(app)}$ = 70.35 ± 21.03 nM,

n = 1.82 ± 0.13, R^2 = 0.989, standard error of regression = 0.0415; NV-5440 treatment (●): $K_{i(app)}$ = 19.48 ± 4.79 nM, n = 1.50 ± 0.12, R^2 = 0.989, standard error of regression = 0.0387; CB treatment (○): $K_{i(app)}$ = 125.5 ± 37.1 nM, n = 1.077 ± 0.067, R^2 = 0.991, standard error of regression = 0.0338; The residuals of the fits (for BAY-876, NV-5440 and CB data) are plotted beneath the inhibition plot. **C,** Docking of BAY-876 (blue), NV-5440 (orange) and CB (pale green) to GLUT1-e1 (light gray cartoon). **D,** BAY-876 interferes with the concentration dependence of CB inhibition of 3MG uptake. Results are shown for CB–treated cells (○), and CB–treated cells plus 15 nM BAY-876 (△). The curves drawn through data points were computed by nonlinear regression using equation 1, and with the following results: CB only treatment (○): $K_{i(app)}$ = 107.7 ± 10.02 nM, R^2 = 0.977, standard error of regression = 0.052; CB + 15 nM BAY-876 treatment (△): $K_{i(app)}$ = 191.6 ± 33.06 nM, R^2 = 0.923, standard error of regression = 0.041.

CB, BAY-876 and NV-5440 binding to GLUT1 are mutually exclusive but that the binding of BAY-876 and NV-5440 is cooperative.

BAY-588, NV-5440 and its analogs, but not caffeine overlap with BAY-876 binding to GLUT1

The presence of BAY-876 (15 nM) increases $K_{i(app)}$ for BAY-588 inhibition of human erythrocytes sugar uptake from 0.668 ± 0.074 μM to 2.264 ± 0.510 μM (figure 4.6A), suggesting that BAY-876 and BAY-588 share similar GLUT1 binding sites. This is supported by our docking studies showing that BAY-876 overlaps with BAY-588 (its analog; figure 4.6B), NV-5440 (figure 4.6C), NV-5981 (less potent NV-5440 analog; figure 4.6D) and NV-6091 (more potent NV-5440 analog; figure 4.6E). Caffeine, which interacts with the endofacial nucleotide binding site of GLUT1, and which has been shown to inhibit CB binding to GLUT1 (197), does not appear to interfere with BAY-876 binding to, and inhibition of GLUT1 (figure 4.6F and G).

Comparison between ligand inhibitory potency and docking to GLUT1-e1

The observed inhibitory constants ($K_{i(app)}$) of the endofacial GLUT1 inhibitors tested in this study, appear to correlate with the extent of contacts and steric hindrance the inhibitor makes with the putative ß-D-glucose docking sites in GLUT1-e1 (figure 4.7A). $K_{i(app)}$ for the ligands follows the order: NV-6091 > NV-5902 > NV-5440 ≈ BAY-876 > NV-6346 > NV-5770 >> CB > BAY-588 >> NV-5981 >> caffeine (figure 4.1B and C). $K_{i(app)}$ reported for CB and caffeine are 150–300 nM (117), and 3.5 mM (197) respectively. Our ligand docking studies predict that ligand binding at the core 2 ß-D-glucose docking site will produce the least inhibition of transport (caffeine; figure 4.7B), followed by binding at both

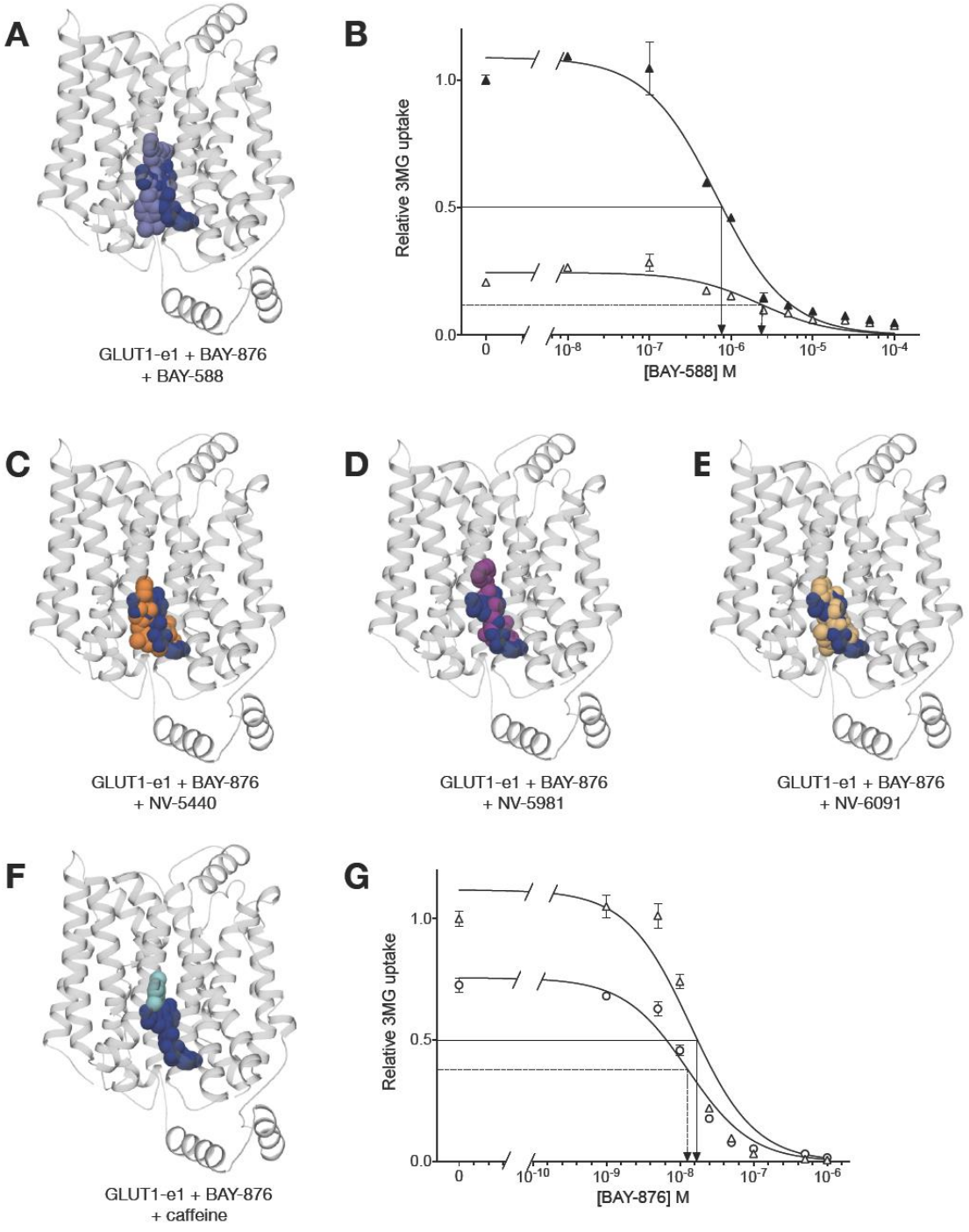

Figure 4.6: BAY-588, NV-5440 and its analogs, but not caffeine, interfere with BAY-876 binding to GLUT1-e1

A, Docking of BAY-588 (light blue) and BAY-876 (blue) to GLUT1-e1 (light gray cartoon). **B,** Dose-dependent inhibition of human erythrocyte 3MG (0.1 mM) uptake by BAY-588 (▲) or BAY-

588 plus 15 nM BAY-876 (△). Ordinate: Relative 3MG uptake; Abscissa: Increasing [BAY-588] in M (axis expressed in log scale). Each data point represents mean ± SEM of 3 duplicate measurements. Curves drawn through data points were computed by nonlinear regression using equation 4.1, and with the following results: BAY-588–treated cells (▲): $K_{i(app)}$ = 6.68 x 10^{-7} ± 7.38 x 10^{-8} M, R^2 = 0.971, standard error of mean = 0.073; BAY-588 + 15 nM BAY-876–treated cells (△): $K_{i(app)}$ = 2.26 x 10^{-6} ± 5.10 x 10^{-7} M, R^2 = 0.834, standard error of mean = 0.036. **C–E,** Docking of NV-5440 (orange; C), NV-5981 (purple; D), and NV-6091 (light orange, E), with BAY-876 (blue) to GLUT1-e1 (light gray cartoon). **F,** Docking of caffeine (cyan) and BAY-876 (blue) to GLUT1-e1 (light gray cartoon). **G,** Dose-dependent inhibition of human erythrocyte 3MG (0.1 mM) uptake by BAY-876 (△) or BAY-876 plus 3.5 mM caffeine (○). Ordinate: Relative 3MG uptake; Abscissa: Increasing [BAY-876] in M (axis expressed in log scale). Each data point represents mean ± SEM of 3 duplicate measurements. Curves drawn through data points were computed by nonlinear regression using equation 4.1, and with the following results: BAY-876–treated cells (△): $K_{i(app)}$ = 1.41 x 10^{-8} ± 2.10 x 10^{-9} M, R^2 = 0.922, standard error of mean = 0.131; BAY-876 + 3.5 mM caffeine–treated cells (○): $K_{i(app)}$ = 1.28 x 10^{-8} ± 1.35 x 10^{-9} M, R^2 = 0.957, standard error of mean = 0.062.

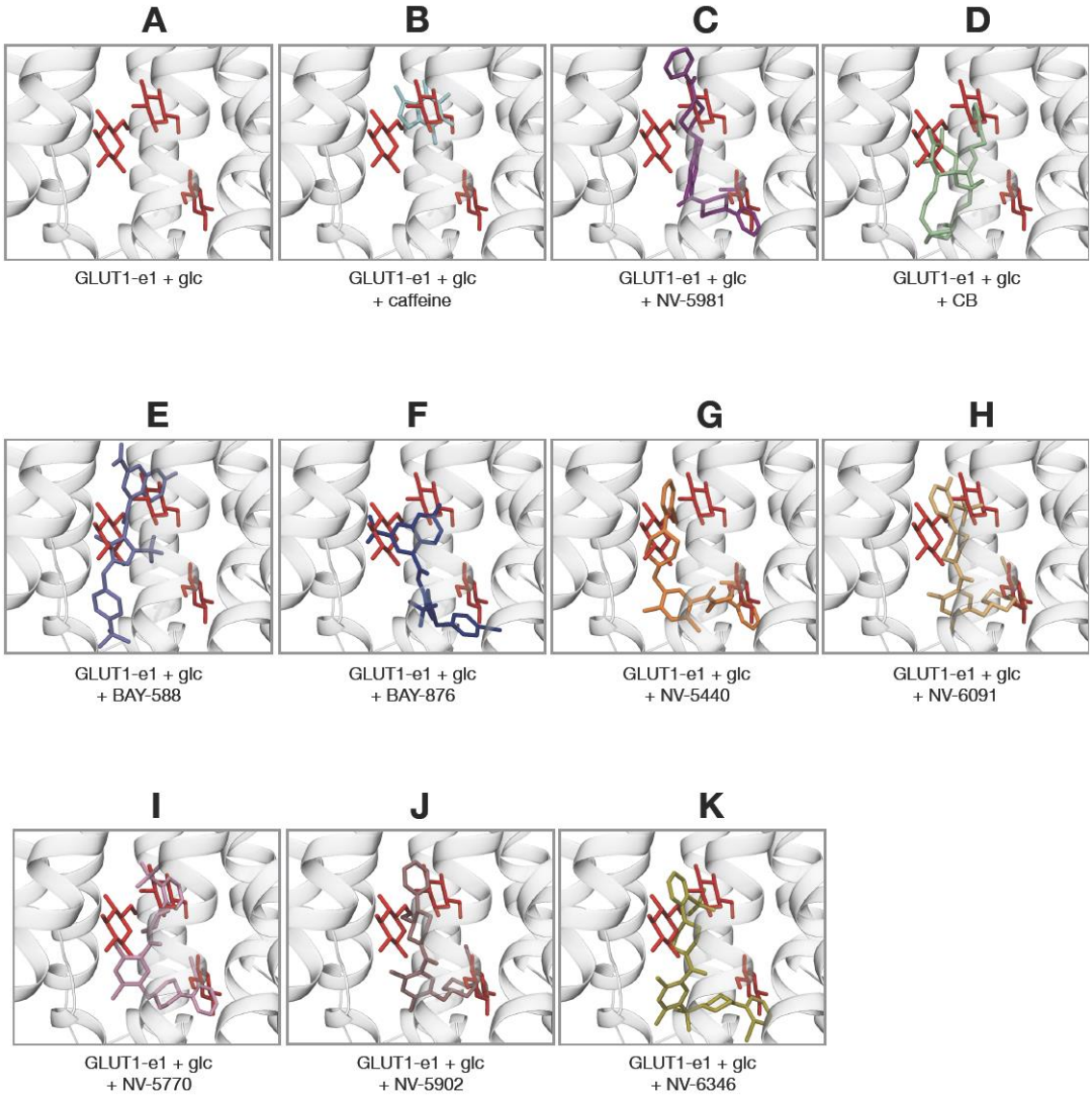

Figure 4.7: Ligand interaction with all three putative glucose binding sites of GLUT1-e1 correlates with greater GLUT1 inhibition

GLUT1-e1 is shown as light gray cartoon (a zoomed in view of the same orientation as in Figure 4A). Ligands are shown as sticks with the following color code: glucose (red), CB (pale green), caffeine (cyan), BAY-876 (blue), BAY-588 (light blue), NV-5440 (orange), NV-6091 (light orange); NV-5981 (purple), NV-5770 (light pink), NV-5902 (light brown), NV-6346 (olive green).

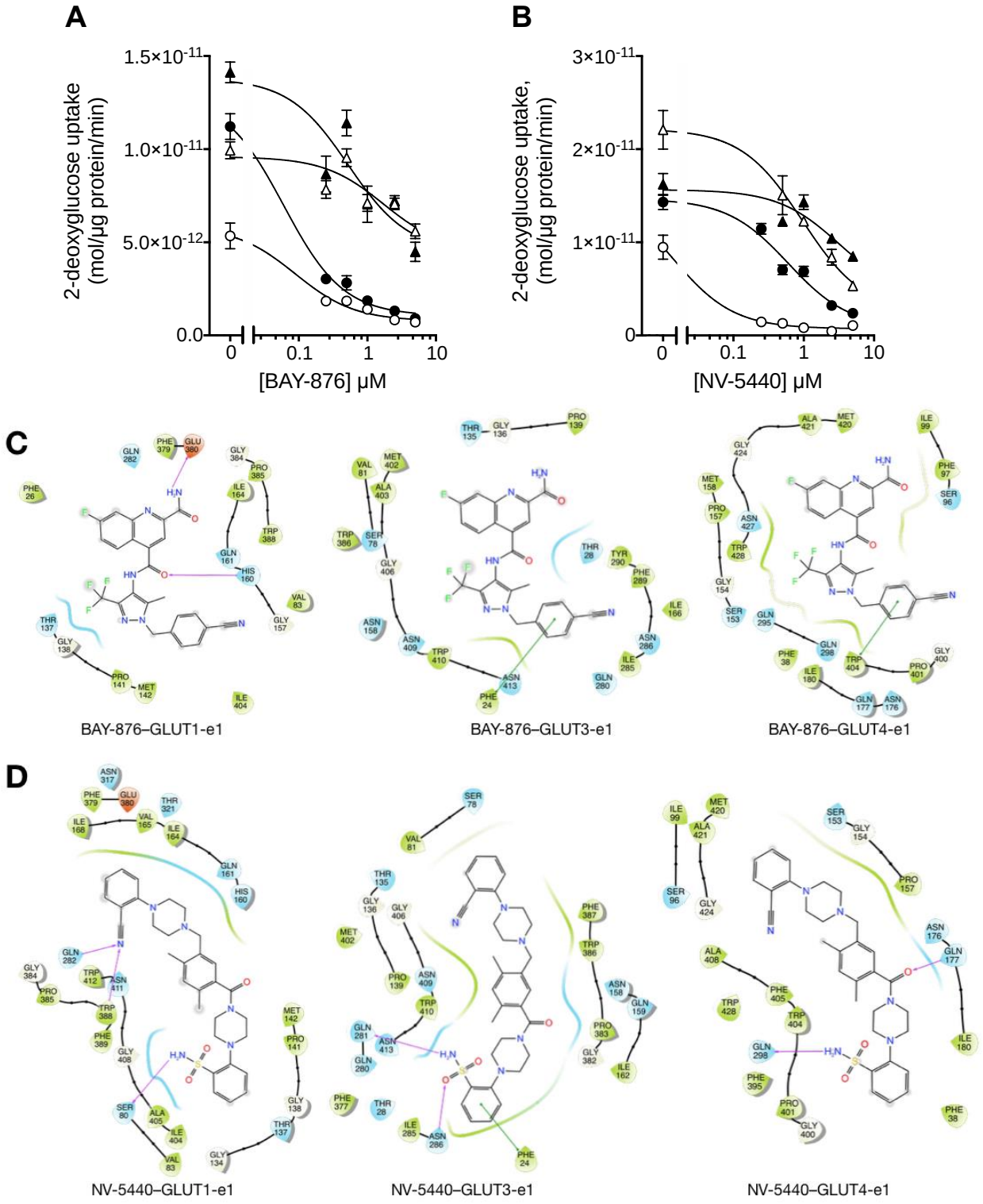

Figure 4.8: Isoform specificity of sugar transport inhibition by BAY-876 and NV-5440

A & B, Ordinate: 2-deoxyglcuose uptake in mol/µg protein/min; Abscissa: inhibitor concentration in µM (axis expressed as log scale). Results are shown for transport inhibition by BAY-876 (**A**) and NV-5440 (**B**) in untransfected (○), and in transfected HEK293 cells stably expressing hGLUT1 (●), hGLUT3 (△) or hGLUT4 (▲). The curves drawn through the data points were computed by nonlinear regression using equation 4.1, with the following results: BAY-876–treated cells: untransfected cells (○), $K_{i(app)}$ = 0.089 ± 0.036 µM, R^2 = 0.983, standard error of regression = 2.86 x 10^{-13}; hGLUT1-transfected cells (●): $K_{i(app)}$ = 0.061 ± 0.019 µM, R^2 = 0.994, standard error of regression = 3.88 x 10^{-13}, hGLUT3-transfected cells (△): $K_{i(app)}$ = 1.726 ± 2.757 µM, R^2 = 0.760, standard error of regression = 1.04 x 10^{-12}; hGLUT4-transfected cells (▲): $K_{i(app)}$ = 0.527 ± 0.567 µM, R^2 = 0.800, standard error of regression = 1.99 x 10^{-12}; NV-5440–treated cells: untransfected cells (○), $K_{i(app)}$ = 0.014 ± 0.012 µM, R^2 = 0.996, standard error of regression = 2.96 x 10^{-13}; hGLUT1-transfected cells (●): $K_{i(app)}$ = 0.603 ± 0.238 µM, R^2 = 0.969, standard error of regression = 1.06 x 10^{-12}, hGLUT3-transfected cells (△): $K_{i(app)}$ = 0.958 ± 0.145 µM, R^2 = 0.997, standard error of regression = 4.90 x 10^{-13}; hGLUT4-transfected cells (▲): $K_{i(app)}$ = 3.177 ± 5.544 µM, R^2 = 0.844, standard error of regression = 1.71 x 10^{-12}. **C & D,** 2-dimensional representations of interactions between GLUT1-e1, GLUT3-e1, GLUT4-e1 and BAY-876 (C), and NV-5440 (D). Residues and contacts are shown as: hydrophobic (green); polar (blue); negatively charged (orange); hydrogen bond (magenta arrow), Pi–Pi stacking (green line); Pi cation (red line).

core 2 and intermediate docking sites (NV-5981; figure 4.7C). Ligand binding at both core 1 and core 2 sites (CB and BAY-588; figure 4.7D and E) will increase transport inhibition but the greatest inhibition ($K_{i(app)}$ ≈ 15 nM) is observed with ligands interacting with all 3 putative ß-D-glucose binding sites (figure 4.7F – K).

Isoform specificity of sugar transport inhibition by BAY-876 and NV-5440

Siebeneicher et al (167) used a cell-based assay, with an indirect ATP read-out, to show that BAY-876 is GLUT1-specific. They reported that BAY-876 has an inhibitory potency for GLUT1 that is more than 100-fold greater than its affinity for GLUT2, GLUT3 and GLUT4 (167). Here, we assayed for the dose-dependent inhibition of 2-deoxy-D-glucose (2DG) uptake at 37 ºC by BAY-876 and NV-5440 in HEK293 cells stably expressing hGLUT1, GLUT3 or GLUT4, and show that BAY-876 and NV-5440 inhibit GLUT1-, GLUT3-, and GLUT4-mediated 2DG uptake in HEK293 in a dose-dependent manner (figure 4.8A and B). In our hands, BAY-876 shows a ≥10-fold greater potency with GLUT1 than GLUT3 and GLUT4 (figure 4.8A), while NV-5440 shows similar affinities for GLUT1 and GLUT3, but is 5-fold less potent against GLUT4 (figure 4.8B). Molecular docking studies reveal that BAY-876, as well as NV-5440, interact with identical residues in GLUT1, GLUT3 and GLUT4 (figure 4.8C and D).

Discussion

BAY-876 and NV-5440 inhibit the glucose transporter, GLUT1, by acting as noncompetitive inhibitors of human erythrocyte sugar uptake, and as competitive inhibitors of net glucose exit, suggesting that BAY-876 and NV-5440 interact with GLUT1 at, or close to, the endofacial sugar binding site. This conclusion is supported by ligand binding and

molecular docking analyses which reveal that these compounds overlap with glucose and cytochalasin B (CB, an extensively characterized endofacial ligand of GLUT1) for binding to the endofacial sugar binding site of GLUT1.

Indeed, BAY-876, NV-5440 and CB are endofacial inhibitors that inhibit GLUT1 by a common mechanism (29,117,118,186). We demonstrated this by showing that: 1) BAY-876 and NV-5440 decrease the V_{max} for sugar uptake but increase K_m for sugar exit from cells, indicating that BAY-876 and NV-5440, just like CB (116,117), compete with glucose for the sugar exit site, but not the sugar uptake site; 2) BAY-876 and NV-5440 dock within the CB binding pocket revealed recently by the CB–bound hGLUT1-e1 crystal structure (29). Molecular docking predicts that BAY-876, NV-5440 and CB interact with common GLUT1 residues. Each forms hydrophobic interactions with Ile164, Phe379 and Trp388, and NV-5440 forms an additional hydrophobic contact with Trp412 and a hydrogen bond with Trp388 as shown for the CB–hGLUT1 crystal structure (29). 3) BAY-876 and NV-5440 inhibit CB binding to the endofacial sugar binding site in a dose-dependent manner but in a way that suggests that there are multiple, cooperative endofacial ligand biding sites in the transporter complex. Exofacial inhibitors of GLUT1 also inhibit CB binding to the endofacial sugar binding site by acting at multiple exofacial binding sites (see figures 2.7 & 3.4). Collectively, these results suggest that ligand binding to GLUT1 is much more complex than is described by the simple, alternating access model for how GLUT1 functions.

Like CB (120,239), subsaturating concentrations of BAY-876, BAY-588 and NV-5440 stimulate erythrocyte sugar uptake (figure 4.3). This action of endofacial inhibitors on GLUT1-mediated glucose transport is termed trans-allostery (120), because the

stimulating ligands interacts with GLUT1 at the opposite (trans) side of the membrane relative to the transported substrate. This trans-allosteric effect is lost as inhibitor concentration is raised, resulting in inhibition of sugar uptake (figure 4.3). If GLUT1 functions as a simple alternating access carrier, as is suggested by published interpretations of recent crystal structures of human GLUTs 1 and 3 (16,28-30,119), trans-allostery should be impossible. Instead, these crystal structures inform us that monomeric GLUT1: 1) alternates between outward-facing and the inward-facing conformations; 2) is capable of binding multiple exofacial ligands when in the outward-facing conformation, but, 3) can bind only a single large ligand when in the inward-facing orientation. This present study, however, strengthens the argument that operationally, the glucose transporter simultaneously presents exofacial and endofacial sugar binding sites. Given the positive cooperativity observed at low inhibitor concentrations, we propose that GLUT1 functions as an oligomeric complex of alternating access subunits. This hypothesis is supported by previous reports that show GLUT1 also exhibits cis-allostery with low concentrations of exofacial inhibitors (120,122,124,239) and the report by De Zutter *et. al.* (123) implicating TM9 as the GLUT1 tetramerization interface.

With an apparent inhibitory constant of ~ 13 nM for inhibiting human erythrocyte glucose transport, BAY-876 and NV-5440 are the most potent inhibitors of GLUT1 reported to date. We show that the structural analogs of NV-5440 that retain the benzonitrile group inhibit GLUT1-mediated sugar transport in human RBCs with similar inhibitory potencies as NV-5440, whereas NV-5981 in which the benzonitrile group is replaced with a benzaldehyde group is more than 200-fold less potent than NV-5440. Likewise, substituting the nitrile group in BAY-876 with a tert-butyl group to form BAY-588 reduces its inhibitory potency

by at least 40-fold. While BAY-876 and NV-5440 are structurally different, the presence of a benzonitrile group confers similar inhibitory potencies on BAY-876 and NV-5440.

Many benzonitrile-containing drugs have been developed to treat a wide range of disease conditions including cancers (e.g. breast (273-275), prostate (276), pancreatic (277), myeloid leukemia (278-280), and lung cancer (281)), acne (282,283), heart failure (284), hypertension (285), mood disorders (286), arthritis (287) and HIV AIDS (288). The nitrile substituents in drugs usually act as hydrogen bond acceptors (e.g. fadrozole hydrochloride and letrozole – aromatase enzyme inhibitors used to treat breast cancer (273,274)). There are cases, however, where the nitrile group forms no specific interactions with the protein target. An example of this is seen with BMS-214662 (a farnesyltransferase inhibitor developed for chronic myeloid leukemia), where the nitrile group forms no specific interactions with farnesyltransferase, but enhances solubility of the drug by about 10-fold more than its bromo analog (280). The nitrile group in BAY-876 shows no specific interactions in GLUT1, GLUT3 and GLUT4 (figure 4.8C). Similarly, the nitrile unit in NV-5440 shows no specific interactions with GLUT3 and GLUT4, but forms hydrogen bonds with Gln282 and Trp388 in GLUT1 (figure 4.8D). Regardless of whether the nitrile groups in BAY-876 and NV-5440 form specific interactions with GLUT1, or not, our experimental data clearly show that nitrile unit confers greater inhibitory potency to the GLUT1 inhibitors.

Siebeneicher *et. al.* (167) tested the inhibitory effects of BAY-876 on GLUT1, GLUT2, GLUT3 and GLUT4 in a cell-based assay, and reported that BAY-876 is more selective towards GLUT1 than GLUT2, GLUT3 and GLUT4 by a selectivity factor of > 100-fold. Consistent with this report, our isoform specificity data reveal that BAY-876 is more selective towards GLUT1 than GLUT3 and GLUT4, although we only observed a

selectivity factor of ≥ 10-fold for GLUT1 (figure 4.8A). To resolve the disparity between the selectivity factor observed in this present study and the one previously reported, much more data points will be needed at high BAY-876 concentrations, and this will only be achievable by automating the sugar uptake experiments used in this study. NV-5440 shows similar affinities towards GLUT1 and GLUT3 but is 5-fold less selective for GLUT4 (figure 4.8B). While specificity of these compounds for GLUT1 is important, treatment of patients with GLUT1 inhibitors will adversely impact non-diseased tissues, like the brain, that depend on GLUT1-mediated glucose uptake for proper function. A better treatment regimen, therefore, is to combine GLUT1-mediated glucose transport inhibition, with ketogenic diet (which will provide a source of metabolic fuel to healthy tissues while cancer cells are starved of glucose (289)). With this treatment strategy, specificity of the inhibitor for GLUT1, GLUT3 and GLUT4 becomes less important, instead what is more important is the ability of the inhibitors to effectively limit glucose availability to the cancer cells.

BAY-876, NV-5440 and the nitrile-containing analogs of NV-5440 are very promising novel anticancer therapeutics. *In vitro* and *in vivo* pharmacokinetic studies on BAY-876 show that it has an excellent oral bioavailability and a long terminal half-life (167). Similar pharmacokinetic analyses are needed for NV-5440 and its analogs, as well as further tests that show how these nitrile-containing inhibitors of GLUT1 impact normal carbohydrate homeostasis within a host. This present report provides important mechanistic information about how BAY-876, NV-5440 and their analogs inhibit GLUT1 and should serve to stimulate more research into finding suitable GLUT1 inhibitors that can eventually be used as anticancer therapeutics.

Chapter V

Conclusion and future directions

Inhibition of GLUT1 and glucose metabolism in cancer is a viable strategy for killing cancer cells. There is an increased interest to develop small molecule anticancer drugs that specifically target GLUT1, with several groups using different approaches, including high-throughput and virtual screening to identify compounds that impair the glucose transport function of GLUT1. These efforts are beginning to yield dividends with several glycolytic enzyme inhibitors at different phases of clinical trials (193,290), and also with the recent report of compounds that inhibit GLUT1 at low nanomolar concentrations.

However, for this strategy to be therapeutically viable in cancer treatment it is important to understand the potency and specificity of candidate GLUT1 inhibitors. Once, this is established, it becomes feasible to modify any treatment regimen to take into account the potential adverse effects of inhibiting GLUT1 on normal brain glucose metabolism, in particular, and, more generally, on the overall carbohydrate homeostasis of the patient.

This study provides a fundamental framework for characterizing candidate GLUT1 inhibitors for their inhibitory potencies, and sidedness of action on GLUT1 by performing specific sugar transport and ligand binding experiments in human erythrocytes. We tested 21 previously uncharacterized candidate GLUT1 inhibitors for their mechanisms of GLUT1 inhibition in freshly isolated human red blood cells. We show that WZB117, quercetin, EGCG and ECG act as exofacial inhibitors that interact with GLUT1 at, or close to the extracellular sugar binding site. BAY-876 and NV-5440 are endofacial GLUT1 inhibitors that compete with glucose for binding at the intracellular sugar binding site. Furthermore,

STF-31 and the PUG series (PUG-1 – PUG8) failed to inhibit human erythrocyte sugar transport (figure 5.1).

Chan *et. al.* (166), identified STF-31 by high-throughput screening and reported that STF-31 inhibited GLUT1–mediated glucose uptake by renal cell carcinomas (RCCs), resulting in the selective killing of these cancer cells. We sought to extend this finding by investigating the mechanism by which STF-31 inhibits GLUT1. Contrary to the findings of Chan *et. al.* that showed up to 70 % inhibition of human erythrocytes glucose transport with 5 µM of STF-31 (166), we found no inhibition of human erythrocyte GLUT1 by STF-31, either at the reported 5 µM concentration or by a 10-fold higher (50 µM) concentration of STF-31 (figure 5.1A). Indeed, recent studies showed that STF-31 is instead an inhibitor of nicotinamide phosphoribosyltransferase (NAMPT), an enzyme of the NAD^+ salvage pathway (291,292). Precisely how STF-31 inhibition of NAMPT decreases GLUT1–mediated glucose uptake is unknown, but this could be related to cell death initiation by STF-31.

Ung et. al. (185) identified PUG-1 – PUG-8 as GLUT1 inhibitors by virtual screening of several chemical libraries of compounds. They followed up their virtual screening by testing the effects of these compounds on 2-deoxyglucose uptake in CHO-K1 cells, and reported IC50s of 0.45 – 58.6 µM for PUG-1 – PUG-8. Again, we sought to identify the mechanisms of GLUT1 inhibition by these compounds but found that they do not inhibit GLUT1–mediated sugar uptake in human erythrocytes (figure 5.1B), in GLUT1-transfected HEK293 cells (figure 5.1C) and in untransfected HEK293 cells (figure 5.1D). PUG1 (0.5 µM) and PUG5 (25 µM) stimulate GLUT1-mediated 3MG uptake by human erythrocytes by 57% and 98% respectively (figure 5.1 B). This indicates possible cis- or

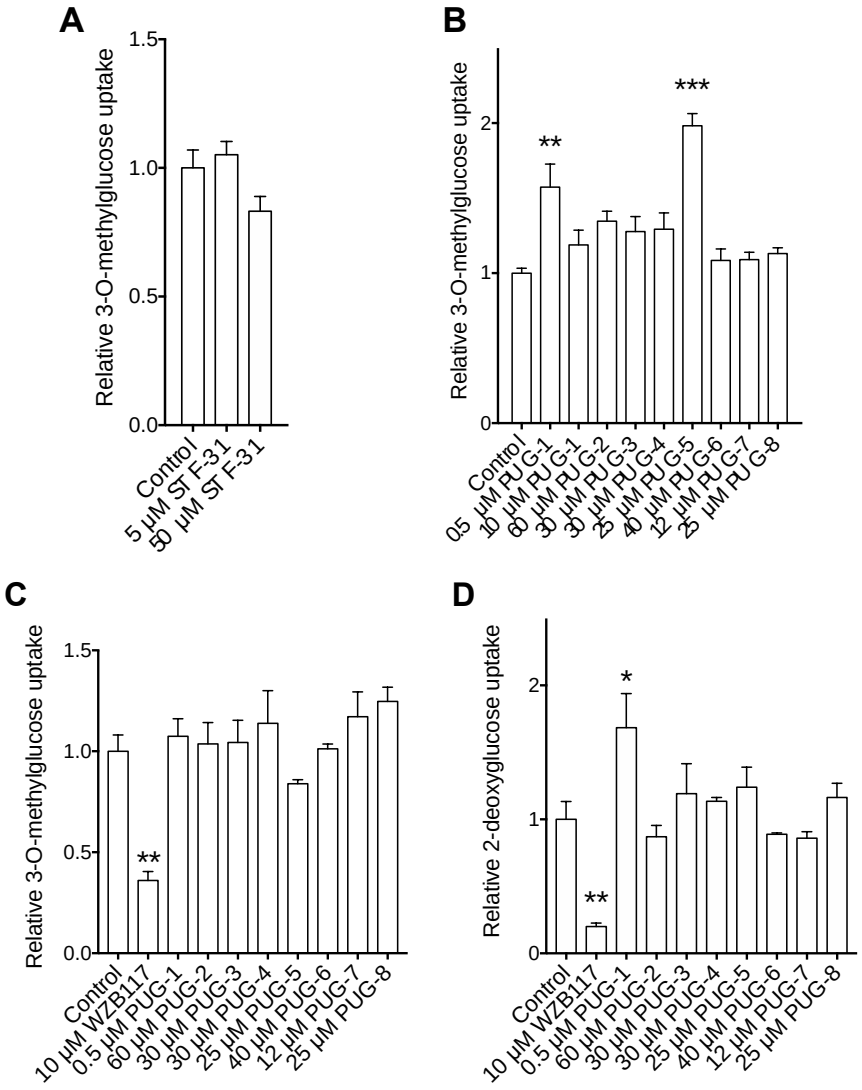

Figure 5.1: STF-31 (A) and PUG-1 – PUG-8 (B–D) do not inhibit GLUT1

Each bar represents the mean ± S.E.M of 3 duplicate measurements, and statistical analysis was done by ordinary one-way ANOVA. **A,** 3MG uptake ± STF-31 in human RBCs. There is no significant difference ($p > 0.05$) between control and STF-31–treated cells. **B,** 3MG uptake ± PUG-1–PUG-8 in human RBCs. PUG-1 (0.5 µM) and PUG-5 (25 µM) significantly increase 3MG uptake in human erythrocytes by 57% and 98% respectively (B), (**, $p = 0.0051$; ***, $p < 0.0001$). The other PUG compounds show no significance difference from control ($p \geq 0.206$). **C,** 3MG uptake ± PUG-1–PUG-8 or WZB117 in HEK293 cells stably expressing GLUT1. WZB117 significantly inhibit 3MG uptake (**, $p = 0.003$); PUG-1–8 show no significant difference ($p \geq 0.685$). **D,** 2DG uptake ± PUG-1–PUG-8 or WZB117 in untransfected HEK293. WZB117 significantly inhibit 2DG uptake (**, $p = 0.011$); PUG-1 significantly simulate 2DG uptake by up to 70% (*, $p = 0.042$); PUG-2–8 show no significant difference ($p \geq 0.947$) compared to control.

trans-allosteric effects by these ligands on GLUT1, and also suggests that the ligands interact with GLUT1. However, raising the concentration of PUG1 by 20 fold (10 μM) failed to inhibit sugar uptake by human RBCs (figure 5.1B).

The lack of inhibition of human erythrocyte sugar transport by STF-31 and PUGs 1–8, underscores the importance of validating the candidate GLUT1 inhibitors in human erythrocytes, as these cells abundantly express GLUT1 as the only glucose transporter.

Once we established the mechanisms of action of GLUT1 inhibitors in human red blood cells, we moved on to test their specificity for class 1 GLUTs (GLUT1, GLUT3 and GLUT4), which transport glucose as their primary substrate. This we did in cultured HEK293 cells stably expressing these GLUT isoforms. With the exception of WZB117, that inhibits GLUT4 more strongly (up to 10-fold more) than GLUT1 in HEK293 cells, we show that the inhibitors tested in this study inhibit GLUT1 with greater or equal potency than GLUT3 or GLUT4. The fact that these molecules inhibit GLUT1, GLUT3 and GLUT4, indicates that their ability to serve as anticancer agents does not derive from their specificity for GLUT1, but rather from the extreme sensitivity of cancer cells to limited glucose uptake. Consequently, the use of these compounds in cancer therapy may impair glucose uptake by astrocytes, neurons and insulin-sensitive tissues (e.g. fat and skeletal muscle cells) which depend on GLUT1-, GLUT3- and GLUT4-mediated glucose uptake respectively. A way to mitigate against adverse consequences in normal, differentiated cells is to combine small molecule inhibition of GLUT1 with application of a ketogenic diet which will serve as an alternative source of metabolic fuel for normal tissues with adaptable metabolism while cancer cells are starved of glucose (289).

BAY-876 and NV-5440 are benzonitrile–containing compounds, and are the most potent inhibitors of GLUT1 reported to date. We show that analogs of NV-5440 retaining the benzonitrile group inhibited GLUT1 with similar avidity, while analogs of both BAY-876 and NV-5440 lacking the benzonitrile group are less potent inhibitors of GLUT1, with reduced inhibitory potency of 40- to 200-fold. It will be interesting to see if introduction of nitrile groups on phenyls of the exofacial inhibitors, WZB117, quercetin, EGCG and ECG, will improve their inhibition of GLUT1.

Furthermore, we report that GLUT1 ligands, regardless of their mechanisms of GLUT1 inhibition, stimulate glucose uptake at low, subsaturating concentrations, followed by inhibition of glucose uptake as inhibitor concentration is raised. We interpret this finding as evidence that GLUT1 simultaneously presents multiple ligand binding sites, with the possibility of exposing 2 exofacial and 2 endofacial binding sites at any instant (figure 5.2; (266)). We reason that at low concentrations, inhibitor binding to a high affinity site stimulates glucose transport, but binding of inhibitor to the second lower affinity site, at high [inhibitor], leads to inhibition of glucose transport. Glucose uptake stimulation at low flavonoid concentrations could also explain the beneficial effects of these compounds against diabetes, where increased GLUT1–mediated glucose uptake could lower blood sugar concentration.

This present study, as well as another recent study from our lab reveal that the exofacial GLUT1 ligands, maltose (120) and WZB117 (239), can bind to the outward-open conformation of GLUT1 in orientations that still expose the catalytic (core) exofacial glucose binding site, which may be responsible for cis-allostery observed with these ligands (120,239,266). Further studies can explore this finding to identify molecules that

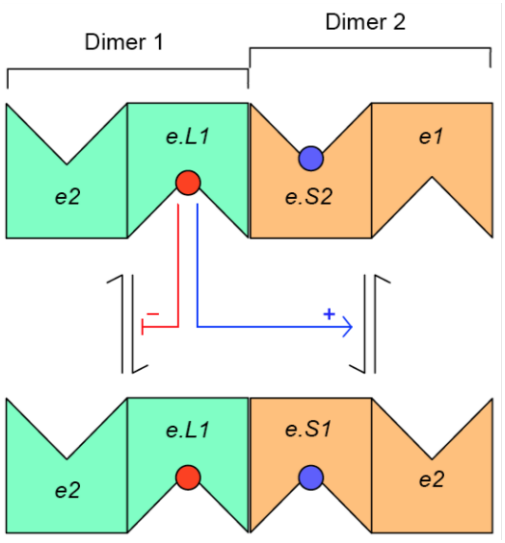

Figure 5.2: GLUT1 as a tetramer of alternating access subunits

GLUT1 is considered a dimer of dimers (a tetramer) of alternating access transporters in which each dimer must present subunits in opposite conformations (e.g. one subunit presents an e2 conformation and the second an e1 conformation or vice versa). If an e1 subunit of a dimer undergoes the e1 to e2 conformational change, the adjacent e2 subunit within the same dimer must undergo the e2 to e1 conformational change. If a dimer contains an inhibitor in its e1 subunit (e.L1), that dimer is trapped in an inhibited state. If the adjacent dimer does not contain an inhibitory ligand (i.e. its e1 subunit is ligand-free), the occupancy state of the neighboring liganded dimer is communicated to the uninhibited dimer and transport of sugar via the e2 subunit is accelerated either via increased affinity of sugar binding or via increased translocation.

preferentially bind at sites (peripheral and intermediate glucose docking sites) that still permit glucose binding to the core site, in an attempt to develop small molecules that directly bind to GLUT1 to stimulate glucose uptake. This will be useful in treatment of diseases including GLUT1 deficiency syndrome, diabetes, and neurological disorders (Alzheimer's and Parkinson's disease), where glucose uptake into cells is greatly diminished.

We took advantage of the increasing proficiency of *in silico* ligand docking methodologies such as GLIDE (293-295) and homology modeling techniques (241,242) to predict the interactions between ligands and GLUT isoforms in this study. This allowed us to predict protein–ligand interactions in the absence of crystal structures of the ligand bound to its target. However, this method is limited because it treats the protein target as a static structure and generates multiple docking poses ranked by their glide scores (GS) which are related to but not necessarily predictive of the standard free energy (ΔG) for binding (293-295). While glide scores are successful in selecting the best or most probable ligand–protein docking pose, they are less successful in predicting experimental K_d values for ligand binding. In this study, we chose the ligand–protein docking poses with the most favorable docking scores for ligands for which experimental ligand–protein interactions data are unavailable. For glucose–GLUT1 interactions, we chose only docking poses that predicted hydrogen bonds that are consistent with previously published biochemical data (86,87). We also relied heavily on our sugar transport data to decide how best to interpret our ligand docking studies. For instance, GLIDE predicted better glide scores for cytochalasin B (CB) docking to GLUT1-e2 (GS = –8.31 to –5.42 kcal/mol) than CB docking to GLUT1-e1 (GS = –7.14 to –3.72 kcal/mol). Whereas extensive biochemical and kinetic characterization of CB, and even a recent GLUT1–CB crystal structure show that CB

interacts only with GLUT1-e1 (29,117,118,186). Therefore, docking analysis must be guided by experimental data. Also, in the absence of ligand–GLUT1 crystal structures, combination with a method that allows dynamic movement of the protein target (i.e. allowing for induced fits by incorporating molecular dynamic stimulations) may better predict GLUT residues involved in ligand interaction.

To ultimately verify the conclusions in this study (oligomeric complexes of allosteric, alternating access transporters each presenting multiple exofacial ligand binding sites, and antiparallel functional arrangement of exofacial and endofacial substrate binding sites), we must visualize structures of GLUT1 with ligands bound. Detergents disrupt the oligomeric state of GLUT1 (111,215,296), and detergent–solubilized GLUTs do not bind ligands efficiently (215,297). One way to verify functional GLUT1 structures may be to isolate GLUT1 from cell membranes by detergent-free techniques, such as by using styrene maleic acid copolymers to isolate proteins from membranes surrounded by their native lipids (298) producing SMALPs (Styrene Maleic Acid LipoProteins) which retain ligand binding function. Cryo-EM can then be used to obtain structures of GLUTs with ligands bound. Efforts to achieve this are underway in our laboratory.

APPENDIX

Acute AMPK stimulation of glucose transport in cultured brain capillary endothelial cells does not occur via inhibition of GLUT1 endocytosis

Rationale, Results & Discussion

Acute metabolic stress dependent activation of AMPK in cultured murine brain capillary endothelial cells (bEnd.3 cells) results in a 2- to 3-fold increase in plasma membrane (PM) GLUT1 content, and a corresponding increase in glucose uptake (ref: (132); and figure A.1). This stimulation of glucose transport does not result from increasing total GLUT1 mRNA or protein levels (132,151), suggesting that acute AMPK activation controls GLUT1 trafficking between the intracellular and cell surface membranes in bEnd.3 cells. Here we used a reversible cell surface biotinylation technique (figure A.2A – D and A.4A) to test if AMPK regulates GLUT1-mediated glucose uptake in blood-brain barrier (BBB) endothelial cells by stimulating exocytosis of intracellular GLUT1 to the PM or by inhibiting endocytosis of PM GLUT1, or a combination of both.

Our data (figure A.3) reveal little or no internalization of PM GLUT1 in basal, unstimulated bEnd.3 cells. Whereas, we observe up to 30% net internalization of PM TfR in these cells (figure A3), suggesting that AMPK does not increase PM GLUT1 levels in bEnd.3 cells by inhibiting GLUT1 endocytosis. Assuming changes in cell surface GLUT1 biotinylation reveal changes in cell surface [GLUT1] not cell surface GLUT1 lysine accessibility, AMPK activation must stimulate GLUT1 exocytosis in order to produce increased PM GLUT1 and increased glucose uptake (figure A.4). However, it has been challenging to conclusively demonstrate AMPK stimulation of GLUT1 exocytosis using cell surface biotinylation at

37ºC where membrane trafficking may be too rapid to capture the time course of GLUT1 externalization by biotinylation. More definitive experimental proof may require alternative approaches such as immunohistochemistry.

Additionally, we show that while acute treatment of bEnd.3 cells with GLUT1 antagonists inhibits glucose uptake (figure A.5A), acute application (0 to 1 hour) of these inhibitors does not lead to AMPK activation or increased cell surface GLUT1 levels (figure A.5B – C).

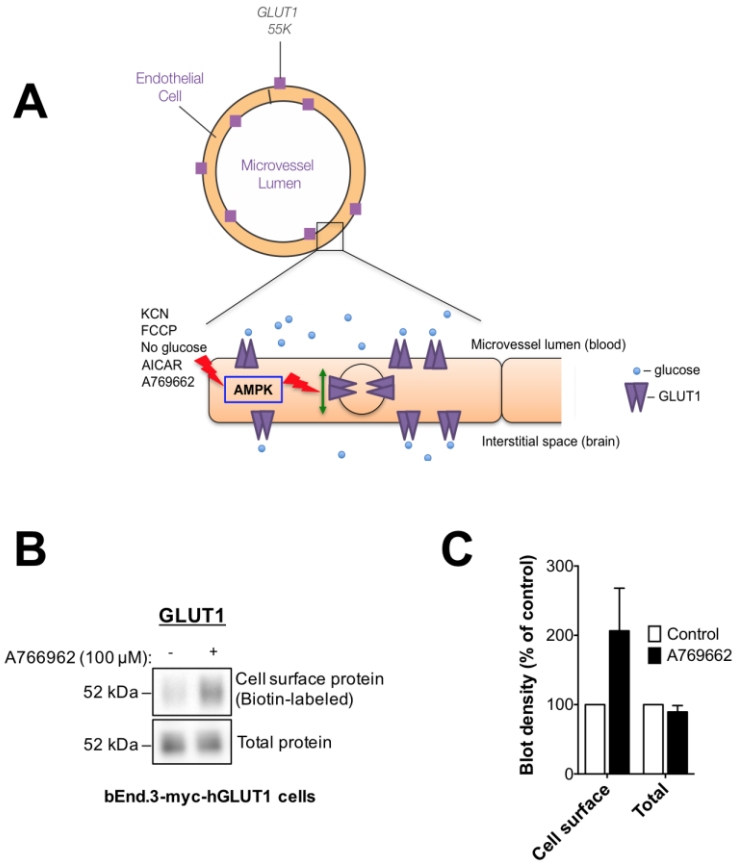

Figure A.1: BBB endothelial cells increase cell surface GLUT1 levels in response to acute metabolic stress of agonist-induced activation of AMPK

A, Illustration summarizing the observation that AMPK activation either by acute metabolic stress or agonist increases cell surface GLUT1 content by 2- to 3-fold. **B,** A766962 activation of AMPK results in up to a 3-fold in cell surface GLUT1 without increasing total GLUT1 protein. **C,** Blot quantitation of B.

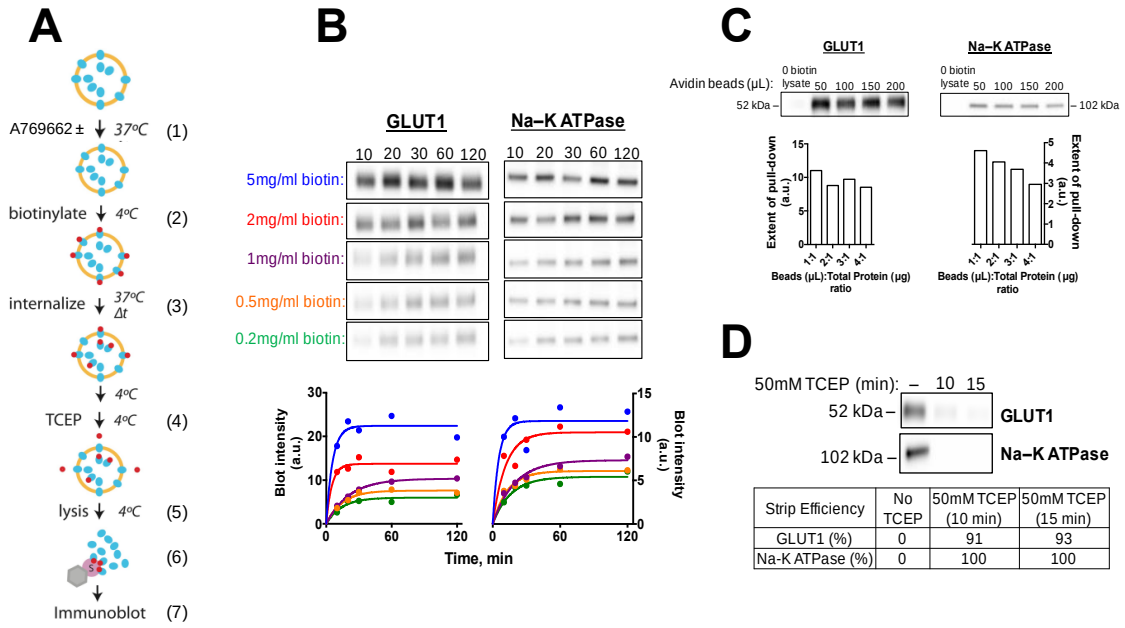

Strip Efficiency	No TCEP	50mM TCEP (10 min)	50mM TCEP (15 min)
GLUT1 (%)	0	91	93
Na-K ATPase (%)	0	100	100

Figure A.2: Technique of reversible cell surface biotinylation to measure net GLUT1 internalization

A, Step-by-step protocol for measuring net PM GLUT1 internalization. The PM is shown as an orange circle and GLUT1 as cyan ellipses present both at the PM and inside the cell. (1) AMPK activation: cells are treated with or without AMPK agonist (0.1 mM A769662 for 1 hr or 2 mM AICAR for 2 hrs at 37 ºC). (2) PM protein biotinylation: cells are transferred to 4 ºC to halt membrane trafficking and cell impermeant sulfo-NHS-SS-biotin applied to biotinylate (red dots) amino groups of cell surface exposed lysine residues. GLUT1 has at least 4 potentially NHS ester accessible lysine residues (ref: (17)), and α–subunit of Na–K ATPase has at least 1 (ref: (224)). (3) Unreacted biotin is quenched with excess glycine (100 mM) or Tris (5 mM) at 4 ºC and the cells are warmed back to 37 ºC for varying time periods to restore membrane trafficking. (4) Cells are transferred back to 4 ºC and treated with the cell impermeable reductant (TCEP; 50 mM) for 2 x 15 min, to cleave off any biotin label remaining at the PM. (5) Cell are washed extensively to remove any residual TCEP, followed by lysis. (6) Clarified lysate [Total protein] is determined by BCA and a normalized amount of each sample is loaded onto avidin beads to capture biotinylated proteins that were protected from extracellular TCEP by internalization. (7) Pulled-down proteins are eluted from avidin beads and quantitated by immunoblotting using appropriate antibody. **B – D,** Optimization of major steps in the reversible cell surface biotinylation technique. B, Optimization of the biotinylation step (step 2 in A). Cells were labeled with 0.2 – 5 mg/mL sulfo-NHS-SS-biotin for 10 – 120 min at 4 ºC. The extent of PM GLUT1 and Na–ATPase biotinylation depends on the concentration of the biotinylating reagent and the duration of biotinylation. **C,** Optimization of the avidin pull-down step (step 6 in A). Ratio of bead volume (50 – 200 µL) to the concentration of total protein lysate (50 µg) from cells treated with or without 0.5 mg/mL sulfo-NHS-SS-biotin for 30 min, was varied from 1:1 to 4:1, and the extent of GLUT1 and Na–K ATPase pull-down was assessed by immunoblot. Figure shows that a ratio 1:1 ratio of beads to total protein lysate is sufficient to capture PM proteins biotinylated with 0.5 mg/mL biotin reagent. **D,** Optimization of TCEP stripping step (step 4 in A). PM proteins were biotinylated with 0.5 mg/mL sulfo-NHS-SS-biotin for 30 min (step 2 in A). After quenching unreacted biotin, biotinylated PM proteins were cleaved with 50 mM TCEP for 10 – 15 min. 100% stripping efficiency was obtained for Na–K ATPase at 10 or 15 min strip, while 91 – 93% stripping efficiency was obtained for GLUT1. In subsequent assays, the 50 mM TCEP stripping step was performed for 2 x 15 min.

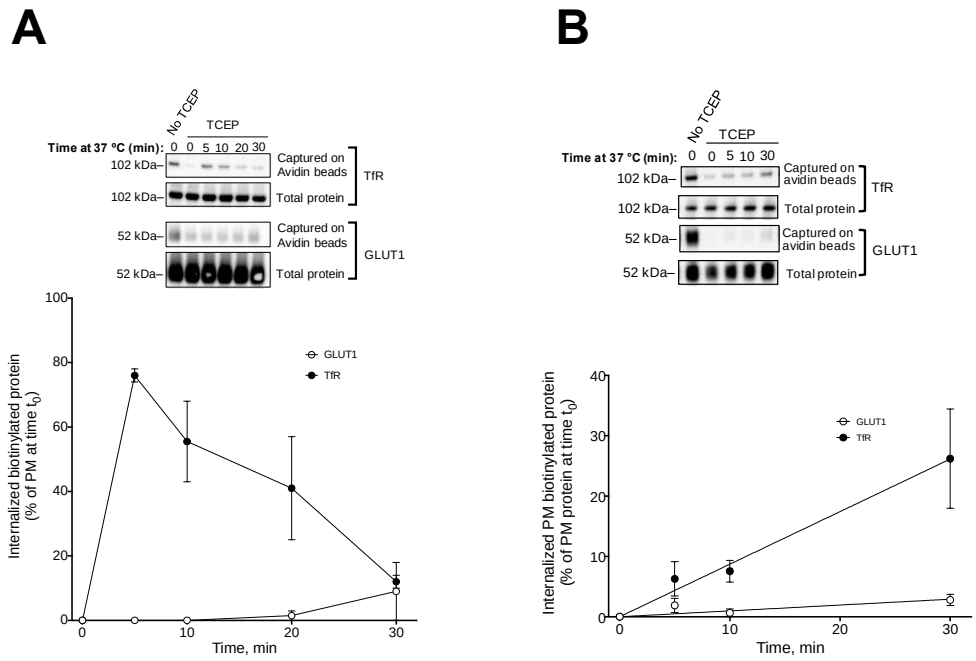

Figure.A.3: Net internalization of cell surface GLUT1 and transferrin receptor (TfR) in cultured cells (HEK293 cells (A) and bEnd.3 cells (B)) stably expressing GLUT1

The reversible cell surface biotinylation protocol reveals robust net internalization of TfR in HEK293 cells (up to 80% internalization after 5 min) followed by a decline in signal to about 20% (after 30 min), suggesting re-externalization of internalized biotinylated TfR. In bEnd.3 cells we see only about 30% net internalization of TfR after 30 min, suggesting a slower rate of internalization in these cells. In both HEK293 and bEnd.3 cells, GLUT1 internalization is extremely slow with about 10% and 5% internalized GLUT1 after 30 min in HEK293 and bEnd.3 cells respectively.

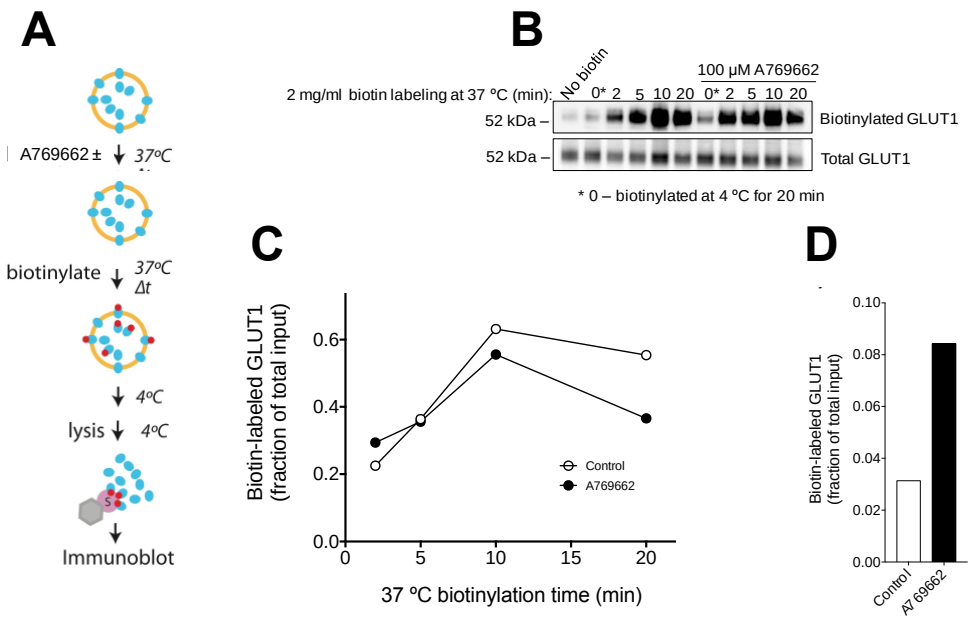

Figure.A.4: Measuring GLUT1 externalization by cell surface biotinylation in bEnd.3 cells stably expressing GLUT1

A, Modified cell-surface biotinylation protocol for measuring GLUT1 exocytosis. Here, biotinylation of PM proteins is performed at 37 ºC. The rationale is that if AMPK activation stimulates GLUT1 exocytosis, we should obtain more biotinylated PM GLUT1 in AMPK-activated cells versus basal control cells. B, A western blotting readout of the experiment described in A. C and D are graphical representation of data presented in B. As shown in **B & C,** we observed about 50% increase in PM membrane GLUT1 in AMPK-activated cells vs unstimulated control cells at 2 min, and as the time course progresses this increase is lost. This suggests that the rate of GLUT1 externalization is much faster than this technique can resolve. We still observe a 2-fold increase cell surface [GLUT1] in AMPK-activated cells vs basal control cells when biotinylation is performed at 4 ºC (**D**).

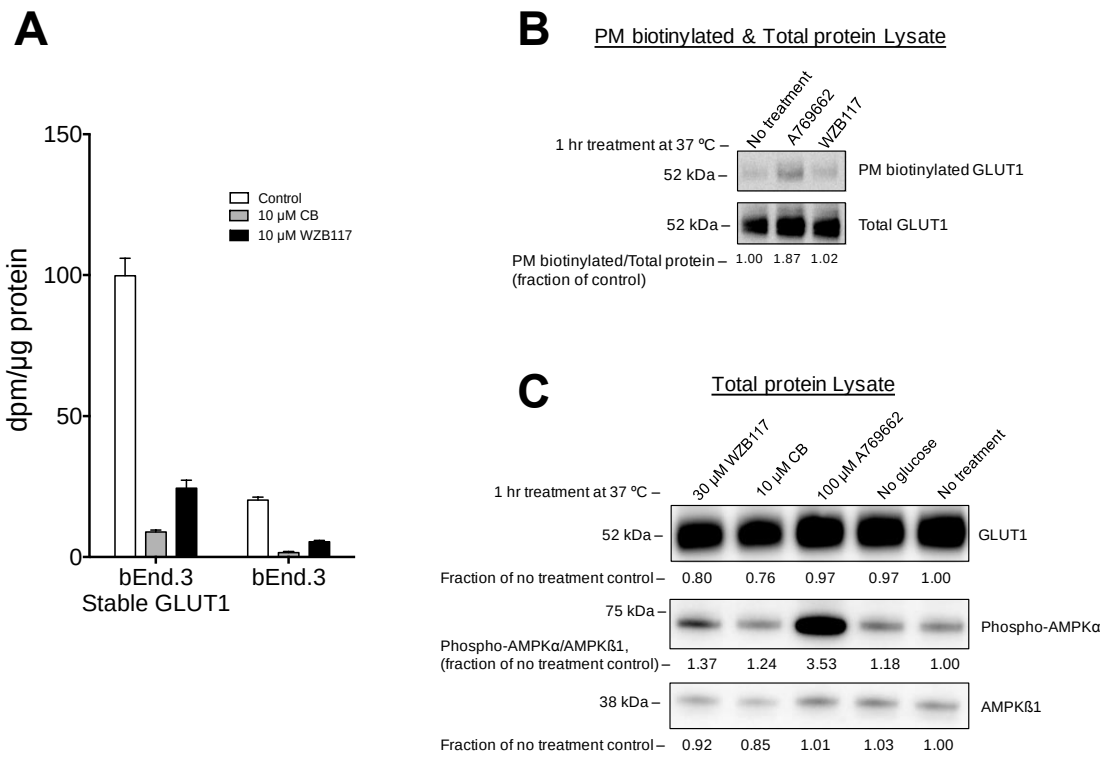

Figure A.5: Acute treatment of bEnd.3 cells with GLUT1 inhibitors inhibit glucose uptake but is without effect on AMPK or PM GLUT1 content.

A, 5 min 2-deoxyglucose uptake in untransfected bEnd.3 cells and in bEnd.3 cells stably expressing GLUT1 treated with or without 10 µM WZB117 or 10 µM cytochalasin B (CB) for 5 min. WZB117 and CB inhibit sugar uptake by greater than 75% in both transfected and untransfected cells. **B**, Treatment of bEnd.3-stable GLUT1 cells with 10 µM WZB117 did not increase PM GLUT1 but the AMPK agonist, A769662 increased PM GLUT1 by 87%. **C**, A769662, but not GLUT1 inhibitors or 1 hr glucose withdrawal, activated AMPK in bEnd.3–GLUT1-transfected stable cells.

REFERENCES

1. Alberts, B., Johnson, A., Lewis, J., Morgan, D., Raff, M., Roberts, K., and Walter, P. (2015) *Molecular biology of the cell*, Garland Science, New York
2. Yang, N. J., and Hinner, M. J. (2015) Getting across the cell membrane: An overview for small molecules, peptides, and proteins. *Methods in Molecular Biology* **1266**, 29-53
3. Stein, W. D. (1986) *Transport and diffusion across cell membranes*, Academic Press, New York
4. Cooper, G. M., and Hausman, R. E. (2007) *The cell: A molecular approach*, 4th ed., Sinauer Associates, Sunderland, MA
5. Cura, A. J., and Carruthers, A. (2012) Role of monosaccharide transport proteins in carbohydrate assimilation, distribution, metabolism, and homeostasis. *Comprehensive Physiology* **2**, 863-914
6. Carruthers, A. (1990) Facilitated diffusion of glucose. *Physiological Reviews* **70**, 1135-1176
7. Stein, W. D., and Litman, T. (2015) Carrier-mediated transport: Facilitated diffusion. in *Channels, Carriers, and Pumps*, 2nd Ed., Elsevier, London. pp 131-178
8. Klepper, J., and Voit, T. (2002) Facilitated glucose transporter protein type 1 (GLUT1) deficiency syndrome: impaired glucose transport into brain – a review. *European Journal of Pediatrics* **161**, 295-304
9. Gordon, N., and Newton, R. W. (2003) Glucose transporter type1 (GLUT1) deficiency. *Brain and Development* **25**, 477-480
10. Wang, D., Kranz-Eble, P., and De Vivo, D. C. (2000) Mutational analysis of GLUT1 (SLC2A1) in GLUT1 deficiency syndrome. *Human Mutation* **16**, 224-231
11. Chillaron, J., Font-Llitjos, M., Fort, J., Zorzano, A., Goldfarb, D. S., Nunes, V., and Palacin, M. (2010) Pathophysiology and treatment of cystinuria. *Nature Reviews Nephrology* **6**, 424-434
12. Cutting, G. R. (2015) Cystic fibrosis genetics: from molecular understanding to clinical application. *Nature Reviews Genetics* **16**, 45-56
13. Thorens, B., and Mueckler, M. (2010) Glucose transporters in the 21st Century. *American Journal of Physiology - Endocrinology and Metabolism* **298**, E141-E145
14. Wright, E. M. (2013) Glucose transport families SLC5 and SLC50. *Molecular Aspects of Medicine* **34**, 183-196
15. Feng, L., and Frommer, W. B. (2015) Structure and function of SemiSWEET and SWEET sugar transporters. *Trends in Biochemical Sciences* **40**, 480-486
16. Deng, D., and Yan, N. (2016) GLUT, SGLT, and SWEET: Structural and mechanistic investigations of the glucose transporters. *Protein Science* **25**, 546-558
17. Wright, E. M., Loo, D. D., and Hirayama, B. A. (2011) Biology of human sodium glucose transporters. *Physiological Reviews* **91**, 733-794
18. Chen, L.-Q. Q., Hou, B.-H. H., Lalonde, S., Takanaga, H., Hartung, M. L., Qu, X.-Q. Q., Guo, W.-J. J., Kim, J.-G. G., Underwood, W., Chaudhuri, B., Chermak, D., Antony, G., White, F. F., Somerville, S. C., Mudgett, M. B., and Frommer, W. B. (2010) Sugar transporters for intercellular exchange and nutrition of pathogens. *Nature* **468**, 527-532
19. Saier, M. H., Beatty, J. T., Goffeau, A., Harley, K. T., Heijne, W. H., Huang, S. C., Jack, D. L., Jähn, P. S., Lew, K., Liu, J., Pao, S. S., Paulsen, I. T., Tseng, T. T., and

Virk, P. S. (1999) The major facilitator superfamily. *Journal of Molecular Microbiology and Biotechnology* **1**, 257-279

20. Reddy, V. S., Shlykov, M. A., Castillo, R., Sun, E. I., and Saier, M. H. (2012) The major facilitator superfamily (MFS) revisited. *The FEBS Journal* **279**, 2022-2035
21. Mueckler, M., and Thorens, B. (2013) The SLC2 (GLUT) family of membrane transporters. *Molecular Aspects of Medicine* **34**, 121-138
22. Joost, H. G., and Thorens, B. (2001) The extended GLUT-family of sugar/polyol transport facilitators: nomenclature, sequence characteristics, and potential function of its novel members (review). *Molecular membrane biology* **18**, 247-256
23. Pao, S. S., Paulsen, I. T., and Saier, M. H. (1998) Major facilitator superfamily. *Microbiology and Molecular Biology Reviews* **62**, 1-34
24. Sato, M., and Mueckler, M. (1999) A conserved amino acid motif (R-X-G-R-R) in the GLUT1 glucose transporter is an important determinant of membrane topology. *The Journal of Biological Chemistry* **274**, 24721-24725
25. Zhao, F.-Q., and Keating, A. F. (2007) Functional properties and genomics of glucose transporters. *Current Genomics* **8**, 113-128
26. Chen, S., Pan, C., Nandigama, K., Mansfield, B., Ambudkar, S., and Chou, J. (2008) The glucose-6-phosphate transporter is a phosphate-linked antiporter deficient in glycogen storage disease type Ib and Ic. *The FASEB Journal* **22**, 2206-2213
27. Augustin, R., Riley, J., and Moley, K. (2005) GLUT8 contains a [DE]XXXL[LI] sorting motif and localizes to a late endosomal/lysosomal compartment. *Traffic* **6**, 1196-1212
28. Deng, D., Xu, C., Sun, P., Wu, J., Yan, C., Hu, M., and Yan, N. (2014) Crystal structure of the human glucose transporter GLUT1. *Nature* **510**, 121-125
29. Kapoor, K., Finer-Moore, J., Pedersen, B., Caboni, L., Waight, A., Hillig, R., Bringmann, P., Heisler, I., Müller, T., Siebeneicher, H., and Stroud, R. (2016) Mechanism of inhibition of human glucose transporter GLUT1 is conserved between cytochalasin B and phenylalanine amides. *Proceedings of the National Academy of Sciences of the United States of America* **113**, 4711-4716
30. Deng, D., Sun, P., Yan, C., Ke, M., Jiang, X., Xiong, L., Ren, W., Hirata, K., Yamamoto, M., Fan, S., and Yan, N. (2015) Molecular basis of ligand recognition and transport by glucose transporters. *Nature* **526**, 391-396
31. Nomura, N., Verdon, G., Kang, H. J., Shimamura, T., Nomura, Y., Sonoda, Y., Hussien, S. A., Qureshi, A. A., Coincon, M., Sato, Y., Abe, H., Nakada-Nakura, Y., Hino, T., Arakawa, T., Kusano-Arai, O., Iwanari, H., Murata, T., Kobayashi, T., Hamakubo, T., Kasahara, M., Iwata, S., and Drew, D. (2015) Structure and mechanism of the mammalian fructose transporter GLUT5. *Nature* **526**, 397-401
32. Sun, L., Zeng, X., Yan, C., Sun, X., Gong, X., Rao, Y., and Yan, N. (2012) Crystal structure of a bacterial homologue of glucose transporters GLUT1-4. *Nature* **490**, 361-366
33. Quistgaard, E. M., Löw, C., Moberg, P., Trésaugues, L., and Nordlund, P. (2013) Structural basis for substrate transport in the GLUT-homology family of monosaccharide transporters. *Nature Structural & Molecular Biology* **20**, 766-768
34. Wisedchaisri, G., Park, M.-S., Iadanza, M. G., Zheng, H., and Gonen, T. (2014) Proton-coupled sugar transport in the prototypical major facilitator superfamily protein XylE. *Nature Communications* **5**, 4521-4532

35. Iancu, C. V., Zamoon, J., Woo, S. B., Aleshin, A., and Choe, J.-y. (2013) Crystal structure of a glucose/H+ symporter and its mechanism of action. *Proceedings of the National Academy of Sciences of the United States of America* **110**, 17862-17867
36. Västermark, Å., and Saier, M. H. (2014) Evolutionary relationship between 5+5 and 7+7 inverted repeat folds within the amino acid-polyamine-organocation superfamily. *Proteins: Structure, Function, and Bioinformatics* **82**, 336-346
37. Turk, E., and Wright, E. M. (1997) Membrane topology motifs in the SGLT cotransporter family. *Journal of Membrane Biology* **159**, 1-20
38. Hirayama, B. A., Lostao, M. P., Panayotova-Heiermann, M., Loo, D. D., Turk, E., and Wright, E. M. (1996) Kinetic and specificity differences between rat, human, and rabbit Na+-glucose cotransporters (SGLT1). *American Journal of Physiology - Gastrointestinal and Liver Physiology* **270**, G919-G926
39. Hummel, C. S., Lu, C., Loo, D. D. F., Hirayama, B. A., Voss, A. A., and Wright, E. M. (2011) Glucose transport by human renal Na+/D-glucose cotransporters SGLT1 and SGLT2. *American Journal of Physiology - Cell Physiology* **300**, C14-C21
40. Uldry, M., Ibberson, M., Hosokawa, M., and Thorens, B. (2002) GLUT2 is a high affinity glucosamine transporter. *FEBS Letters* **524**, 199-203
41. Takata, K., Kasahara, T., Kasahara, M., Ezaki, O., and Hirano, H. (1990) Erythrocyte/HepG2-type glucose transporter is concentrated in cells of blood-tissue barriers. *Biochemical & Biophysical Research Communications* **173**, 67-73
42. Zhao, F., Glimm, D., Kennelly, J. M., Postic, C., and Girard, J. (1993) Distribution of mammalian facilitative glucose transporter messenger RNA in bovine tissues. *International Journal of Biochemistry* **25**, 1897-1903
43. Johnson, J. H., Newgard, C. B., Milburn, J. L., Lodish, H. F., and Thorens, B. (1990) The high Km glucose transporter of islets of Langerhans is functionally similar to the low affinity transporter of liver and has an identical primary sequence. *Journal of Biological Chemistry* **265**, 6548-6551
44. Colville, C. A., Seatter, M. J., Jess, T. J., Gould, G. W., and Thomas, H. M. (1993) Kinetic analysis of the liver-type (GLUT2) and brain-type (GLUT3) glucose transporters in Xenopus oocytes: substrate specificities and effects of transport inhibitors. *Biochemical Journal* **290**, 701-706
45. Fukumoto, H., Seino, S., Imura, H., Seino, Y., Eddy, R. L., Fukushima, Y., Byers, M. G., Shows, T. B., and Bell, G. I. (1988) Sequence, tissue distribution, and chromosomal localization of mRNA encoding a human glucose transporter-like protein. *Proceedings of the National Academy of Sciences of the United States of America* **85**, 5434-5438
46. Haber, R. S., Weinstein, S. P., O'Boyle, E., Morgello, S. J., and Gould, G. W. (1993) Tissue distribution of the human GLUT3 glucose transporter. *Endocrinology* **132**, 2538-2543
47. Simpson, I. A., Dwyer, D., Malide, D., Moley, K. H., Travis, A., Vannucci, S. J. r.-S., Ellen M., Vannucci, S. J., and Smith, Q. R. (2008) The facilitative glucose transporter GLUT3: 20 years of distinction. *American Journal of Physiology - Endocrinology and Metabolism* **295**, E242-E253
48. Kasahara, T., Kasahara, M. T., and Lengyel, P. (1997) Characterization of rat Glut4 glucose transporter expressed in the yeast Saccharomyces cerevisiae: comparison with Glut1 glucose transporter. *Biochimica et Biophysica Acta (BBA) - Biomembranes* **1324**, 111-119

49. Rumsey, S., Daruwala, R., Al-Hasani, H., Zarnowski, M., Simpson, I., and Levine, M. (2000) Dehydroascorbic acid transport by GLUT4 in Xenopus oocytes and isolated rat adipocytes. *Journal of Biological Chemistry* **275**, 28246-28253
50. Burant, C. F., Takeda, J., Brot, L. E., Bell, G. I., and Davidson, N. O. T. (1992) Fructose transporter in human spermatozoa and small intestine is GLUT5. *Journal of Biological Chemistry* **267**, 14523-14526
51. Rand, E. B., Depaoli, A. M., Davidson, N. O., Bell, G. I., and Burant, C. F. (1993) Sequence, tissue distribution, and functional characterization of the rat fructose transporter GLUT5. *American Journal of Physiology* **264**, G1169-G1176
52. Hundal, H. S., Darakhshan, F., Kristiansen, S., Blakemore, S. J., and Richter, E. A. (1998) GLUT5 expression and fructose transport in human skeletal muscle. in *Skeletal Muscle Metabolism in Exercise and Diabetes* (Richter, E. A., Kiens, B., Galbo, H., and Saltin, B. eds.), Springer US, Boston, MA. pp 35-45
53. Doege, H., Schurmann, A., Bahrenberg, G., Brauers, A., and Joost, H. (2000) GLUT8, a novel member of the sugar transport facilitator family with glucose transport activity. *Journal of Biological Chemistry* **275**, 16275-16280
54. Barron, C. C., Bilan, P. J., Tsakiridis, T., and Tsiani, E. (2016) Facilitative glucose transporters: Implications for cancer detection, prognosis and treatment. *Metabolism: Clinical and Experimental* **65**, 124-139
55. Li, Q., Manolescu, A., Ritzel, M., Yao, S., Slugoski, M., Young, J., Chen, X., Cheeseman, C., and Bennett, J. (2004) Cloning and functional characterization of the human GLUT7 isoform SLC2A7 from the small intestine. *American Journal of Physiology - Gastrointestinal and Liver Physiology* **287**, G236-242
56. Ibberson, M., Uldry, M., and Thorens, B. (2000) GLUTX1 (GLUT8), a novel mammalian glucose transporter expressed in the central nervous system and insulin-sensitive tissues. *Journal of Biological Chemistry* **275**, 4607-4612
57. Doblado, M., and Moley, K. H. (2009) Facilitative glucose transporter 9, a unique hexose and urate transporter. *American Journal of Physiology - Endocrinology and Metabolism* **297**, E831-E835
58. Anzai, N., Ichida, K., Jutabha, P., Kimura, T., Babu, E., Jin, C. J., Srivastava, S., Kitamura, K., Hisatome, I., Endou, H., and Sakurai, H. (2008) Plasma urate level is directly regulated by a voltage-driven urate efflux transporter URATv1 (SLC2A9) in humans. *Journal of Biological Chemistry* **283**, 26834-26838
59. Dawson, P. A., Mychaleckyj, J. C., Fossey, S. C., Mihic, S. J., Craddock, A. L., Bowden, D. W. n., G.E., and Lodish, H. F. (2001) Sequence and functional analysis of glut10: A glucose transporter in the type 2 diabetes-linked region of chromosome 20q12-13.1. *Molecular Genetics and Metabolism* **74**, 186-199
60. McVie-Wylie, A. J., Lamson, D. R., Chen, Y. T. K. E., Ferdman, B. A., and Lublin, D. M. (2001) Molecular cloning of a novel member of the GLUT family of transporters, SLC2a10 (GLUT10), localized on chromosome 20q13.1: a candidate gene for NIDDM susceptibility. *Genomics* **72**, 113-117
61. Wu, X., Li, W., Sharma, V., Godzik, A., Freeze, H. H. l., P.F., Bell, G. I., Seino, S. k., N. A., and Agre, P. (2002) Cloning and characterization of glucose transporter 11, a novel sugar transporter that is alternatively spliced in various tissues. *Molecular Genetics and Metabolism* **76**, 37-45
62. Manolescu, A., Augustin, R., Moley, K., and Cheeseman, C. (2007) A highly conserved hydrophobic motif in the exofacial vestibule of fructose transporting

SLC2A proteins acts as a critical determinant of their substrate selectivity. *Molecular Membrane Biology* **24**, 455-463

63. Sasaki, T., Minoshima, S., Shiohama, A., Shintani, A., Shimizu, A., Asakawa, S., Kawasaki, K., and Shimizu, N. (2001) Molecular cloning of a member of the facilitative glucose transporter gene family GLUT11 (SLC2A11) and identification of transcription variants. *Biochemical and Biophysical Research Communications* **289**, 1218-1224
64. Scheepers, A., Schmidt, S., Manolescu, A., Cheeseman, C. I., Bell, A., Zahn, C., Joost, H. G., and Schurmann, A. (2005) Characterization of the human SLC2A11 (GLUT11) gene: alternative promoter usage, function, expression, and subcellular distribution of three isoforms, and lack of mouse orthologue. *Molecular Membrane Biology* **22**, 339-351
65. Rogers, S., Chandler, J. D., Clarke, A. L., Petrou, S., and Best, J. D. (2003) Glucose transporter GLUT12-functional characterization in Xenopus laevis oocytes. *Biochemical and Biophysical Research Communications* **308**, 422-426
66. Uldry, M., Ibberson, M., Horisberger, J., Chatton, J., Riederer, B., and Thorens, B. (2001) Identification of a mammalian H(+)-myo-inositol symporter expressed predominantly in the brain. *The EMBO Journal* **20**, 4467-4477
67. Wu, X., and Freeze, H. (2002) GLUT14, a duplicon of GLUT3, is specifically expressed in testis as alternative splice forms. *Genomics* **80**, 553-557
68. Faham, S., Watanabe, A., Besserer, G. M., Cascio, D., Specht, A., Hirayama, B. A., Wright, E. M., and Abramson, J. (2008) The crystal structure of a sodium galactose transporter reveals mechanistic insights into Na+/sugar symport. *Science* **321**, 810-814
69. Watanabe, A., Choe, S., Chaptal, V., Rosenberg, J. M., Wright, E. M., Grabe, M., and Abramson, J. (2010) The mechanism of sodium and substrate release from the binding pocket of vSGLT. *Nature* **468**, 988-991
70. Yee, D. C., Shlykov, M. A., Västermark, Å., Reddy, V. S., Arora, S., Sun, E. I., and Saier, M. H. (2013) The transporter–opsin–G protein-coupled receptor (TOG) superfamily. *The FEBS Journal* **280**, 5780-5800
71. Chen, L.-Q., Hou, B.-H., Lalonde, S., Takanaga, H., Hartung, M. L., Qu, X.-Q., Guo, W.-J., Kim, J.-G., Underwood, W., Chaudhuri, B., Chermak, D., Antony, G., White, F. F., Somerville, S. C., Mudgett, M. B., and Frommer, W. B. (2010) Sugar transporters for intercellular exchange and nutrition of pathogens. *Nature* **468**, 527-532
72. Chen, L.-Q., Qu, X.-Q., Hou, B.-H., Sosso, D., Osorio, S., Fernie, A. R., and Frommer, W. B. (2012) Sucrose efflux mediated by SWEET proteins as a key step for phloem transport. *Science* **335**, 207-211
73. Chen, L.-Q., Lin, I. W., Qu, X.-Q., Sosso, D., McFarlane, H. E., Londoño, A., Samuels, A. L., and Frommer, W. B. (2015) A Cascade of Sequentially Expressed Sucrose Transporters in the Seed Coat and Endosperm Provides Nutrition for the Arabidopsis Embryo. *The Plant Cell Online* **27**, 607-619
74. Lin, I. W., Sosso, D., Chen, L.-Q., Gase, K., Kim, S.-G., Kessler, D., Klinkenberg, P. M., Gorder, M. K., Hou, B.-H., Qu, X.-Q., Carter, C. J., Baldwin, I. T., and Frommer, W. B. (2014) Nectar secretion requires sucrose phosphate synthases and the sugar transporter SWEET9. *Nature* **508**, 546-549
75. Chardon, F., Bedu, M., Calenge, F., Klemens, Patrick A. W., Spinner, L., Clement, G., Chietera, G., Léran, S., Ferrand, M., Lacombe, B., Loudet, O., Dinant, S., Bellini,

C., Neuhaus, H. E., Daniel-Vedele, F., and Krapp, A. (2013) Leaf fructose content is controlled by the vacuolar transporter SWEET17 in Arabidopsis. *Current Biology* **23**, 697-702

76. Klemens, P. A. W., Patzke, K., Deitmer, J., Spinner, L., Le Hir, R., Bellini, C., Bedu, M., Chardon, F., Krapp, A., and Neuhaus, H. E. (2013) Overexpression of the vacuolar sugar carrier AtSWEET16 modifies germination, growth and stress tolerance in Arabidopsis thaliana. *Plant Physiology* **163**, 1338-1352
77. Xu, Y., Tao, Y., Cheung, L. S., Fan, C., Chen, L.-Q., Xu, S., Perry, K., Frommer, W. B., and Feng, L. (2014) Structures of bacterial homologues of SWEET transporters in two distinct conformations. *Nature* **515**, 448-452
78. Wang, J., Yan, C., Li, Y., Hirata, K., Yamamoto, M., Yan, N., and Hu, Q. (2014) Crystal structure of a bacterial homologue of SWEET transporters. *Cell Research* **24**, 1486-1489
79. Lee, Y., Nishizawa, T., Yamashita, K., Ishitani, R., and Nureki, O. (2015) Structural basis for the facilitative diffusion mechanism by SemiSWEET transporter. *Nature Communications* **6**, 6112-6120
80. Patching, S. G. (2017) Glucose transporters at the blood-brain barrier: function, regulation and gateways for drug delivery. *Molecular Neurobiology* **54**, 1046-1077
81. Gruetter, R., Novotny, E. J., Boulware, S. D., Rothman, D. L., Mason, G. F., Shulman, G. I., Shulman, R. G., and Tamborlane, W. V. (1992) Direct measurement of brain glucose concentrations in humans by 13C NMR spectroscopy. *Proceedings of the National Academy of Sciences of the United States of America* **89**, 1109-1112
82. Appelboom, J. W. T., Brodsky, W. A., and Rehm, W. S. (1959) The concentration of glucose in mammalian liver. *The Journal of General Physiology* **43**, 467-479
83. Rumsey, S. C., Kwon, O., Xu, G. W., Burant, C. F., Simpson, I., and Levine, M. (1997) Glucose transporter isoforms GLUT1 and GLUT3 transport dehydroascorbic acid. *Journal of Biological Chemistry* **272**, 18982-18989
84. Sage, J., and Carruthers, A. (2014) Human erythrocytes transport dehydroascorbic acid and sugars using the same transporter complex. *American Journal of Physiology - Cell Physiology* **306**, C910-C917
85. Lieb, W. R., and Stein, W. D. (1986) Facilitated diffusion: The simple carrier. in *Transport and diffusion across cell membranes*, Academic Press, New York. pp 231-361
86. Barnett, J. E., Holman, G. D., Chalkley, R. A., and Munday, K. A. (1975) Evidence for two asymmetric conformational states in the human erythrocyte sugar-transport system. *Biochemical Journal* **145**, 417-429
87. Barnett, J., Holman, G., and Munday, K. (1973) Structural requirements for binding to the sugar-transport system of the human erythrocyte. *Biochemical Journal* **131**, 211-221
88. Barnett, J. E., Holman, G. D., and Munday, K. A. (1973) An explanation of the asymmetric binding of sugars to the human erythrocyte sugar-transport systems. *Biochemical Journal* **135**, 539-541
89. Baker, G. F., and Widdas, W. F. (1973) The asymmetry of the facilitated transfer system for hexoses in human red cells and the simple kinetics of a two component model. *The Journal of Physiology* **231**, 143-165
90. Lowe, A. G., and Walmsley, A. R. (1986) The kinetics of glucose transport in human red blood cells. *Biochimica et Biophysica Acta* **857**, 146-154

91. Carruthers, A., and Melchior, D. (1983) Asymmetric or symmetric? Cytosolic modulation of human erythrocyte hexose transfer. *Biochimica et Biophysica Acta* **728**, 254-266
92. Blodgett, D., De Zutter, J., Levine, K., Karim, P., and Carruthers, A. (2007) Structural Basis of GLUT1 Inhibition by Cytoplasmic ATP. *The Journal of General Physiology* **130**, 157-168
93. Carruthers, A., Dezutter, J., Ganguly, A., and Devaskar, S. (2009) "Will the Original Glucose Transporter Isoform Please Stand Up!". *American Journal of Physiology - Endocrinology and Metabolism* **297**, E836-8489
94. Levine, M., Oxender, D. L., and Stein, W. D. (1965) The substrate facilitated transport of the glucose carrier across the human erythrocyte membrane. *Biochimica et Biophysica Acta (BBA) - Biophysics including Photosynthesis* **109**, 151–163
95. Widdas, W. F. (1952) Inability of diffusion to account for placental glucose transfer in the sheep and consideration of the kinetics of a possible carrier transfer. *The Journal of Physiology* **118**, 23-39
96. Toyoda, N., Flanagan, J. E., and Kono, T. (1987) Reassessment of insulin effects on the Vmax and Km values of hexose transport in isolated rat epididymal adipocytes. *Journal of Biological Chemistry* **262**, 2737-2745
97. Vollers, S. S., and Carruthers, A. (2012) Sequence determinants of GLUT1-mediated accelerated-exchange transport: Analysis by homology-scanning mutagenesis. *Journal of Biological Chemistry* **287**, 42533-42544
98. Mueckler, M., Caruso, C., Baldwin, S. A., Panico, M., Blench, I., Morris, H. R., Allard, W. J., Lienhard, G. E., and Lodish, H. F. (1985) Sequence and structure of a human glucose transporter. *Science* **229**, 941-945
99. Gorga, F., R., Baldwin, S., A., and Lienhard, G., E. (1979) The monosaccharide transporter from human erythrocytes is heterogeneously glycosylated. *Biochemical and Biophysical Research Communications* **91**, 955-961
100. Asano, T., Katagiri, H., Takata, K., Lin, J. L., Ishihara, H., Inukai, K., Tsukuda, K., Kikuchi, M., Hirano, H., and Yazaki, Y. (1991) The role of N-glycosylation of GLUT1 for glucose transport activity. *Journal of Biological Chemistry* **266**, 24632-24636
101. Abramson, J., Smirnova, I., Kasho, V., Verner, G., Kaback, R. H., and Iwata, S. (2003) Structure and mechanism of the lactose permease of Escherichia coli. *Science* **301**, 610-615
102. Huang, Y., Lemieux, M. J., Song, J., Auer, M., and Wang, D. N. (2003) Structure and mechanism of the glycerol-3-phosphate transporter from Escherichia coli. *Science* **301**, 616-620
103. Jardetzky, O. (1966) Simple allosteric model for membrane pumps. *Nature* **211**, 969-970
104. Krupka, R. M., and Devés, R. (1981) An experimental test for cyclic versus linear transport models. The mechanisms of glucose and choline transport in erythrocytes. *Journal of Biological Chemistry* **256**, 5410-5416
105. Lieb, W. R., and Stein, W. D. (1974) Testing and characterizing the simple carrier. *Biochimica et Biophysica Acta* **373**, 178-196
106. Baker, P. F., and Carruthers, A. (1981) 3-O-methylglucose transport in internally dialysed giant axons of Loligo. *The Journal of Physiology* **316**, 503-525
107. Naftalin, R. J. (2008) Alternating carrier models of asymmetric glucose transport violate the energy conservation laws. *Biophysical Journal* **95**, 4300-4314

108. Sogin, D. C., and Hinkle, P. C. (1980) Binding of cytochalasin B to human erythrocyte glucose transport. *Biochemistry* **19**, 5417–5420
109. Gorga, F. R., and Lienhard, G. E. (1981) Equilibria and kinetics of ligand binding to the human erythrocyte glucose transporter. Evidence for an alternating conformation model for transport. *Biochemistry* **20**, 5108-5113
110. Baldwin, S. A., Baldwin, J. M., Gorga, F. R., and Lienhard, G. E. (1979) Purification of the cytochalasin B binding component of the human erythrocyte monosaccharide transport system. *Biochimica et Biophysica Acta - Biomembranes* **552**, 183-188
111. Carruthers, A. (1986) ATP regulation of the human red cell sugar transporter. *Journal of Biological Chemistry* **261**, 11028-11037
112. Coderre, L., Monfar, M. M., Chen, K. S., Heydrick, S. J., Kurowski, T. G., Ruderman, N. B., and Pilch, P. F. (1992) Alteration in the expression of GLUT-1 and GLUT-4 protein and messenger RNA levels in denervated rat muscles. *Endocrinology* **131**, 1821-1825
113. Hebert, D. N., and Carruthers, A. (1991) Cholate-solubilized erythrocyte glucose transporters exist as a mixture of homodimers and homotetramers. *Biochemistry* **30**, 4654-4658
114. Hebert, D. N., and Carruthers, A. (1992) Glucose transporter oligomeric structure determines transporter function. Reversible redox-dependent interconversions of tetrameric and dimeric GLUT1. *Journal of Biological Chemistry* **267**, 23829-23838
115. Zottola, R. J., Cloherty, E. K., Coderre, P. E., Hansen, A., Hebert, D. N., and Carruthers, A. (1995) Glucose transporter function is controlled by transporter oligomeric structure. A single, intramolecular disulfide promotes GLUT1 tetramerization. *Biochemistry* **34**, 9734-9747
116. Helgerson, A. L., and Carruthers, A. (1987) Equilibrium ligand binding to the human erythrocyte sugar transporter. Evidence for two sugar-binding sites per carrier. *Journal of Biological Chemistry* **262**, 5464-5475
117. Basketter, D., and Widdas, W. (1978) Asymmetry of the hexose transfer system in human erythrocytes. Comparison of the effects of cytochalasin B, phloretin and maltose as competitive inhibitors. *The Journal of Physiology* **278**, 389-401
118. Carruthers, A., and Helgerson, A. (1991) Inhibitions of sugar transport produced by ligands binding at opposite sides of the membrane. Evidence for simultaneous occupation of the carrier by maltose and cytochalasin B. *Biochemistry* **30**, 3907-3915
119. Yan, N. (2017) A glimpse of membrane transport through structures—Advances in the structural biology of the GLUT glucose transporters. *Journal of Molecular Biology* **429**, 2710-2725
120. Lloyd, K. P., Ojelabi, O. A., De Zutter, J. K., and Carruthers, A. (2017) Reconciling contradictory findings: Glucose transporter 1 (GLUT1) functions as an oligomer of allosteric, alternating access transporters. *Journal of Biological Chemistry* **292**, 21035-21046
121. Robichaud, T., Appleyard, A., Herbert, R., Henderson, P., and Carruthers, A. (2011) Determinants of ligand binding affinity and cooperativity at the GLUT1 endofacial site. *Biochemistry* **50**, 3137-3148
122. Cloherty, E. K., Levine, K. B., and Carruthers, A. (2001) The red blood cell glucose transporter presents multiple, nucleotide-sensitive sugar exit sites. *Biochemistry* **40**, 15549-15561

123. De Zutter, J. K., Levine, K. B., Deng, D., and Carruthers, A. (2013) Sequence determinants of GLUT1 oligomerization: Analysis by homology-scanning mutagenesis. *Journal of Biological Chemistry* **288**, 20734-20744
124. Hamill, S., Cloherty, E. K., and Carruthers, A. (1999) The human erythrocyte sugar transporter presents two sugar import sites. *Biochemistry* **38**, 16974-16983
125. Haworth, R. A., and Berkoff, H. A. (1986) The control of sugar uptake by metabolic demand in isolated adult rat heart cells. *Circulation Research* **58**, 157-165
126. Holman, G. D., Kozka, I. J., Clark, A. E., Flower, C. J., Saltis, J., Habberfield, A. D., Simpson, I. A., and Cushman, S. W. (1990) Cell surface labeling of glucose transporter isoform GLUT4 by bis-mannose photolabel. Correlation with stimulation of glucose transport in rat adipose cells by insulin and phorbol ester. *Journal of Biological Chemistry* **265**, 18172-18179
127. Simpson, I., Carruthers, A., and Vannucci, S. (2007) Supply and demand in cerebral energy metabolism: the role of nutrient transporters. *Journal of Cerebral Blood Flow and Metabolism* **27**, 1766-1791
128. Simpson, I. A., and Cushman, S. W. (1986) Hormonal regulation of mammalian glucose transport. *Annual Review of Biochemistry* **55**, 1059-1089
129. Wilson, C., and Cushman, S. (1994) Insulin stimulation of glucose transport activity in rat skeletal muscle: increase in cell surface GLUT4 as assessed by photolabelling. *Biochemical Journal* **299** 755-759
130. Jacquez, J. A. (1984) Red blood cell as glucose carrier: significance for placental and cerebral glucose transfer. *American Journal of Physiology* **246**, R289-R298
131. Gerritsen, M., Burke, T., Allen, L., Silverstein, S., and Stern, D. (1988) Glucose starvation is required for insulin stimulation of glucose uptake and metabolism in cultured microvascular endothelial cells. *Microvascular Research* **35**, 153-166
132. Cura, A., and Carruthers, A. (2010) Acute modulation of sugar transport in brain capillary endothelial cell cultures during activation of the metabolic stress pathway. *Journal of Biological Chemistry* **285**, 15430-15439
133. Sone, H., Deo, B. K., and Kumagai, A. K. (2000) Enhancement of glucose transport by vascular endothelial growth factor in retinal endothelial cells. *Investigative Ophthalmology & Visual Science* **41**, 1876-1884
134. Simpson, I., Appel, N., Hokari, M., Oki, J., Holman, G., Maher, F., Koehler-Stec, E., Vannucci, S., and Smith, Q. (1999) Blood-brain barrier glucose transporter: effects of hypo- and hyperglycemia revisited. *Journal of Neurochemistry* **72**, 238-247
135. Diamond, D., and Carruthers, A. (1993) Metabolic control of sugar transport by derepression of cell surface glucose transporters: an insulin-independent, recruitment-independent mechanism of regulation. *Journal of Biological Chemistry* **268**, 6437-6444
136. Hebert, D. N., and Carruthers, A. (1986) Direct evidence for ATP modulation of sugar transport in human erythrocyte ghosts. *Journal of Biological Chemistry* **261**, 10093-10099
137. Carruthers, A. (1986) Anomalous asymmetric kinetics of human red cell hexose transfer: role of cytosolic adenosine 5'-triphosphate. *Biochemistry* **25**, 3592-3602
138. Levine, K. B., Cloherty, E. K., Fidyk, N. J., and Carruthers, A. (1998) Structural and physiologic determinants of human erythrocyte sugar transport regulation by adenosine triphosphate. *Biochemistry* **37**, 12221-12232
139. Carruthers, A., and Helgerson, A. L. (1989) The human erythrocyte sugar transporter is also a nucleotide binding protein. *Biochemistry* **28**, 8337-8346

140. Heard, K., Fidyk, N., and Carruthers, A. (2000) ATP-dependent substrate occlusion by the human erythrocyte sugar transporter. *Biochemistry* **39**, 3005-3014
141. Jacquez, J. A. (1983) Modulation of glucose transport in human red blood cells by ATP. *Biochimica et Biophysica Acta (BBA) - Biomembranes* **727**, 367-378
142. Leitch, J., and Carruthers, A. (2007) ATP-dependent sugar transport complexity in human erythrocytes. *American Journal of Physiology - Cell Physiology* **292**, C974-C986
143. Levine, K. B., Cloherty, E. K., Hamill, S., and Carruthers, A. (2002) Molecular determinants of sugar transport regulation by ATP. *Biochemistry* **41**, 12629-12638
144. Cloherty, E. K., Diamond, D. L., Heard, K. S., and Carruthers, A. (1996) Regulation of GLUT1-mediated sugar transport by an antiport/uniport switch mechanism. *Biochemistry* **35**, 13231-13239
145. Helgerson, A. L., Hebert, D. N., Naderi, S., and Carruthers, A. (1989) Characterization of two independent modes of action of ATP on human erythrocyte sugar transport. *Biochemistry* **28**, 6410-6417
146. Levine, K. B., Hamill, S., Cloherty, E. K., and Carruthers, A. (2001) Alanine scanning mutagenesis of the human erythrocyte glucose transporter putative ATP binding domain. *Blood Cells, Molecules, and Diseases* **27**, 139-142
147. Harik, S. I., Behmand, R. A., and LaManna, J. C. (1994) Hypoxia increases glucose transport at blood-brain barrier in rats. *Journal of Applied Physiology* **77**, 896-901
148. McCall, A., Fixman, L., Fleming, N., Tornheim, K., Chick, W., and Ruderman, N. (1986) Chronic hypoglycemia increases brain glucose transport. *American Journal of Physiology* **251**, E442-E447
149. Abbud, W., Habinowski, S., Zhang, J.-Z., Kendrew, J., Elkairi, F. S., Kemp, B. E., Witters, L. A., and Ismail-Beigi, F. (2000) Stimulation of AMP-Activated Protein Kinase (AMPK) Is Associated with Enhancement of Glut1-Mediated Glucose Transport. *Archives of Biochemistry and Biophysics* **380**, 347-352
150. Barnes, K., Ingram, J., Porras, O., Barros, L., Hudson, E., Fryer, L., Foufelle, F., Carling, D., Hardie, D., Baldwin, S. K., Kikuchi, M., Oka, Y., and Asano, T. (2002) Activation of GLUT1 by metabolic and osmotic stress: potential involvement of AMP-activated protein kinase (AMPK). *Journal of Cell Science* **115**, 2433-2442
151. Cura, A., and Carruthers, A. (2012) AMP kinase regulation of sugar transport in brain capillary endothelial cells during acute metabolic stress. *American Journal of Physiology - Cell Physiology* **303**, C808-C814
152. Mu, J., Brozinick, J. T., Jr., Valladares, O., Bucan, M., and Birnbaum, M. J. (2001) A role for AMP-activated protein kinase in contraction- and hypoxia- regulated glucose transport in skeletal muscle. *Molecular Cell* **7**, 1085-1094.
153. Hardie, D. G., Ross, F. A., and Hawley, S. A. (2012) AMPK: a nutrient and energy sensor that maintains energy homeostasis. *Nature Reviews Molecular Cell Biology* **13**, 251-262
154. Hardie, D. G., Ross, Fiona A., and Hawley, Simon A. (2012) AMP-activated protein kinase: A target for drugs both ancient and modern. *Chemistry & Biology* **19**, 1222-1236
155. Boado, R. J., and Pardridge, W. M. (1993) Glucose deprivation causes posttranscriptional enhancement of brain capillary endothelial glucose transporter gene expression via GLUT1 mRNA stabilization. *Journal of Neurochemistry* **60**, 2290-2296

156. Boado, R. J., Wu, D., and Windisch, M. (1999) In vivo upregulation of the blood-brain barrier GLUT1 glucose transporter by brain-derived peptides. *Neuroscience Research* **34**, 217-224
157. Fazakerley, D. J., Holman, G. D., Marley, A., James, D. E., Stöckli, J., and Coster, A. C. F. (2010) Kinetic evidence for unique regulation of GLUT4 trafficking by insulin and AMP-activated protein kinase activators in L6 myotubes. *Journal of Biological Chemistry* **285**, 1653-1660
158. Kurth-Kraczek, E. J., Hirshman, M. F., Goodyear, L. J., and Winder, W. W. (1999) 5' AMP-activated protein kinase activation causes GLUT4 translocation in skeletal muscle. *Diabetes* **48**, 1667-1671
159. Lauritzen, H. P. M. M., Galbo, H., Toyoda, T., and Goodyear, L. J. (2010) Kinetics of contraction-induced GLUT4 translocation in skeletal muscle fibers from living mice. *Diabetes* **59**, 2134-2144
160. Geraghty, K. M., Chen, S., Harthill, J. E., Ibrahim, A. F., Toth, R., Morrice, N. A., Vandermoere, F., Moorhead, G. B., Hardie, D. G., and MacKintosh, C. (2007) Regulation of multisite phosphorylation and 14-3-3 binding of AS160 in response to IGF-1, EGF, PMA and AICAR. *Biochemical Journal* **407**, 231-241
161. Treebak, J. T., Glund, S., Deshmukh, A., Klein, D. K., Long, Y. C., Jensen, T. E., Jørgensen, S. B., Viollet, B., Andersson, L., Neumann, D., Wallimann, T., Richter, E. A., Chibalin, A. V., Zierath, J. R., and Wojtaszewski, J. F. P. (2006) AMPK-mediated AS160 phosphorylation in skeletal muscle is dependent on AMPK catalytic and regulatory subunits. *Diabetes* **55**, 2051-2058
162. Wu, N., Zheng, B., Shaywitz, A., Dagon, Y., Tower, C., Bellinger, G., Shen, C., Wen, J., Asara, J., McGraw, T., Kahn, B., and Cantley, L. (2013) AMPK-dependent degradation of TXNIP upon energy stress leads to enhanced glucose uptake via GLUT1. *Molecular Cell* **49**, 1167-1175
163. Bloch, R. (1973) Inhibition of glucose transport in the human erythrocyte by cytochalasin B. *Biochemistry* **12**, 4799-4801
164. LeFevre, P. G., Marshall, J. K., Glozman, R., and Elazar, Z. (1959) The attachment of phloretin and analogues to human erythrocytes in connection with inhibition of sugar transport. *Journal of Biological Chemistry* **234**, 3022–3027
165. Liu, Y., Cao, Y., Zhang, W., Bergmeier, S., Qian, Y., Akbar, H., Colvin, R., Ding, J., Tong, L., Wu, S., Hines, J., and Chen, X. (2012) A small-molecule inhibitor of glucose transporter 1 downregulates glycolysis, induces cell-cycle arrest, and inhibits cancer cell growth in vitro and in vivo. *Molecular Cancer Therapeutics* **11**, 1672-1682
166. Chan, D., Sutphin, P., Nguyen, P., Turcotte, S., Lai, E., Banh, A., Reynolds, G., Chi, J., Wu, J., Solow-Cordero, D., Bonnet, M., Flanagan, J., Bouley, D., Graves, E., Denny, W., Hay, M., and Giaccia, A. (2011) Targeting GLUT1 and the Warburg effect in renal cell carcinoma by chemical synthetic lethality. *Science Translational Medicine* **3**, 94ra70
167. Siebeneicher, H., Cleve, A., Rehwinkel, H., Neuhaus, R., Heisler, I., Müller, T., Bauser, M., and Buchmann, B. (2016) Identification and optimization of the first highly selective GLUT1 inhibitor BAY-876. *ChemMedChem* **11**, 2261-2271
168. Lin, S., Lin, D. C., and Flanagan, M. D. (1978) Specificity of the effects of cytochalasin B on transport and motile processes. *Proceedings of the National Academy of Sciences of the United States of America* **75**, 329-333

169. Lin, S., Santi, D. V., and Spudich, J. A. (1974) Biochemical studies on the mode of action of cytochalasin B: Preparation of [3H]cytochalasin B and studies on its cinding to cells. *Journal of Biological Chemistry* **249**, 2268-2274
170. Calvo, M. B., Figueroa, A., Pulido, E. G., Campelo, R. G., and Aparicio, L. A. (2010) Potential Role of Sugar Transporters in Cancer and Their Relationship with Anticancer Therapy. *International Journal of Endocrinology* **1**, 1-14
171. Craik, J. D., Cheeseman, C. I., and Young, J. D. (1995) Rapid entry of D-glucose into erythrocytes from bottlenose dolphins (Tursiops truncatus). *Marine Mammal Science* **11**, 584-589
172. Craik, J., Young, J., Cheeseman, C., PMW, and Chishti, A. (1998) GLUT-1 mediation of rapid glucose transport in dolphin (Tursiops truncatus) red blood cells. *American Journal of Physiology* **274**, R112-119
173. De Vos, A., Heimberg, H., Quartier, E., Huypens, P., Bouwens, L., Pipeleers, D., and Schuit, F. (1995) Human and rat beta cells differ in glucose transporter but not in glucokinase gene expression. *Journal of Clinical Investigation* **96**, 2489-2495
174. Mohanasundaram, D., Drogemuller, C., Brealey, J., Jessup, C., Milner, C., Murgia, C., Lang, C., Milton, A., Zalewski, P., Russ, G., and Coates, P. (2011) Ultrastructural analysis, zinc transporters, glucose transporters and hormones expression in new world primate (Callithrix jacchus) and human pancreatic islets. *General and Comparative Endocrinology* **174**, 71-79
175. Plentz, R., Palagani, V., Wiedemann, A., Diekmann, U., Glage, S., Naujok, O., Jorns, A., and Muller, T. (2012) Islet microarchitecture and glucose transporter expression of the pancreas of the marmoset monkey display similarities to the human. *Islets* **4**, 123-129
176. Moore, M., Coate, K., Winnick, J., An, Z., and Cherrington, A. (2012) Regulation of hepatic glucose uptake and storage in vivo. *Advances in Nutrition* **3**, 286-294
177. Winnick, J., An, Z., Moore, M., Ramnanan, C., Farmer, B., Shiota, M., and Cherrington, A. (2009) A physiological increase in the hepatic glycogen level does not affect the response of net hepatic glucose uptake to insulin. *American Journal of Physiology - Endocrinology and Metabolism* **297**, E358-E366
178. Freemerman, A. J., Johnson, A. R., Sacks, G. N., Milner, J. J., Kirk, E. L., Troester, M. A., Macintyre, A. N., Goraksha-Hicks, P., Rathmell, J. C., and Makowski, L. (2014) Metabolic reprogramming of macrophages glucose transporter 1 (GLUT1)-mediated glucose metabolism drives a proinflammatory phenotype. *Journal of Biological Chemistry* **289**, 7884-7896
179. MacIver, N. J., Jacobs, S. R., Wieman, H. L., Wofford, J. A., Coloff, J. L., and Rathmell, J. C. (2008) Glucose metabolism in lymphocytes is a regulated process with significant effects on immune cell function and survival. *Journal of Leukocyte Biology* **84**, 949-957
180. Kelly, B., and O'Neill, L. A. J. (2015) Metabolic reprogramming in macrophages and dendritic cells in innate immunity. *Cell Research* **25**, 771-784
181. Vander Heiden, M., Cantley, L., and Thompson, C. (2009) Understanding the Warburg effect: The metabolic requirements of cell proliferation. *Science* **324**, 1029-1033
182. Kim, J., and Dang, C. V. (2006) Cancer's molecular sweet tooth and the Warburg effect. *Cancer Research* **66**, 8927-8930
183. Klepper, J., and Leiendecker, B. (2007) GLUT1 deficiency syndrome - 2007 update. *Developmental Medicine and Child Neurology* **49**, 707-716

184. Winkler, E. A., Nishida, Y., Sagare, A. P., Rege, S. V., Bell, R. D., Perlmutter, D., Sengillo, J. D., Hillman, S., Kong, P., Nelson, A. R., Sullivan, J. S., Zhao, Z., Meiselman, H. J., Wenby, R. B., Soto, J., Abel, E. D., Makshanoff, J., Zuniga, E., De Vivo, D. C., and Zlokovic, B. V. (2015) GLUT1 reductions exacerbate Alzheimer's disease vasculo-neuronal dysfunction and degeneration. *Nature Neuroscience* **18**, 521-530
185. Ung, P. M.-U., Song, W., Cheng, L., Zhao, X., Hu, H., Chen, L., and Schlessinger, A. (2016) Inhibitor discovery for the human GLUT1 from homology modeling and virtual screening. *ACS Chemical Biology* **11**, 1908-1916
186. Baker, G. F., Basketter, D. A., and Widdas, W. F. (1978) Asymmetry of the hexose transfer system in human erythrocytes. Experiments with non-transportable inhibitors. *Journal of Physiology (London)* **278**, 377-388
187. Palorini, R., Cammarata, F., Balestrieri, C., Monestiroli, A., Vasso, M., Gelfi, C., Alberghina, L., and Chiaradonna, F. (2013) Glucose starvation induces cell death in K-ras-transformed cells by interfering with the hexosamine biosynthesis pathway and activating the unfolded protein response. *Cell Death and Disease* **4**, e732-e746
188. Warburg, O. (1956) On the origin of cancer cells. *Science* **123**, 309-314
189. De Giorgis, V., and Veggiotti, P. (2013) GLUT1 deficiency syndrome 2013: current state of the art. *Seizure* **22**, 803-811
190. Pelicano, H., Martin, D., Xu, R., and Huang, P. (2006) Glycolysis inhibition for anticancer treatment. *Oncogene* **25**, 4633-4646
191. Baracca, A., Chiaradonna, F., Sgarbi, G., Solaini, G., Alberghina, L., and Lenaz, G. (2010) Mitochondrial Complex I decrease is responsible for bioenergetic dysfunction in K-ras transformed cells. *Biochimica et Biophysica Acta* **1797**, 314-323
192. Chiaradonna, F., Sacco, E., Manzoni, R., Giorgio, M., Vanoni, M., and Alberghina, L. (2006) Ras-dependent carbon metabolism and transformation in mouse fibroblasts. *Oncogene* **25**, 5391-5404
193. Xintaropoulou, C., Ward, C., Wise, A., Marston, H., Turnbull, A., and Langdon, S. (2015) A comparative analysis of inhibitors of the glycolysis pathway in breast and ovarian cancer cell line models. *Oncotarget* **6**, 25677-25695
194. Joost, H. G., Bell, G. I., Best, J. D., Birnbaum, M. J., Charron, M. J., Chen, Y. T., Doege, H., James, D. E., Lodish, H. F., Moley, K. H., Moley, J. F., Mueckler, M., Rogers, S., Schurmann, A., Seino, S., and Thorens, B. (2002) Nomenclature of the GLUT/SLC2A family of sugar/polyol transport facilitators. *American Journal of Physiology - Endocrinology and Metabolism* **282**, E974-E976
195. Ganapathy, V., Thangaraju, M., and Prasad, P. D. k. (2009) Nutrient transporters in cancer: Relevance to Warburg hypothesis and beyond. *Pharmacology and Therapeutics* **121**, 29-40
196. Deves, R., and Krupka, R. M. (1978) Cytochalasin B and the kinetics of inhibition of biological transport: a case of asymmetric binding to the glucose carrier. *Biochimica et Biophysica Acta* **510**, 339-348
197. Sage, J. M., Cura, A. J., Lloyd, K. P., and Carruthers, A. (2015) Caffeine inhibits glucose transport by binding at the GLUT1 nucleotide-binding site. *American Journal of Physiology - Cell Physiology* **308**, C827-C834
198. Cunningham, P., Afzal-Ahmed, I., Naftalin, R., and Jtalmans, W. (2006) Docking studies show that D-glucose and quercetin slide through the transporter GLUT1. *Journal of Biological Chemistry* **281**, 5797-5803

199. Naftalin, R. J., Afzal, I., Cunningham, P., Halai, M., Ross, C., Salleh, N., and Milligan, S. R. (2003) Interactions of androgens, green tea catechins and the antiandrogen flutamide with the external glucose-binding site of the human erythrocyte glucose transporter GLUT1. *British Journal of Pharmacology* **140**, 487-499
200. Cairns, R., Harris, I., and Mak, T. (2011) Regulation of cancer cell metabolism. *Nature Reviews Cancer* **11**, 85-95
201. Gambhir, S. (2002) Molecular imaging of cancer with positron emission tomography. *Nature Reviews Cancer* **2**, 683-693
202. Shibuya, K., Okada, M., Suzuki, S., Seino, M., Seino, S., Takeda, H., and Kitanaka, C. (2015) Targeting the facilitative glucose transporter GLUT1 inhibits the self-renewal and tumor-initiating capacity of cancer stem cells. *Oncotarget* **6**, 651-661
203. Zhang, W., Liu, Y., Chen, X., and Bergmeier, S. (2010) Novel inhibitors of basal glucose transport as potential anticancer agents. *Bioorganic & Medicinal Chemistry Letters* **20**, 2191-2194
204. Leitch, J., and Carruthers, A. (2009) Alpha- and beta-monosaccharide transport in human erythrocytes. *American Journal of Physiology - Cell Physiology* **296**, C151-C161
205. Cloherty, E. K., Heard, K. S., and Carruthers, A. (1996) Human erythrocyte sugar transport is incompatible with available carrier models. *Biochemistry* **35**, 10411-10421
206. Segel, I. H. (1975) Multisite and allosteric enzymes. in *Enzyme kinetics*, Wiley, New York. pp 355-385
207. Murata, H., Hruz, P. W., and Mueckler, M. (2000) The mechanism of insulin resistance caused by HIV protease inhibitor therapy. *Journal of Biological Chemistry* **275**, 20251-20254
208. Cunningham, P., and Naftalin, R. (2013) Implications of aberrant temperature-sensitive glucose transport via the glucose transporter deficiency mutant (GLUT1DS) T295M for the alternate-access and fixed-site transport models. *The Journal of Membrane Biology* **246**, 495-511
209. Madej, M., Sun, L., Yan, N., and Kaback, H. (2014) Functional architecture of MFS D-glucose transporters. *Proceedings of the National Academy of Sciences of the United States of America* **111**, E719-727
210. James, D., Brown, R., Navarro, J., and Pilch, P. (1988) Insulin-regulatable tissues express a unique insulin-sensitive glucose transport protein. *Nature* **333**, 183-185
211. James, D., Strube, M., and Mueckler, M. (1989) Molecular cloning and characterization of an insulin-regulatable glucose transporter. *Nature* **338**, 83-87
212. Fukumoto, H., Kayano, T., Buse, J., Edwards, Y., Pilch, P., Bell, G., and Seino, S. (1989) Cloning and characterization of the major insulin-responsive glucose transporter expressed in human skeletal muscle and other insulin-responsive tissues. *Journal of Biological Chemistry* **264**, 7776-7779
213. Carruthers, A. (1991) Mechanisms for the facilitated diffusion of substrates across cell membranes. *Biochemistry* **30**, 3898-3906
214. Jardetzky, O. (1966) Simple allosteric model for membrane pumps. *Nature* **211**, 969-970
215. Graybill, C., van Hoek, A., Desai, D., Carruthers, A., and Carruthers, A. (2006) Ultrastructure of human erythrocyte GLUT1. *Biochemistry* **45**, 8096-8107

216. Cunningham, P., and Naftalin, R. (2014) Reptation-induced coalescence of tunnels and cavities in Escherichia Coli XylE transporter conformers accounts for facilitated diffusion. *Journal of Membrane Biology* **247**, 1161-1179
217. Blodgett, D., Nowosielska, A., Afik, S., Pechhold, S., Cura, A., Kennedy, N., Kim, S., Kucukural, A., Davis, R., Kent, S., Greiner, D., Garber, M., Harlan, D., and diIorio, P. (2015) Novel observations from next-generation RNA sequencing of highly purified human adult and fetal islet cell subsets. *Diabetes* **64**, 3172-3181
218. Brockmann, K. (2009) The expanding phenotype of GLUT1-deficiency syndrome. *Brain and Development* **31**, 545-552
219. Klepper, J. (2008) Glucose transporter deficiency syndrome (GLUT1DS) and the ketogenic diet. *Epilepsia* **49**, 46-49
220. De Vivo, D. C., Leaiy, L., and Wang, D. (2002) Glucose transporter 1 deficiency syndrome and other glycolytic defects. *Journal of Child Neurology* **17**, 3S15-13S25
221. Del Rio, D., Rodriguez-Mateos, A., Spencer, J. P., Tognolini, M., Borges, G., and Crozier, A. (2013) Dietary (poly)phenolics in human health: structures, bioavailability, and evidence of protective effects against chronic diseases. *Antioxid Redox Signal* **18**, 1818-1892
222. Hung, C. H., Chan, S. H., and Chu, P. M. (2015) Quercetin is a potent anti-atherosclerotic compound by activation of SIRT1 signaling under oxLDL stimulation. *Molecular Nutrition & Food Research* **59**, 1905-1917
223. Kerry, N. L., and Abbey, M. (1997) Red wine and fractionated phenolic compounds prepared from red wine inhibit low density lipoprotein oxidation in vitro. *Atherosclerosis* **135**, 93-102
224. Martínez-Pérez, C., Ward, C., and Turnbull, A. K. (2016) Antitumour activity of the novel flavonoid Oncamex in preclinical breast cancer models. *British Journal of Cancer* **114**, 905–916
225. Nijveldt, R. J., van Nood, E., van Hoorn, D. E., Boelens, P. G., van Norren, K., and van Leeuwen, P. A. (2001) Flavonoids: A review of probable mechanisms of action and potential applications. *The American Journal of Clinical Nutrition* **74**, 418-425
226. Formica, J. V., and Regelson, W. (1995) Review of the biology of quercetin and related bioflavonoids. *Food and Chemical Toxicology* **33**, 1061-1080
227. Kühnau, J. (1976) The flavonoids. A class of semi-essential food components: Their role in human nutrition. *World Review of Nutrition and Dietetics* **24**, 117-191
228. Nishimuro, H., Ohnishi, H., Sato, M., Ohnishi-Kameyama, M., Matsunaga, I., Naito, S., Ippoushi, K., Oike, H., Nagata, T., Akasaka, H., Saitoh, S., Shimamoto, K., and Kobori, M. (2015) Estimated daily intake and seasonal food sources of quercetin in Japan. *Nutrients* **7**, 2345-2358
229. Sutherland, B. A., Rahman, R. M., and Appleton, I. (2006) Mechanisms of action of green tea catechins, with a focus on ischemia-induced neurodegeneration. *The Journal of Nutritional Biochemistry* **17**, 291-306
230. Singh, B. N., Shankar, S., and Srivastava, R. K. (2011) Green tea catechin, epigallocatechin-3-gallate (EGCG): Mechanisms, perspectives and clinical applications. *Biochemical Pharmacology* **82**, 1807-1821
231. Hertog, M. G. L., and Hollman, P. C. H. (1993) Content of potentially anticarcinogenic flavonoids of tea infusions, wines, and fruit juices. *Journal of Agricultural and Food Chemistry* **41**, 1242-1246
232. McDonald, M. S., Hughes, M., Burns, J., Lean, M. E. J., Matthews, D., and Crozier, A. (1998) Survey of the free and conjugated myricetin and quercetin content of red

wines of different geographical origins. *Journal of Agricultural and Food Chemistry* **46**, 368-375
233. Yang, C. S., and Wang, H. (2016) Cancer preventive activities of tea catechins. *Molecules* **21**, 1679-1698
234. Kim, H. S., Quon, M. J., and Kim, J. A. (2014) New insights into the mechanisms of polyphenols beyond antioxidant properties; lessons from the green tea polyphenol, epigallocatechin 3-gallate. *Redox Biology* **2**, 187-195
235. Strobel, P., Allard, C., Perez-Acle, T., Calderon, R., Aldunate, R., and Leighton, F. (2005) Myricetin, quercetin and catechin-gallate inhibit glucose uptake in isolated rat adipocytes. *Biochemical Journal* **386**, 471-478
236. Vera, J. C., Reyes, A. M., Velasquez, F. V., Rivas, C. I., Zhang, R. H., Strobel, P., Slebe, J. C., Nunez-Alarcon, J., and Golde, D. W. (2001) Direct inhibition of the hexose transporter GLUT1 by tyrosine kinase inhibitors. *Biochemistry* **40**, 777-790
237. Araujo, J. R., Goncalves, P., and Martel, F. (2008) Modulation of Glucose Uptake in a Human Choriocarcinoma Cell Line (BeWo) by Dietary Bioactive Compounds and Drugs of Abuse. *Journal of Biochemistry* **144**, 177-186
238. Szablewski, L. (2013) Expression of glucose transporters in cancers. *Biochimica et Biophysica Acta (BBA) - Reviews on Cancer* **1835**, 164-169
239. Ojelabi, O. A., Lloyd, K. P., Simon, A. H., De Zutter, J. K., and Carruthers, A. (2016) WZB117 (2-fluoro-6-(m-hydroxybenzoyloxy) phenyl m-hydroxybenzoate) inhibits GLUT1-mediated sugar transport by binding reversibly at the exofacial sugar binding site. *Journal of Biological Chemistry* **291**, 26762-26772
240. Larkin, M., Blackshields, G., Brown, N., Chenna, R., McGettigan, P., McWilliam, H., Valentin, F., Wallace, I., Wilm, A., Lopez, R., Thompson, J., Gibson, T., and Higgins, D. (2007) Clustal W and Clustal X version 2.0. *Bioinformatics* **23**, 2947-2948
241. Eswar, N., Eramian, D., Webb, B., Shen, M.-Y., and Sali, A. (2008) Protein structure modeling with MODELLER. in *Structural proteomics: High-throughput methods* (Kobe, B., Guss, M., and Huber, T. eds.), Humana Press, Totowa, NJ. pp 145-159
242. Laskowski, R. A., Macarthur, M. W., Moss, D. S., and Thornton, J. M. (1993) {PROCHECK}: a program to check the stereochemical quality of protein structures. *Journal of Applied Crystallography* **26**, 283-291
243. Cermak, R., Landgraf, S., and Wolffram, S. (2004) Quercetin glucosides inhibit glucose uptake into brush-border-membrane vesicles of porcine jejunum. *British Journal of Nutrition* **91**, 849-855
244. Johnston, K., Sharp, P., Clifford, M., and Morgan, L. (2005) Dietary polyphenols decrease glucose uptake by human intestinal Caco-2 cells. *FEBS Letters* **579**, 1653-1657
245. Moreira, L., Araujo, I., Costa, T., Correia-Branco, A., Faria, A., Martel, F., and Keating, E. (2013) Quercetin and epigallocatechin gallate inhibit glucose uptake and metabolism by breast cancer cells by an estrogen receptor-independent mechanism. *Experimental Cell Research* **319**, 1784-1795
246. Perez, A., Ojeda, P., Ojeda, L., Salas, M., Rivas, C. I., Vera, J. C., and Reyes, A. M. (2011) Hexose transporter GLUT1 harbors several distinct regulatory binding sites for flavones and tyrphostins. *Biochemistry* **50**, 8834-8845
247. Sultzman, L., and Carruthers, A. (1999) Stop-flow analysis of cooperative interactions between GLUT1 sugar import and export sites. *Biochemistry* **38**, 6640-6650

248. Sirk, T. W., Brown, E. F., Friedman, M., and Sum, A. K. (2009) Molecular binding of catechins to biomembranes: relationship to biological activity. *Journal of Agricultural and Food Chemistry* **57**, 6720-6728
249. Uekusa, Y., Kamihira, M., and Nakayama, T. (2007) Dynamic behavior of tea catechins interacting with lipid membranes as determined by NMR spectroscopy. *Journal of Agricultural and Food Chemistry* **55**, 9986-9992
250. Vaidyanathan, J. B., and Walle, T. (2003) Cellular uptake and efflux of the tea flavonoid (-)epicatechin-3-gallate in the human intestinal cell line Caco-2. *Journal of Pharmacology and Experimental Therapeutics* **307**, 745-752
251. Walgren, R. A., Lin, J. T., Kinne, R. K., and Walle, T. (2000) Cellular uptake of dietary flavonoid quercetin 4'-beta-glucoside by sodium-dependent glucose transporter SGLT1. *Journal of Pharmacology and Experimental Therapeutics* **294**, 837-843
252. Wolffram, S., Block, M., and Ader, P. (2002) Quercetin-3-glucoside is transported by the glucose carrier SGLT1 across the brush border membrane of rat small intestine. *Journal of Nutrition* **132**, 630-635
253. Kao, Y.-h., Hiipakka, R. A., and Liao, S. (2000) Modulation of obesity by a green tea catechin. *The American Journal of Clinical Nutrition* **72**, 1232-1233
254. Tsuneki, H., Ishizuka, M., Terasawa, M., Wu, J.-B., Sasaoka, T., and Kimura, I. (2004) Effect of green tea on blood glucose levels and serum proteomic patterns in diabetic (db/db) mice and on glucose metabolism in healthy humans. *BMC Pharmacology* **4**, 1-10
255. Wu, L.-Y., Juan, C.-C., Hwang, L. S., Hsu, Y.-P., Ho, P.-H., and Ho, L.-T. (2004) Green tea supplementationameliorates insulin resistance and increases glucose transporter IV content in a fructose-fed rat model. *European Journal of Nutrition* **43**, 116-124
256. Choi, Y. T., Jung, C. H., Lee, S. R., Bae, J. H., Baek, W. K., Suh, M. H., Park, J., Park, C. W., and Suh, S. I. (2001) The green tea polyphenol (-)-epigallocatechin gallate attenuates beta-amyloid-induced neurotoxicity in cultured hippocampal neurons. *Life Sciences* **70**, 603-614
257. Choi, J.-Y., Park, C.-S., Kim, D.-J., Cho, M.-H., Jin, B.-K., Pie, J.-E., and Chung, W.-G. (2002) Prevention of nitric oxide-mediated 1-methyl-4-phenyl-1,2,3,6-tetrahydropyridine-induced Parkinson's disease in mice by tea phenolic epigallocatechin 3-gallate. *NeuroToxicology* **23**, 367-374
258. Jeon, S.-Y., Bae, K., Seong, Y.-H., and Song, K.-S. (2003) Green tea catechins as a BACE1 (β-Secretase) inhibitor. *Bioorganic & Medicinal Chemistry Letters* **13**, 3905-3908
259. Mandel, S., and Youdim, M. B. H. (2004) Catechin polyphenols: Neurodegeneration and neuroprotection in neurodegenerative diseases. *Free Radical Biology and Medicine* **37**, 304-317
260. Yang, C., and Wang, H. (2016) Cancer preventive activities of tea catechins. *Molecules* **21**, 1679-1698
261. Yang, C. S., Sang, S., Lambert, J. D., and Lee, M.-J. (2008) Bioavailability issues in studying the health effects of plant polyphenolic compounds. *Molecular Nutrition & Food Research* **52**, S139-S151
262. Day, A. J., Cañada, F. J., Díaz, J. C., and Kroon, P. A. (2000) Dietary flavonoid and isoflavone glycosides are hydrolysed by the lactase site of lactase phlorizin hydrolase. *FEBS Letters* **468**, 166-170

263. Gee, J. M., DuPont, M. S., Day, A. J., and Plumb, G. W. (2000) Intestinal transport of quercetin glycosides in rats involves both deglycosylation and interaction with the hexose transport pathway. *The Journal of Nutrition* **130**, 2765-2771
264. Baker, G., and Naftalin, R. (1979) Evidence of multiple operational affinities for D-glucose inside the human erythrocyte membrane. *Biochimica et Biophysica Acta* **550**, 474-484
265. Naftalin, R. J. (1988) Pre-steady-state uptake of D-glucose is inconsistent with a circulating carrier mechanism. *Biochimica et Biophysica Acta* **946**, 431-438
266. Lloyd, K. C., Ojelabi, O. A., Simon, A. H., De Zutter, J. K., and Carruthers, A. (2017) Kinetic basis of cis- and trans-allostery in GLUT1-mediated sugar transport. *Journal of Membrane Biology*, in press
267. Hanahan, D., and Weinberg, R. A. (2011) Hallmarks of cancer: the next generation. *Cell* **144**, 646-674
268. Qian, Y., Wang, X., and Chen, X. (2014) Inhibitors of glucose transport and glycolysis as novel anticancer therapeutics. *World Journal of Translational Medicine* **3**, 37-52
269. Warburg, O., Wind, F., and Negelein, E. (1927) The metabolism of tumors in the body. *The Journal of General Physiology* **8**, 519-530
270. DeBerardinis, R. J., Lum, J. J., Hatzivassiliou, G., and Thompson, C. B. (2008) The biology of cancer: Metabolic reprogramming fuels cell growth and proliferation. *Cell Metabolism* **7**, 11-20
271. Upadhyay, M., Samal, J., Kandpal, M., Singh, O. V., and Vivekanandan, P. (2013) The Warburg effect: Insights from the past decade. *Pharmacology & Therapeutics* **137**, 318-330
272. Gorga, F. R., and Lienhard, G. E. (1982) Changes in the intrinsic fluorescence of the human erythrocyte monosaccharide transporter upon ligand binding. *Biochemistry* **21**, 1905-1908
273. Kelloff, G. J., Lubet, R. A., Lieberman, R., Eisenhauer, K., Steele, V. E., Crowell, J. A., Hawk, E. T., Boone, C. W., and Sigman, C. C. (1998) Aromatase inhibitors as potential cancer chemopreventives. *Cancer Epidemiology Biomarkers & Prevention* **7**, 65-78
274. Browne, L. J., Gude, C., Rodriguez, H., Steele, R. E., and Bhatnager, A. (1991) Fadrozole hydrochloride: a potent, selective, nonsteroidal inhibitor of aromatase for the treatment of estrogen-dependent disease. *Journal of Medicinal Chemistry* **34**, 725-736
275. Bhatnagar, A. S. (2008) The discovery and mechanism of action of letrozole. *Breast Cancer Research and Treatment* **112**, 385-385
276. Wellington, K., and Keam, S. J. (2007) Spotlight on bicalutamide 150mg in the treatment of locally advanced prostate cancer. *Drugs & Aging* **24**, 169-171
277. Martin, N. E., Brunner, T. B., Kiel, K. D., DeLaney, T. F., Regine, W. F., Mohiuddin, M., Rosato, E. F., Haller, D. G., Stevenson, J. P., Smith, D., Pramanik, B., Tepper, J., Tanaka, W. K., Morrison, B., Deutsch, P., Gupta, A. K., Muschel, R. J., McKenna, W. G., Bernhard, E. J., and Hahn, S. M. (2004) A phase I trial of the dual farnesyltransferase and geranylgeranyltransferase inhibitor L-778,123 and radiotherapy for locally advanced pancreatic cancer. *Clinical Cancer Research* **10**, 5447-5454
278. Jørgensen, H. G., and Holyoake, T. L. (2007) Characterization of cancer stem cells in chronic myeloid leukaemia. *Biochemical Society Transactions* **35**, 1347-1351

279. Reid, T. S., and Beese, L. S. (2004) Crystal structures of the anticancer clinical candidates R115777 (Tipifarnib) and BMS-214662 complexed with protein farnesyltransferase suggest a mechanism of FTI selectivity. *Biochemistry* **43**, 6877-6884
280. Hunt, J. T., Ding, C. Z., Batorsky, R., Bednarz, M., Bhide, R., Cho, Y., Chong, S., Chao, S., Gullo-Brown, J., Guo, P., Kim, S. H., Lee, F. Y. F., Leftheris, K., Miller, A., Mitt, T., Patel, M., Penhallow, B. A., Ricca, C., Rose, W. C., Schmidt, R., Slusarchyk, W. A., Vite, G., and Manne, V. (2000) Discovery of (R)-7-cyano-2,3,4,5-tetrahydro-1-(1H-imidazol-4-ylmethyl)-3- (phenylmethyl)-4-(2-thienylsulfonyl)-1H-1,4-benzodiazepine (BMS-214662), a farnesyltransferase inhibitor with potent preclinical antitumor activity. *Journal of Medicinal Chemistry* **43**, 3587-3595
281. Fleming, F. F., Yao, L., Ravikumar, P. C., Funk, L., and Shook, B. C. (2010) Nitrile-containing pharmaceuticals: Efficacious roles of the nitrile pharmacophore. *Journal of Medicinal Chemistry* **53**, 7902-7917
282. Van Dort, M. E., and Jung, Y.-W. (2001) Synthesis and structure–activity studies of side-chain derivatized arylhydantoins for investigation as androgen receptor radioligands. *Bioorganic & Medicinal Chemistry Letters* **11**, 1045-1047
283. Li, J. J., Lula, D. M., Nguyen, M. N., Hu, L.-Y., Dettling, D., Johnson, T. R., Du, D. Y., Shanmugasundaram, V., Van Camp, J. A., Wang, Z., Harter, W. G., Yue, W.-S., Boys, M. L., Wade, K. J., Drummond, E. M., Samas, B. M., Lefker, B. A., Hoge, G. S., Lovdahl, M. J., Asbill, J., Carroll, M., Meade, M. A., Ciotti, S. M., and Krieger-Burke, T. (2008) Rational design and synthesis of 4-((1R,2R)-2-hydroxycyclohexyl)-2(trifluoromethyl)benzonitrile (PF-998425), a novel, nonsteroidal androgen receptor antagonist devoid of phototoxicity for dermatological indications. *Journal of Medicinal Chemistry* **51**, 7010-7014
284. Bayram, M., De Luca, L., Massie, M. B., and Gheorghiade, M. (2005) Reassessment of Dobutamine, Dopamine, and Milrinone in the Management of Acute Heart Failure Syndromes. *The American Journal of Cardiology* **96**, 47-58
285. Violetta, C., Oriana, T., and Stefano, S. (2006) From cromakalim to different structural classes of K(ATP) channel openers. *Current Topics in Medicinal Chemistry* **6**, 1049-1068
286. Sánchez, C. (2006) The pharmacology of citalopram enantiomers: The antagonism by R-citalopram on the effect of S-citalopram. *Basic & Clinical Pharmacology & Toxicology* **99**, 91-95
287. Pascual, E., Sivera, F., Yasothan, U., and Kirkpatrick, P. (2009) Febuxostat. *Nature Reviews Drug Discovery* **8**, 191-192
288. Hughes, C. A., Robinson, L., Tseng, A., and MacArthur, R. D. (2009) New antiretroviral drugs: a review of the efficacy, safety, pharmacokinetics, and resistance profile of tipranavir, darunavir, etravirine, rilpivirine, maraviroc, and raltegravir. *Expert Opinion on Pharmacotherapy* **10**, 2445-2466
289. Klement, R. J. (2017) Beneficial effects of ketogenic diets for cancer patients: a realist review with focus on evidence and confirmation. *Medical Oncology* **34**, 132
290. Chen, X.-s., Li, L.-y., Guan, Y.-d., Yang, J.-m., and Cheng, Y. (2016) Anticancer strategies based on the metabolic profile of tumor cells: therapeutic targeting of the Warburg effect. *Acta Pharmacologica Sinica* **37**, 1013-1019
291. Kropp, E. M., Oleson, B. J., Broniowska, K. A., Bhattacharya, S., Chadwick, A. C., Diers, A. R., Hu, Q., Sahoo, D., Hogg, N., Boheler, K. R., Corbett, J. A., and Gundry, R. L. (2015) Inhibition of an NAD+ salvage pathway provides efficient and selective

toxicity to human pluripotent stem cells. *Stem Cells Translational Medicine* **4**, 483-493

292. Adams, D. J., Ito, D., Rees, M. G., Seashore-Ludlow, B., Puyang, X., Ramos, A. H., Cheah, J. H., Clemons, P. A., Warmuth, M., Zhu, P., Shamji, A. F., and Schreiber, S. L. (2014) NAMPT is the cellular target of STF-31-like small-molecule probes. *ACS Chemical Biology* **9**, 2247-2254
293. Halgren, T. A., Murphy, R. B., Friesner, R. A., Beard, H. S., Frye, L. L., Pollard, W. T., and Banks, J. L. (2004) Glide: A new approach for rapid, accurate docking and scoring. 2. Enrichment factors in database screening. *Journal of Medicinal Chemistry* **47**, 1750-1759
294. Friesner, R. A., Murphy, R. B., Repasky, M. P., Frye, L. L., Greenwood, J. R., Halgren, T. A., Sanschagrin, P. C., and Mainz, D. T. (2006) Extra precision glide: Docking and scoring incorporating a model of hydrophobic enclosure for protein−ligand complexes. *Journal of Medicinal Chemistry* **49**, 6177-6196
295. Friesner, R. A., Banks, J. L., Murphy, R. B., Halgren, T. A., Klicic, J. J., Mainz, D. T., Repasky, M. P., Knoll, E. H., Shelley, M., Perry, J. K., Shaw, D. E., Francis, P., and Shenkin, P. S. (2004) Glide: A new approach for rapid, accurate docking and scoring. 1. Method and assessment of docking accuracy. *Journal of Medicinal Chemistry* **47**, 1739-1749
296. Sogin, D. C., and Hinkle, P. C. (1980) Immunological identification of the human erythrocyte glucose transporter. *Proceedings of the National Academy of Sciences of the United States of America* **77**, 5725-5729
297. Kasahara, M., and Hinkle, P. C. (1977) Reconstitution and purification of the D-glucose transporter from human erythrocytes. *Journal of Biological Chemistry* **252**, 7384-7390
298. Knowles, T. J., Finka, R., Smith, C., Lin, Y.-P., Dafforn, T., and Overduin, M. (2009) Membrane proteins solubilized intact in lipid containing nanoparticles bounded by styrene maleic acid copolymer. *Journal of the American Chemical Society* **131**, 7484-7485